

# THE VALIDATION OF THE LMC DEVICE

Analysis of Icelandic basaltic rocks

Johanna Ruether



UNIVERSITY OF ICELAND



TECHNISCHE  
UNIVERSITÄT  
DARMSTADT

# **THE VALIDATION OF THE LMC DEVICE**

Analysis of Icelandic basaltic rocks

Johanna Ruether

A 30 ECTS credit units Master's thesis

Supervisors

Prof. Dr. Ingo Sass

Prof. Dr. Axel Björnsson

Dipl. Ing. Sebastian Homuth MSc

A Master's thesis done at

RES | The School for Renewable Energy Science

in affiliation with

University of Iceland &

University of Akureyri

Akureyri, February 2011

The validation of the LMC device

Analysis of Icelandic basaltic rocks

A 30 ECTS credit units Master's thesis

© Johanna Ruether, 2010

RES | The School for Renewable Energy Science

Solborg at Nordurslod

IS600 Akureyri, Iceland

Telephone + 354 464 0100

[www.res.is](http://www.res.is)

### **Declaration of authorship**

I, Johanna Ruether, hereby declare that this thesis and the work presented in it is entirely my own. Where I have consulted the work of others, this is always clearly stated.

A handwritten signature in black ink, reading 'Johanna Ruether'. The signature is fluid and cursive, with a long horizontal stroke extending from the end.

February 16, 2011

Printed in February 2011

at Stell Printing in Akureyri, Iceland

## **ABSTRACT**

Thermal conductivity and diffusivity are geothermal parameters that characterize and categorize a geothermal reservoir. These physical features can be determined by optical scanning techniques. To improve the geothermal exploration of bedrocks a new optical scanning device called Lambda Measuring Center (LMC) has been developed. The instrument is able to measure the thermal conductivity and diffusivity of solids. The approach of this thesis is to validate the LMC device proceeding via statistical analyses of Icelandic basaltic rocks' thermal conductivity and diffusivity. The geological analysis is supplemented by an Icelandic study. 270 samples are collected and analyzed with respect to thermal conductivity and diffusivity for the program. Additionally 120 of the samples have been observed by the state-of-the-art instrument Thermal Conductivity Scanning (TCS). As a result of the comparison of the two data series the new tool is statistically analyzed and evaluated. The calibration of the LMC device to the TCS tool is rudimentary implemented. Tributary to the validation of the tool, the relation of thermal conductivity to varying texture in basalts is analyzed.

The study shows that the LMC device cannot be recommended for routine field measurements. Otherwise laboratory measurements done by the LMC have a slightly higher quality than the results obtained by the TCS. The comparison of the two devices shows that the analyzed geothermal parameters differ. Variations in the results are caused by differing deployed standards and heating intensities.

## ACKNOWLEDGEMENT

I would like to thank my thesis advisors Prof. Dr. Axel Björnsson and Prof. Dr. Ingo Sass for their multidisciplinary and intra-European cooperation. On the basis of this liaison it was possible to work on a project which combines my educational background of applied geosciences with the at RES newly acquired knowledge of geothermal energy. I thank Prof. Sass for his trust in my responsibility for the LMC device. Without Prof. Björnsson's support and translation related to Orkustofnun the thesis would not have been realized.

Thank you especially to the Orkustofnun employees Hjalti Franzson and Ásgrímur Guðmundsson who provided me with samples and data from the Öskjuhlíð outcrop. The cooperation was a great benefit for my thesis.

I thank Julia Jóhannsson and Sana'a Al-Zyoud who analyzed samples for me. The additional data was very helpful for the progress of my thesis.

I would like to thank Prof. Dr. Hrefna Kristiansdóttir for her support with the x-ray analyses and discussions about the mineralogy of my samples.

My special thanks to Sebastian Homuth who always had a supporting answer to my questions during my time in Germany.

Thank you to Sigrun Lóa Kristjánsdóttir for her effort with regard to the accounting.

Thanks to Þorkell Einarsson at the company Grásteinn, Reykjavík for cutting the samples into cuboids.

My special thanks to my supportive fellow students Eneja Osterman, Joseph Batir and Alicja Stokłosa who transported samples in Iceland and to Germany. Additionally I would like to thank Svanhildur Helgadóttir who picked up the samples at the stonecutter and borrowed me her trolley to transport the LMC tool to Germany.

I would like to thank my fellow students Marcin Wronowski and Michael Thompson for a really diversified thesis. Thank you for the emotional support.

Finally I want to thank my parents for their unrestricted help and understanding.

# TABLE OF CONTENTS

1	Motivation.....	13
2	Fundamentals .....	15
2.1	Geology of Iceland .....	15
2.2	Conductive Heat Transfer in the Earth's Crust.....	17
2.3	Optical Scanning Method .....	19
2.4	Statistics.....	21
2.4.1	Descriptive Statistics .....	21
2.4.2	Inductive Statistics .....	23
2.4.3	Regression and Correlation .....	24
3	Methodology.....	26
3.1	Logistics.....	26
3.1.1	Description of Location.....	26
3.1.2	Description of Samples .....	29
3.1.3	Analysis Program .....	29
3.2	Determination of Geothermal Parameters .....	30
3.2.1	Lambda Measuring Center (LMC).....	30
3.2.2	Thermal Conductivity Scanning (TCS).....	32
4	Geological Interpretation .....	35
4.1	Lithologic Interpretation .....	35
4.2	Petrologic and Physical Interpretation.....	38
4.3	Geodynamic Interpretation .....	46
5	Analysis of Thermal Conductivity.....	48
5.1	Interpretation of the Data.....	48
5.1.1	Hand Probes .....	48
5.1.2	Cuboids.....	50
5.1.3	Cores.....	51
5.1.4	Entire Sample Base .....	52
5.2	Statistical Analysis.....	54
5.2.1	Entire Sample Base Determined by the LMC Device.....	54
5.2.2	Comparison of LMC and TCS Instruments .....	57
5.3	Calibration .....	62
5.3.1	Basic Concept.....	62
5.3.2	Validation of Measurement Conditions .....	63

5.3.3 Derivation.....	64
6 Analysis of Thermal Diffusivity .....	68
6.1 Interpretation of Data.....	68
6.1.1 Hand Probes .....	68
6.1.2 Cuboids.....	70
6.1.3 Cores.....	71
6.1.4 Entire Sample Base .....	73
6.2 Statistical Analysis.....	74
6.2.1 Entire Sample Base Determined by the LMC Device.....	74
6.2.2 Comparison of LMC and TCS Instrument .....	76
6.3 Calibration .....	80
6.3.1 Basic Concept.....	80
6.3.2 Validation of Measurement Conditions .....	81
6.3.3 Derivation.....	82
7 Conclusion .....	89
7.1 Results.....	89
7.2 Outlook .....	90
References .....	89
Appendix A .....	1
Appendix B.....	11

## LIST OF FIGURES

Figure 1: Geotectonic map of Iceland .....	15
Figure 2: Geological map of Iceland .....	17
Figure 3: Thermal conductivity of rocks based on composing minerals and water or air content. ....	19
Figure 4: Sketch of the measuring unit's position related to the surface of the sample. ....	20
Figure 5: Gaussian distribution .....	23
Figure 6: Cumulative distribution function of the Gaussian distribution.....	24
Figure 7: Overview photo of the location of the Öskjuhlið outcrop .....	27
Figure 8: Illustration of the profiles in the Öskjuhlið outcrop.....	27
Figure 9: Sketch of the sampling locations in the several profiles at the Öskjuhlið outcrop .....	28
Figure 10: Photo of the LMC instrument .....	30
Figure 11: Temporal function of temperature at the sample's surface during a thermal conductivity measurement with the LMC instrument .....	31
Figure 12: Sketch of the measurement process for the determination of thermal diffusivity by the LMC device .....	32
Figure 13: Photo of the TCS instrument.....	32
Figure 14: Technical Configuration of the TCS device .....	33
Figure 15: Function of the temperature at the surface of the sample before and after the heating process by the TCS tool. ....	34
Figure 16: Sketch of the geological map of Reykjavik. ....	35
Figure 17: Geological map of southwest Iceland .....	36
Figure 18: Legend of the geological map of southwest Iceland.....	37
Figure 19: Sketch of the zonation in the Öskjuhlið lava flow .....	38
Figure 20: Relation between porosity and permeability in the Öskjuhlið lava flow .....	39
Figure 21: Relation between measured gas porosity and the thin section porosity components in the Öskjuhlið lava flow .....	39
Figure 22: Relation between sonic velocity and porosity in the Öskjuhlið lava flow .....	40
Figure 23: Relation between grain density and sonic velocity in the Öskjuhlið lava flow .	40
Figure 24: Distribution of mineralogical main components for the zone B in the Öskjuhlið lava flow .....	42
Figure 25: Distribution of the mineralogical main components for zone A in the Öskjuhlið lava flow .....	43



Figure 26: Distribution of the mineralogical main components for the Öskjuhlíð lava flow determined by Orkustofnun .....	44
Figure 27: Results of the x-ray fluorescence spectroscopy. Distribution of the chemical components for the Öskjuhlíð lava flow.....	44
Figure 28: Results of the x-ray diffraction analyses. Relation of the reflected x-ray's intensity to the .....	45
Figure 29: Joint measurements of the Öskjuhlíð lava flow illustrated in the Schmidt's grid .....	47
Figure 30: Joint measurements of the Öskjuhlíð lava flow displayed in a rose diagram ....	47
Figure 31: Relation between the thermal conductivity and the temperature difference at uncut and cut hand probes of the Öskjuhlíð lava flow observed by the LMC device.	49
Figure 32: Relation between thermal conductivity and temperature difference for samples classified by their location in the Öskjuhlíð outcrop determined by the LMC device	50
Figure 33: Relation between thermal conductivity and temperature difference of Öskjuhlíð cuboids classified by texture determined by LMC and TCS instruments .....	51
Figure 34: Relation between thermal conductivity and temperature difference of Öskjuhlíð cores determined by the LMC and the TCS device .....	52
Figure 35: Relation between the thermal conductivity and temperature difference of Öskjuhlíð samples determined by the LMC tool .....	53
Figure 36: Histogram of the thermal conductivity Öskjuhlíð data series determined by the LMC device .....	54
Figure 37: Frequency and cumulative normal distribution of the thermal conductivity Öskjuhlíð data series determined by the LMC instrument .....	55
Figure 38: Probability density distribution of the thermal conductivity Öskjuhlíð data series determined by LMC instrument .....	56
Figure 39: Box plot of the thermal conductivity Öskjuhlíð data series determined by the LMC device .....	57
Figure 40: Histograms of the thermal conductivity Öskjuhlíð data series determined by the LMC and the TCS devices.....	57
Figure 41: Frequency and cumulative normal distributions of the thermal conductivity Öskjuhlíð data series determined by the LMC and the TCS instruments .....	59
Figure 42: Probability density distributions of the thermal conductivity Öskjuhlíð data series determined by the LMC and the TCS devices.....	60
Figure 43: Box plot of the thermal conductivity Öskjuhlíð data series determined by the LMC and the TCS instruments .....	61
Figure 44: Linear regression of the thermal conductivity of the Öskjuhlíð data series determined by the LMC and the TCS tool .....	61
Figure 45: Logarithmic Regression of the thermal conductivity Öskjuhlíð data series determined by the LMC and the TCS tools .....	62
Figure 46: Thermal conductivities as observed by the LMC device with respect to the thermal conductivity of the deployed standard.....	63

Figure 47: Thermal conductivities as observed by the LMC device with respect to the deployed heating power.....	64
Figure 48: Thermal conductivities as observed by the LMC device with respect to the temperature difference for different deployed standards.....	65
Figure 49: Thermal conductivities as observed by the LMC device with respect to the temperature difference for different deployed heating power .....	66
Figure 50: Relation between the thermal conductivity Öskjuhlið data series and the temperature difference.....	67
Figure 51: Relation between the thermal diffusivity Öskjuhlið data series and the temperature difference classified by uncut and cut samples .....	69
Figure 52: Relation between the thermal diffusivity Öskjuhlið data series and temperature difference classified by the location in the outcrop.....	70
Figure 53: Relation between the thermal diffusivity of the Öskjuhlið cuboids and the temperature difference determined by the LMC and the TCS devices .....	71
Figure 54: Relation between the thermal diffusivity Öskjuhlið cores and the temperature difference determined by the LMC .....	72
Figure 55: Relation between the thermal diffusivity Öskjuhlið data series and the temperature difference determined by the LMC classified by the texture of the samples .....	73
Figure 56: Histogram of the thermal diffusivity Öskjuhlið data series determined by the LMC .....	74
Figure 57: Frequency and cumulative normal distribution of the thermal diffusivity Öskjuhlið data series determined by the LMC device.....	75
Figure 58: Probability density distribution of the thermal diffusivity Öskjuhlið data series determined by the LMC instrument .....	75
Figure 59: Box plot of the thermal diffusivity Öskjuhlið data series determined by the LMC device .....	76
Figure 60: Histograms of the thermal diffusivity Öskjuhlið data series determined by the LMC and the TCS .....	76
Figure 61: Frequency and cumulative distribution of the thermal diffusivity Öskjuhlið data series determined by the LMC and the TCS devices.....	78
Figure 62: Probability density distributions of the thermal diffusivity Öskjuhlið data series determined by the LMC and the TCS.....	78
Figure 63: Box plots of the thermal diffusivity Öskjuhlið data series determined by the LMC and the TCS instrument .....	79
Figure 64: Linear regression of the thermal diffusivity Öskjuhlið data series determined by the LMC and the TCS device .....	79
Figure 65: Logarithmic regression of the thermal diffusivity Öskjuhlið data series determined by the LMC and the TCS.....	80
Figure 66: Thermal diffusivities as observed by the LMC device with respect to the thermal conductivity of the deployed standard.....	81

Figure 67: Thermal diffusivities as observed by the LMC device with respect to the deployed heating power .....	82
Figure 68: Thermal diffusivities as observed by the LMC device with respect to the temperature difference for different deployed standards .....	82
Figure 69: Thermal diffusivities as observed by the LMC device with respect to the temperature difference for different deployed heating power .....	83
Figure 70: Relation between the thermal diffusivity Öskjuhlíð data series and the temperature difference. ....	84

## LIST OF TABLES

Table 1: Icelandic volcanic rock types categorized related to silica content and origin .....	16
Table 2: Recommended instrument adjustments related to certain thermal conductivities	32
Table 3: Observed properties of two zones A and B in the Öskjuhlið .....	38
Table 4: Comparison of chemical analyses of alkali basalt, olivine tholeiite and tholeiite from Hawaii.....	46
Table 5: Overview of the analysis program of thermal conductivity .....	48
Table 6: Statistical descriptive parameters of the Öskjuhlið data series determined by the LMC instrument .....	55
Table 7: Statistical descriptive parameters of the thermal conductivity Öskjuhlið data series determined by the LMC and the TCS devices.....	58
Table 8: Overview of the analysis program of the thermal diffusivity .....	68
Table 9: Statistical descriptive parameters of the thermal diffusivity Öskjuhlið data series determined by the LMC instrument .....	74
Table 10: Statistical descriptive parameters of the thermal diffusivity Öskjuhlið data series determined by the LMC and the TCS.....	77

# 1 MOTIVATION

Geothermal energy is one of the renewable energy resources besides solar radiation, oceanic waves and tides, wind, biomass, hydropower and the temperature gradient in the oceanic water in the world (Gupta and Roy, 2007). The heat in the earth arises from the initial creation of the planet earth and the decay of radiogenic elements in its crust (Lowrie, 1997). The global heat content adds up to  $12.6 \cdot 10^{24}$  MJ with an additional crust heat content of  $5.4 \cdot 10^{21}$  MJ. This yields a total global heat flow of  $8 \cdot 10^{12}$  W (Dickson and Fanelli, 2004). The transport of heat occurs in three ways. It is transported by convection from the core through the mantle up to the crust where conduction and convection occurs. Furthermore the radiogenic elements  $^{238}\text{U}$ ,  $^{235}\text{U}$ ,  $^{232}\text{Th}$  and  $^{40}\text{K}$  irradiate heat in the crust based on their decay (Lowrie, 1997). A global average conductive heat flow density of 60 to 80 mW/m<sup>2</sup> is finally obtained at the earth's surface. The heat flow varies regionally due to the tectonic localization and the geological bedrock.

To utilize this geothermal energy economically, it is divided into a deep and a shallow nature. Deep geothermal systems are characterized by 20 to 200°C and a depth below 400 m. In 24 nations geothermal energy is utilized to generate electricity (Bertani, 2009). The power originates in Hot Dry Rock reservoirs, also called Enhanced Geothermal Systems, and Hydrothermal Systems. On the other hand the shallow geothermal systems comprise heating, cooling and energy storage. A temperature range of 8 to 25°C up to a depth of 400 m depth under the ground surface is utilized with different kind of heat exchangers like borehole heat exchangers, collectors, energy piles and groundwater circulation well systems (Sass, 2010). Shallow geothermal energy can be exploited worldwide. In 2009 the installed thermal power of 78 countries is about 50,583 MW<sub>th</sub>, which leads to a total annual utilization of 438,071 TJ/yr (Lund et al., 2010).

The most important parameters for the exploration of geothermal systems like these are temperature, pressure, porosity, permeability and chemical composition of the bedrock. Furthermore, the physical properties such as electrical resistivity, magnetization, susceptibility, density, elasticity, seismic velocity, thermal conductivity, electrochemical potential and radioactivity are necessary to evaluate geothermal systems (Björnsson, 2010). On the basis of thermal conductivity and permeability of the bed rock it is possible to characterize the quality of geothermal systems. The grade of a system depends on the occurring heat transfer. Ancillary, to the predominant conduction in the rock matrix, convection of heated groundwater in connected pore volume is possible, thus the permeability of bedrock characterizes the type of heat transfer (Sass, 2010).

The relation of permeability and thermal conductivity in rocks is one of the research fields in the working group Applied Geothermal Science and Technology at the Technical University of Darmstadt, Germany, especially the analysis of basalt caused by its varying texture and alteration.

According to the state of technology, the determination of thermal conductivity of rocks takes place in the laboratory with optical scanning and line source methods. Additionally, an estimation of the bedrock's thermal conductivity is possible in the field with Geothermal Response Tests and Enhanced Geothermal Response Tests (Sass, 2010).

The geothermal exploration technique of bedrocks is extended by a newly developed optical scanning device called Lambda Measuring Center (LMC). This instrument is able

to determine the thermal conductivity and diffusivity of solids. This thesis approaches to validate the LMC instrument via analyses of Icelandic basaltic rocks' thermal conductivity and diffusivity. The new device is calibrated by the comparison of measurements obtained by the Thermal Conductivity Scanning (TCS) state-of-the-art device.

## 2 FUNDAMENTALS

### 2.1 Geology of Iceland

Iceland is the largest volcanic island in the world. It is located in the northern Atlantic Ocean on the Northern American and the Eurasian tectonic plate. In figure 1 it is visible that Iceland is surrounded by the Greenland-Icelandic-Ridge in the northeast, the Kolbeinsey-Ridge in the north, the Iceland-Faroe-Ridge in the southeast and the Reykjanes-Ridge in the southwest. The second and last listed ridges are part of the Mid-Atlantic-Ridge, connected to it by the Tjörnes Fracture Zone (TFZ) in the north and the South Icelandic Seismic Zone (SISZ) in the southwest, which is moving apart 1cm/yr in direction northwest and southeast. This movement is shown by blue arrows in the figure. Along the mid oceanic ridge basalts rise up from the mantle to the earth's crust, which is a phenomenon happening since the early Tertiary 60 Ma ago along the Mid-Atlantic-Ridge. The ages of the basaltic rocks have been determined from the magnetic orientation in their minerals. Due to changes in the earth's magnetic field the magnetization varies in rocks of different ages, which are symbolized in the figure by blue lines. The age of the rock increases with the distance from the Mid-Atlantic-Ridge which is an evidence for the spreading of the two tectonic plates. The volcanic tectonic rift zones that are displayed with a rose color are fed by a mantle plume. Caused by the shifting apart of the tectonic plates, the position of rift zones has changed with time in order to be located above the mantle plume. These tectonic movements create a complex pattern of rift zones and faults (Sædmundsson, 1979).

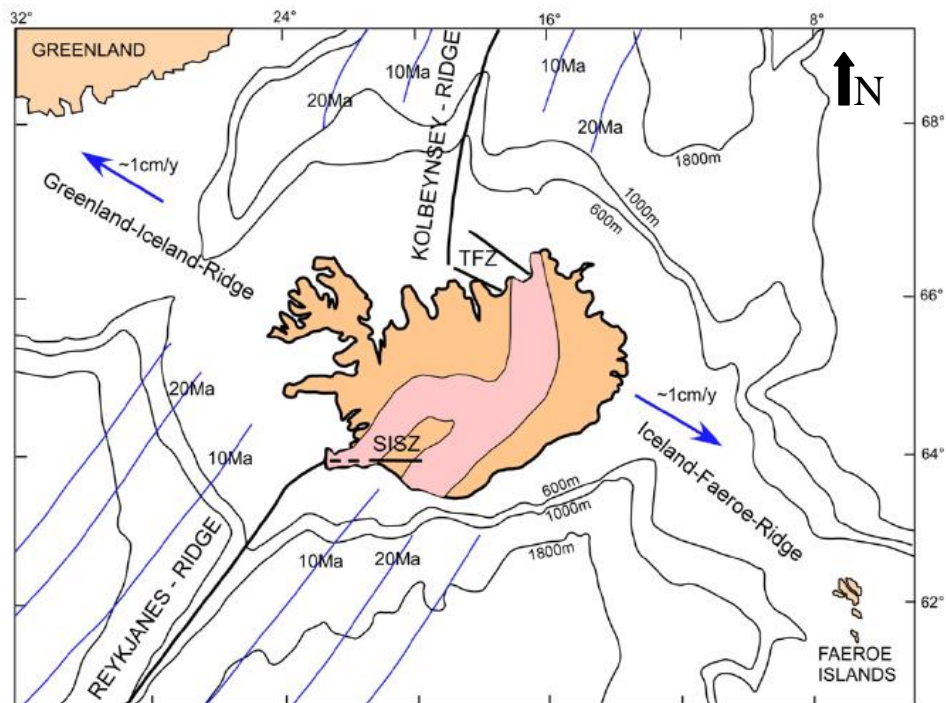


Figure 1: Geotectonic map of Iceland (Björnsson et al., 2007)

The Icelandic volcanic systems consist of fissure swarms and central volcanoes, which feature a high discharge in their center. Calderas and high temperature areas are generated as

well in the center of such volcanic system. Otherwise fissure swarms reaching dimensions of 5 to 15 km width and up to 200 km length are indicators of rift zones, which are commonly 40 to 50 km wide (Sæmundsson, 1979).

The petrology of Icelandic rocks is characterized by volcanic rocks, which is shown by the fact that 90% of the rocks have a volcanic origin. A minority belongs to consolidated sediments like interbedded tuffaceous layers or glacial moraines. Some diagenetic rocks are located in Iceland due to burial diagenesis, palagonitization of hyaloclastic rocks and local hydrothermal alteration in central volcanoes (Jakobsson and Gudmundsson, 2008). The volcanic rocks can be characterized by their origin: Tholeiitic basalts, which are coming directly from the earth mantle, belong to mid oceanic ridges and fissure eruptions. These rocks, with 10 to 19% content of normative hypersthene, poor in sodium, potassium and aluminum, rich in iron and titanium, originate from active volcanic rift zones (Einarsson, 1994). The off-ridge zones produce two other kinds of basalts, namely the transitional and alkaline basalts. These rocks are characterized by a reduced normative-hypersthene content substituted by nepheline content. The different occurring rock types categorized by silica content and igneous series are shown in the subsequent table 1.

*Table 1: Icelandic volcanic rock types categorized related to silica content and origin (Jakobsson et al., 2008)*

<b>Igneous series</b> <b>Silica content</b>	<b>Tholeiitic</b>	<b>Transitional</b>	<b>Alkalic</b>
<b>Basic</b>	Picirite Olivine Tholeiite Tholeiite	Transitional Olivine Basalt Transitional Basalt	Alkali Olive Basalt Alkali Basalt
<b>Intermediate</b>	Basaltic Icelandite Icelandite	Transitional Hawaiite Transitional Mugearite Transitional Benmoreite	Hawaiite Mugearite Benmoreite
<b>Felsic</b>	Dacite Rhyolite	Transitional Trachyte Transitional Rhyolite	Trachyte Alkalic Rhyolite

As mentioned earlier the age of the rocks increases with the distance from the active rift zones. This given fact is once more recognizable on the geological map of Iceland (Figure 2). The fissure swarms and central volcanoes which belong to the rift zone extend from the southwest to the north of the country. They are surrounded by young Holocene sediments, displayed in grey, and pink pictured basaltic postglacial rocks which are younger than 10 ka. Late pleistocenic rocks are divided in subglacial hyaloclasts, shown in brown and interglacial basalts, which are symbolized by a dark grayish color. The center of Iceland is characterized by quaternary basalts with an age of 800ka to 3Ma, which are shown by a green color. The oldest rocks in Iceland, tertiary basalts, 3 to 17Ma old, are located in the east and northwest



and displayed in blue on the map. Acid intrusions are shown in orange, basic intrusions in dark green. Other acid rocks like rhyolite are pictured in yellow.

Due to their age the Icelandic rocks are generally divided into four main groups: The Tertiary Basalt Formation (17 to 3 Ma), the Grey Basalt Formation (3 to 0.01 Ma), the Moberg Formation (0.7 Ma to 10 ka) and the unconsolidated sediments and holocene lava flows (<10 ka) (Einarsson, 1994).

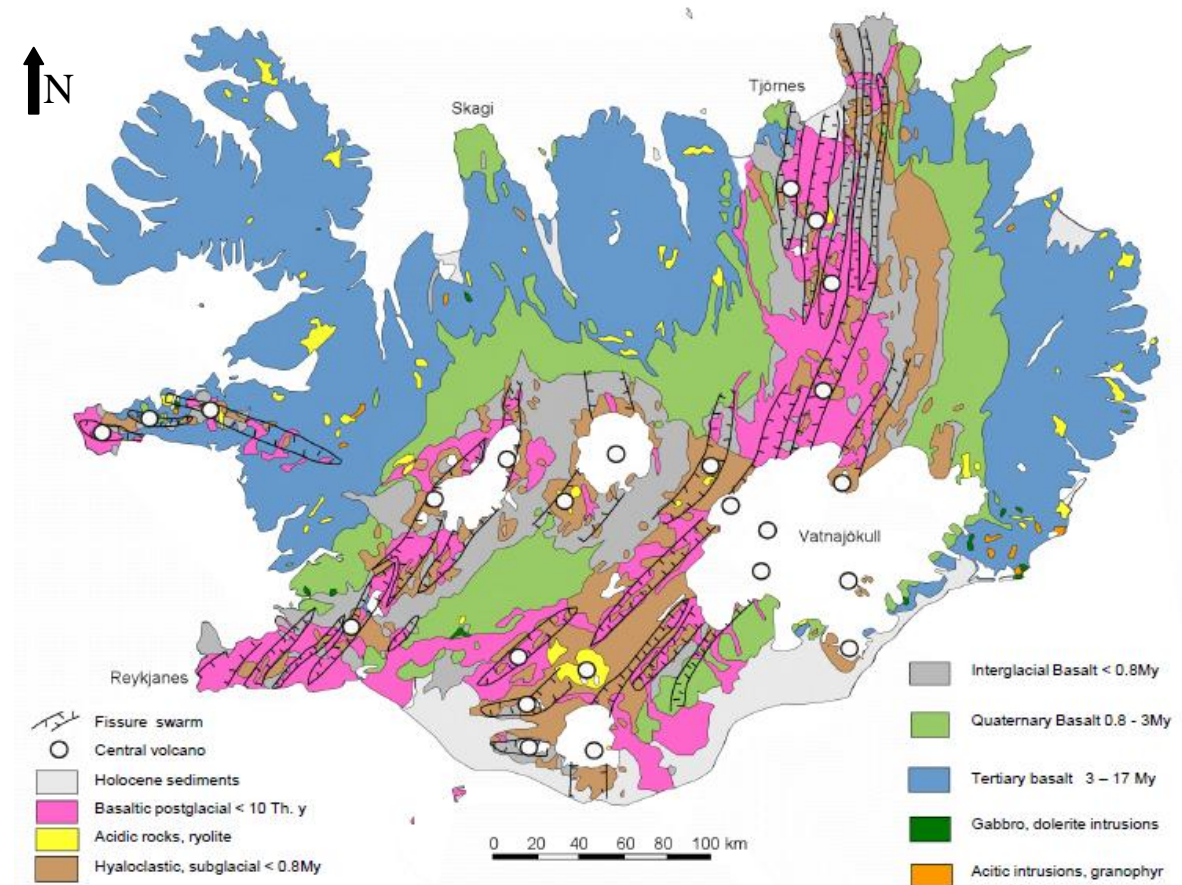


Figure 2: Geological map of Iceland (Adapted from Sædmundsson, 1979)

## 2.2 Conductive Heat Transfer in the Earth's Crust

Conduction is generated by thermal excitation of fixed adjacent atomic particles. It occurs in solids as well as static fluids (Bergmann and Schäfer, 2008). In highly ordered atomic lattices heat conduction is superior to thermal conduction in unordered lattices (Stelzer, 1971). The thermal conductivity varies due to differing material and surrounding temperature. Given that the heat is always transferred from a higher temperature to a lower temperature, the thermal conductivity  $\lambda$  is defined by a negative heat flux  $Q$  which passes through a surrounding temperature field perpendicular to an area  $A$  affected by an temperature gradient  $\frac{dT}{dx}$ . This physical property depends on surrounding temperature

$$\lambda = \frac{-Q}{(A \cdot dT)} dx. \quad \text{Eq. 2.1}$$

The conductive heat flow mainly existing in the earth's crust can be described by the thermal conductivity of the bedrock and the thermal gradient relative to the depth

$$Q = \frac{-\lambda}{dz} dT. \quad \text{Eq. 2.2}$$

With:

$$\begin{aligned} Q &= \text{heat flow} && \left[ \frac{W}{m^2} \right] \\ \lambda &= \text{thermal conductivity} && \left[ \frac{W}{(m \cdot K)} \right] \\ T &= \text{temperature} && [K] \\ z &= \text{depth} && [m] \end{aligned}$$

This equation, the Fourier's law, is only valid, if the temperature T is steady. The unsteady temperature distribution is represented by the diffusion equation, which includes the radiogenic heat production in the crust (Lowrie, 1997)

$$\lambda \cdot \nabla^2 T + R = \rho \cdot c \cdot \frac{dT}{dt}. \quad \text{Eq. 2.3}$$

With:

$$\begin{aligned} R &= \text{radiogenic heat production in the crust} && \left[ \frac{W}{m^3} \right] \\ \rho &= \text{density} && \left[ \frac{kg}{m^3} \right] \\ c &= \text{heat capacity} && \left[ \frac{J}{(kg \cdot ^\circ C)} \right] \end{aligned}$$

The thermal diffusivity, which describes the temporal variation of the temperature's local distribution caused by conduction, is indirectly shown in equation 2.3. It is the quotient of thermal conductivity to density and heat capacity of a material. Its unit is  $\left[ \frac{m^2}{s} \right]$ .

The key parameters of conductive heat flow are the thermal conductivity  $\lambda$  and diffusivity  $\kappa$  of the bedrock. Given that the rocks are porous and filled with water, not only the properties of the rock matrix but also the porosity and the characteristics of the water are important (Björnsson, 2010)

$$\lambda_{in situ} = \lambda_{rock}^{1-\phi} \cdot \lambda_{water}^{\phi}. \quad \text{Eq. 2.4}$$

With:

$$\phi = \text{porosity} \quad [-]$$

Furthermore, the thermal conductivity and diffusivity of rocks or soil depend on the mineral composition and texture. In dense rock the physical parameters are mainly influenced by the quartz content. The density, grain size, water or air content and mineral composition of the water have an impact on thermal conductivity and diffusivity (Sass, 2007). A tendency of thermal conductivities for several rock types is given in figure 3.

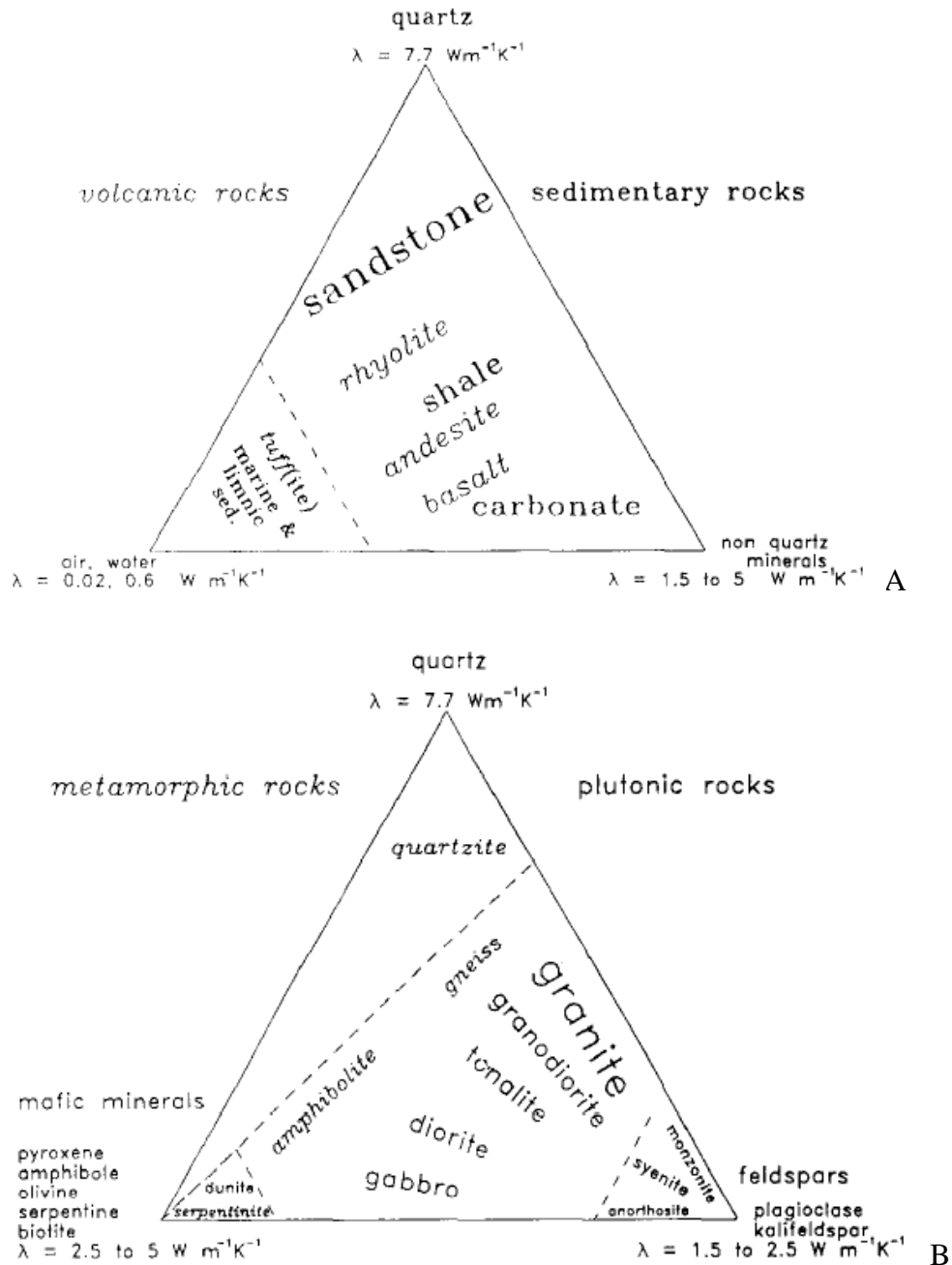


Figure 3: Thermal conductivity of rocks based on composing minerals and water or air content. A) Sedimentary and volcanic rocks. B) Metamorphic and plutonic rocks. Plutonic and sedimentary rocks are not italicized. Metamorphic and volcanic rocks are in italics. (Clauser and Huenges, 1995)

## 2.3 Optical Scanning Method

The optical scanning technique is a contactless method to determine the thermal conductivity and diffusivity of solids. The algorithm to calculate these parameters was derived by Popov et al. (1983) based on the spot welding technique according to Rykalin (1952). Under the assumption that a semi-infinitely sample is irradiated by a mobile point heat source, this sample is heated to a temperature difference  $\Delta T$  after a time  $t$ . The point source moves with a

velocity  $v$  along the  $x$ -axis in a three dimensional coordinate system with the axes  $x$ ,  $y$  and  $z$  as displayed in figure 4. Considered the point  $(x,y,z)$ ,  $R$  is the distance of the point  $(x,y,z)$  to the origin of the system and is equal to  $R = \sqrt{x^2 + y^2 + z^2}$ .

The effected temperature difference in point  $(x,y,z)$  is:

$$\Delta T(x, y, z) = \frac{2 \cdot q}{c \cdot \rho \cdot (4\pi\kappa)^{3/2}} \cdot e^{\left(\frac{-v \cdot x}{2\kappa}\right)} \cdot \int_0^t \frac{1}{t^{3/2}} \cdot e^{\left(\frac{-v^2 t}{4\kappa} - \frac{\kappa^2}{4\kappa \cdot t}\right)} dt. \quad \text{Eq. 2.5}$$

With:

$q$	=	by heat source applied heat amount	$[Ws]$
$c$	=	specific heat capacity of the sample	$\left[\frac{J}{(kg \cdot K)}\right]$
$\rho$	=	density of the sample	$\left[\frac{kg}{m^3}\right]$
$\kappa$	=	thermal diffusivity of the sample	$\left[\frac{m^2}{s}\right]$
$\vec{v}$	=	velocity of the point heat source	$\left[\frac{m}{s}\right]$
$x$	=	$x$ -coordinate of the point $(x,y,z)$	$[m]$
$y$	=	$y$ -coordinate of the point $(x,y,z)$	$[m]$
$z$	=	$z$ -coordinate of the point $(x,y,z)$	$[m]$
$t$	=	time after switching-on the heat source	$[s]$
$R$	=	distance of point $(x,y,z)$ to the origin of the coordinate system	$[m]$
$T$	=	temperature	$[K]$

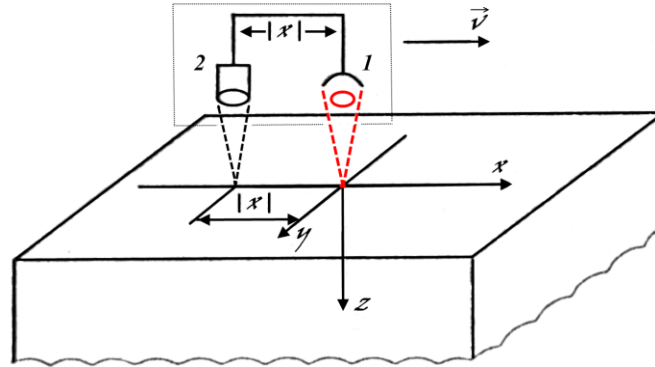


Figure 4: Sketch of the measuring unit's position related to the surface of the sample.

1) infrared emitter, 2) temperature sensor (Schmidt, 2009)

After a certain time the sample is cooled down to a steady state and the temperature difference in point  $(x,y,z)$  equals:

$$\Delta T(x, y, z) = \frac{q}{2\pi \cdot \lambda \cdot R} \cdot e^{\left(\frac{-v \cdot x}{2\kappa} - \frac{v \cdot R}{2\kappa}\right)}. \quad \text{Eq.2.6}$$

With:

$\lambda$	=	thermal conductivity of the sample	$\left[\frac{W}{(m \cdot K)}\right]$
-----------	---	------------------------------------	--------------------------------------

Due to the movement of the heat source only along the x-axis, the assumption  $R = \sqrt{x^2} = |x|$  is valid. Therefore the temperature difference can be derived as following

$$\Delta T(x, 0, 0) = \frac{q}{2\pi \cdot \lambda \cdot |x|} \cdot e^{\left(\frac{-v \cdot x}{2\kappa} - \frac{v|x|}{2\kappa}\right)}. \quad \text{Eq. 2.7}$$

If  $x < 0$ , i.e. x is located behind the origin of the coordinate system, the temperature difference in point (x,0,0) is

$$T(x) = \frac{q}{2\pi \cdot \lambda \cdot |x|}. \quad \text{Eq. 2.8}$$

With a constant distance  $|x|$  to the origin the temperature difference in point (x,0,0) is only dependent on the thermal conductivity of the sample.

If the temperature is measured in a different point (x,y,0), the following temperature difference should be derived:

$$T(x, y, 0) = \frac{q}{2\pi \cdot \lambda \cdot \sqrt{x^2 + y^2}} \cdot e^{\left(\frac{-vx}{2 \cdot \kappa} - \frac{v \cdot \sqrt{x^2 + y^2}}{2\kappa}\right)}. \quad \text{Eq. 2.9}$$

The maximal temperature at a time  $\tau$  in point (x,y,0) can be calculated by assuming that  $x = -v \cdot \tau$ , differentiating with respect to time and deriving to zero (Popov et al., 1985). With a known velocity of the heat source  $v$ , the heat content of the infrared emitter  $q$  and the coordinates of the point (x,y,0) this equation can be solved for the thermal diffusivity of the sample

$$\kappa = \frac{(v\tau)^2 + y^2 - v\tau\sqrt{(v\tau)^2 + y^2}}{2\tau}. \quad \text{Eq. 2.10}$$

The equations 2.5 and 2.8 are only valid according to the assumptions of an optimal point heat source and neglecting convective heat transfer from the sample surface to the surrounding.

## 2.4 Statistics

The method of a statistical analysis is explained on the following pages based on the lecture script “Statistik für Geowissenschaftler“ (statistics for geoscientists) by Weinbruch in 2003.

### 2.4.1 Descriptive Statistics

The first step in a statistical analysis is to establish the characteristics of the feature. A qualitative feature like mineralogy or lithology differs in the type. Quantitative features vary in size like concentration or age. The feature can be discrete, which means there are only a finite number of parameter values. On the other hand a continuous character assumes any value. The second step is to determine the scale of the character. A nominal scale is not sorted and the values are not comparable. In an ordinal scale the values are classified by their intensity, but the distance between the values is not interpretable. The third type of scale is the metric scale. In this scale the data is organized in an order and the distance between the pairs of values is interpretable. This is called order of rank. Furthermore, it is necessary to define the number of meaningful digits for the feature.

In a statistical analysis a character is studied  $n$  times with  $k$  specifications. The direct results belong to the original list. The frequency of values is distinguished in absolute and relative frequency and absolute and relative cumulative frequency and the data is classified by the different frequencies. The frequencies of a data set can be displayed by histograms, characterized by their number of bins and widths, or pie charts.

The measures of location describe the central tendency of a data set. One parameter is the arithmetical mean  $\bar{x}$ , which is the number for which the sum of the cubed deviation is minimal

$$\bar{x} = \frac{1}{n} \sum_{i=1}^n x_i. \quad \text{Eq. 2.11}$$

The median of a data set  $\tilde{x}$  characterizes the middle value in an ordered data set. If  $n$  is even:

$$\tilde{x} = \frac{x_{\frac{n+1}{2}} + x_{\frac{n+2}{2}}}{2}. \quad \text{Eq. 2.12}$$

If  $n$  is odd, than the following equation is valid

$$\tilde{x} = \frac{1}{2} \left( x_{\frac{n}{2}} + x_{\frac{n+1}{2}} \right). \quad \text{Eq. 2.13}$$

The most frequent value of a data set is called mode  $x_{mod}$ .

There are three quartiles, which constitute a data set. In an ordered series the value, which separates the first quarter from the second quarter, is called the lower quartile  $Q_1$ . The second quartile  $Q_2$  is the median, while the third or upper quartile  $Q_3$  cuts of the third from the fourth quarter of the data set.

A further location parameter is the geometric mean  $\bar{x}_G$ . It is never larger than the arithmetical mean  $\bar{x}$

$$\bar{x}_G = \sqrt[n]{x_1 \cdot x_2 \cdot \dots \cdot x_n}. \quad \text{with } x_i > 0 \quad \text{Eq. 2.14}$$

The harmonic mean  $\bar{x}_H$  is defined as the reciprocal of the arithmetical mean of the reciprocal of the data values

$$\bar{x}_H = \frac{n}{\sum_{i=1}^n \frac{1}{x_i}}. \quad \text{with } x_i \neq 0 \quad \text{Eq. 2.15}$$

The measures of statistical dispersion assess the spread of the data set. The variance  $s^2$  is very dependent on outliers

$$s^2 = \frac{\sum_{i=1}^n (x_i - \bar{x})^2}{n-1}. \quad \text{Eq. 2.16}$$

The standard deviation  $s$  is defined as the square root of the variance and is likewise dependent on outliers. It has the same dimension as the observation values

$$s = \sqrt{\frac{\sum_{i=1}^n (x_i - \bar{x})^2}{n-1}}. \quad \text{Eq. 2.17}$$

The dimensionless coefficient of variation  $V$  is a relative spread parameter

$$V = \frac{s}{\bar{x}}. \quad \text{Eq. 2.18}$$

The range  $R$  arises from the subtraction of the maximal from the minimal value of the data set

$$R = x_{max} - x_{min} . \quad \text{Eq. 2.19}$$

The interquartile range IQR, however, is the difference of the upper to the lower quartile

$$IQR = Q_3 - Q_1 . \quad \text{Eq. 2.20}$$

Box plots are charts to represent the spread of a data set. Besides the maximum and minimum value of a series the three quartiles  $Q_1$ ,  $Q_2$  and  $Q_3$  are shown. A box plot is a good medium to visualize outliers of a data set.

The measure of shape of a data set is characterized by the following parameters. The skewness  $g_1$  describes in which direction and how intensely asymmetrical the data distribution is. In the case of  $g_1 = 0$ , the distribution is symmetrical. If  $g_1 < 0$ , then the distribution is negative or left-skewed. A positive skewness  $g_1 > 0$  describes a right-skewed distribution

$$g_1 = \frac{\left(\frac{1}{n} \sum_{i=1}^n (x_i - \bar{x})^3\right)}{\sqrt{\frac{1}{n} \left(\sum_{i=1}^n (x_i - \bar{x})^2\right)^3}} . \quad \text{Eq. 2.21}$$

The kurtosis  $g_2$  indicates whether the absolute maximum of the data values is larger, equal or lower compared to the according normal distribution

$$g_2 = \frac{\frac{1}{n} \sum_{i=1}^n (x_i - \bar{x})^4}{\left(\frac{1}{n} \sum_{i=1}^n (x_i - \bar{x})^2\right)^2} . \quad \text{Eq. 2.22}$$

## 2.4.2 Inductive Statistics

Data sets can be described by distributions. According to the law of large numbers many data sets can be described approximately by a Gaussian distribution. This continuous probability density distribution is only dependent on the arithmetical mean  $\mu$  and the standard deviation  $\sigma$ . The function is symmetrical, bell-shaped with a maximum at the arithmetical mean  $\mu$  and two points of inflection at  $\mu - \sigma$  and  $\mu + \sigma$ .

$$f(x) = \frac{1}{\sigma\sqrt{2\pi}} \cdot e^{-\frac{1}{2} \cdot \left(\frac{x-\mu}{\sigma}\right)^2} \text{ with } -\infty < x < \infty, -\infty < \mu < \infty \text{ and } \sigma > 0 \quad \text{Eq. 2.23}$$

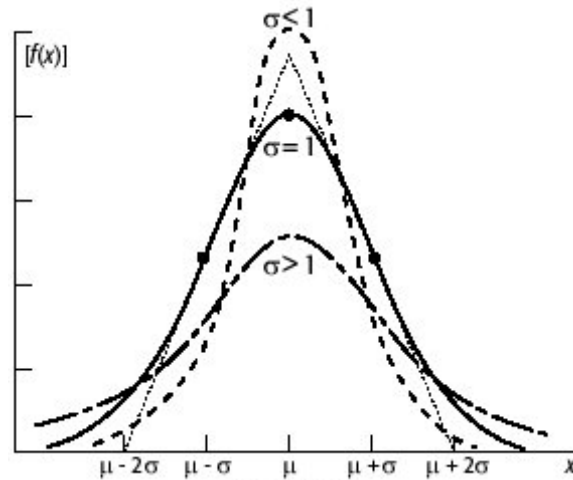


Figure 5: Gaussian distribution ([www.fe-lexikon.info/images/Gauss\\_Kurve.jpg](http://www.fe-lexikon.info/images/Gauss_Kurve.jpg), 2010)

A cumulative frequency of a data set can be approximated by a normal cumulative distribution. This distribution is the integral of the Gaussian function in the interval of  $[-\infty, x]$  (Abramowitz, 1972).

$$F(x; \mu, \sigma^2) = \frac{1}{2} \cdot \left[ 1 + \operatorname{erf} \left( \frac{x - \mu}{\sigma\sqrt{2}} \right) \right] \quad \text{with } \operatorname{erf}(x) = \frac{2}{\pi} \int_{-\infty}^x e^{-t^2} dt \quad \text{Eq. 2.24}$$

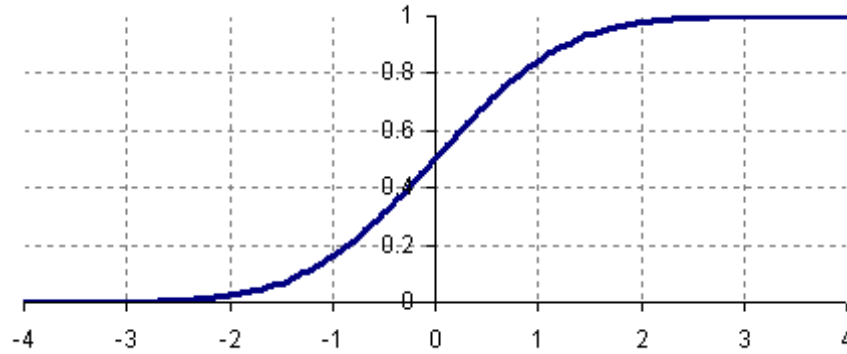


Figure 6: Cumulative distribution function of the Gaussian distribution  
([http://www.knowledgerush.com/kr/encyclopedia/Normal\\_distribution](http://www.knowledgerush.com/kr/encyclopedia/Normal_distribution), 2010)

### 2.4.3 Regression and Correlation

Analysis of regression and correlation of two independent features assess the coherence between them. One can distinguish between a causal and a stochastic interrelation. On the one hand causal relations can be derived with a function. On the other hand stochastic relations are dependent on errors of measurements and a natural variation of the observed feature.

An analysis of regression determines the relation of the variables X and Y. The asked question in this analysis is: Can Y be estimated from X?

Correlations aim for the determination of the existence of a stochastic relation between X and Y.

A linear regression assumes that the following relation exists

$$y = a_x + b_x \cdot x . \quad \text{Eq. 2.25}$$

The coefficient of correlation  $b_x$  can be derived from the variance of the variable X  $s_{x^2}$  and the covariance of X and Y  $s_{xy}$

$$b_x = \frac{s_{xy}}{s_{x^2}} . \quad \text{with } s_{xy} = \frac{1}{n-1} \sum_{i=1}^n (x_i - \bar{x})(y_i - \bar{y}) \quad \text{Eq. 2.26}$$

The axis intercept  $a_x$  can be determined by the arithmetical means of X,  $\bar{x}$ , and Y,  $\bar{y}$ , and the coefficient of correlation  $b_x$

$$a_x = \bar{y} - (b_x \cdot \bar{x}) . \quad \text{Eq. 2.27}$$

The Pearson product-moment coefficient of correlation  $r$  is a measure for the correlation. It ranges from -1 to 1. The closer  $r$  is to  $|1|$ , the larger is the linear correlation. If  $r = 0$ , then there is no linear correlation between X and Y (Plate, 1993)



$$r = \frac{s_{xy}}{s_x s_y}. \quad \text{Eq. 2.28}$$

A nonlinear regression bases e.g. on a logarithmic function

$$\log(y) = \log(a) + b \cdot \log(x). \quad \text{Eq. 2.29}$$

The parameter a and b be can be derived with the help of the geometric means  $\bar{x}_{G,x}$  and  $\bar{x}_{G,y}$

$$b = \frac{s_{\log x \log y}}{s_{\log x}^2} \quad \text{Eq. 2.30}$$

$$a = \frac{\bar{x}_{G,y}}{(\bar{x}_{G,x})^b}. \quad \text{Eq. 2.31}$$

## **3 METHODOLOGY**

### **3.1 Logistics**

#### **3.1.1 Description of Location**

The outcrop, where all basaltic samples were taken, is located in Reykjavik, Iceland. Named after the hill in the capital of Iceland, the location is called Öskjuhlið (Figure 7). The outcrop is a ruined military defense. The decision to use this former defense for sample collection was made for two reasons. First of all, the outcrop contains an individual lava flow from the bottom to the top layer. For this reason samples with a similar mineralogy, but a different porosity and permeability can be collected. Furthermore it is possible to study the homogeneity of geothermal parameters in the flow. The second reason for choosing this outcrop is the fact that a large collection of samples was already taken and analyzed by Orkustofnun between 1997 and 2002. In the 1990's, Orkustofnun, the national energy authority of Iceland, analyzed 509 basaltic samples all over Iceland and 83 samples especially in Öskjuhlið with regard to petrology, mineralogy, chemistry, permeability, porosity, grain density, hydrothermal alteration, acoustic velocity, thermal conductivity and resistivity [Sigurðsson et al, 2000]. The properties already determined by Orkustofnun made it possible to focus on a statistical analysis of geothermal parameter without additional analyses of other geological and mineralogical characteristics in this thesis.

The outcrop extends from NE to SW with a length of 36 m, a height of 4 m and a width of 22 m and consists of the six profiles A-A', B-B', C-C', D-D', E-E' and F-F' (Figure 8 and 9). The first profile A-A' is divided into the four subparts a, b, c and d. All profiles consist of upper and lower sampling locations, which are numerated from 1 to 20. The three upper sampling locations 2, 4 and 15 are substituted by the after Orkustofnun named locations Group I, II and III. Photos of the several profiles are attached in the appendix A.



Figure 7: Overview photo of the location of the Öskjuhlíð outcrop ([www.maps.google.de](http://www.maps.google.de))

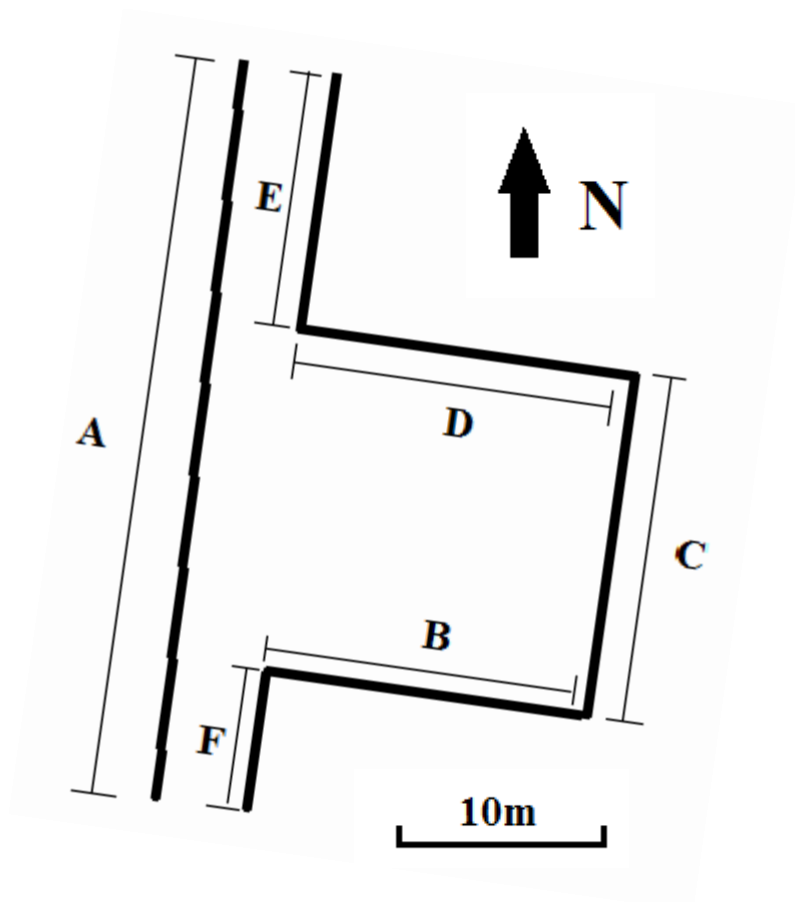


Figure 8: Illustration of the profiles in the Öskjuhlíð outcrop

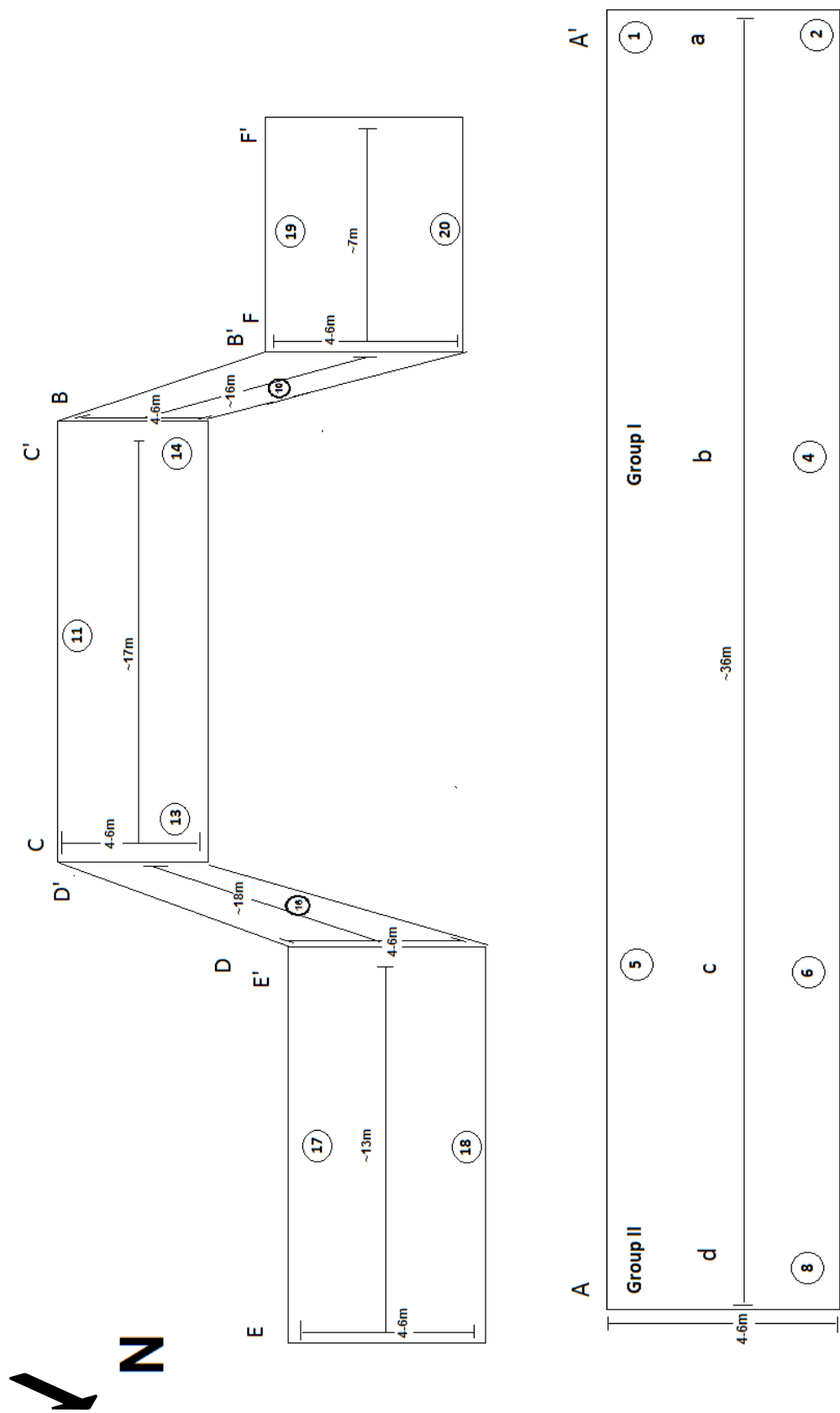


Figure 9: Sketch of the sampling locations in the several profiles at the Öskjuhlíð outcrop

### 3.1.2 Description of Samples

The first 5 samples were taken on September 10, 2010 and were cut into 33 smaller cuboids and then transported to Darmstadt, Germany. The dimensions of the cuboids are 5 cm in height and width and a length of 10 to 20 cm which are samples taken in the two different locations 18 and Group III. The collection of hand probes, which were taken on October 2, 2010, contains 150 samples. They are divided into 15 different groups each including ten samples. All groups represent a location in the outcrop. The hand probes have been analyzed in Akureyri, Iceland. Additionally 10 samples from Orkustofnun, which were taken in 1997 by Hjalti Franzson and Ásgrímur Guðmundsson and in 2002 by Julia Frolova, are measured in this thesis. The earlier collected samples originate from Group II and III, while the samples taken by Julia Frolova belong to Group I. These samples are cores with a diameter of 2.5 cm and a maximal length of 10 cm and have been measured in Darmstadt, Germany. Exemplary photos of the samples are attached in the appendix B.

### 3.1.3 Analysis Program

The determination of the 150 hand probes took place in the laboratory of the University of Akureyri in Iceland from October 14 to 27, 2010. In this period, the thermal conductivity and diffusivity of the basaltic rock was analyzed with the LMC tool. 70 samples of the sample's entirety were measured with a preparation of spraying the analyzed surface with the black polish "Acrylic varnish – deep black RAL9005 – matt". The samples were stored in the laboratory to dry and heated up to room temperature. In order to minimize the falsification of the results, each measurement for one sample has been repeated five times. All 150 hand probes were determined by the LMC device after cutting and varnishing them. After the preparation of the samples, they were stored in the laboratory for the same reason as the uncut samples. Due to a lack of time each of the measurements for the cut samples has been repeated three times in order to maximize the probability of veritable results. All measurements with the LMC were done with a standard of  $2.75 \text{ W}/(\text{m}\cdot\text{K})$  and  $1.35 \text{ mm}^2/\text{s}$ . The heating power of all measurements was set up to 15 % of the maximal electrical performance of the infrared emitter, in which thermal losses and transformation of energy to light are not considered. This equals approximately  $22.5 \text{ W}_e$ .

The samples transported to Germany were analyzed with the LMC instrument and the TCS device. The measurements proceeded from November 5 to 16, 2010. After varnishing with black polish and drying at room temperature, the samples have been analyzed three times with each instrument. All thermal conductivity determinations by the TCS instrument were performed with a standard of  $1.35 \text{ W}/(\text{m}\cdot\text{K})$  and  $0.85 \text{ mm}^2/\text{s}$ . The samples were heated with an intensity of 28 % of the total TCS heating power, which equals approximately  $15.8 \text{ W}_{th}$ . Standards with thermal conductivities of  $0.717$  and  $1.35 \text{ W}/(\text{m}\cdot\text{K})$  as well as thermal diffusivities of  $0.39$  and  $0.85 \text{ mm}^2/\text{s}$  were used for the analysis of the thermal diffusivity based on the TCS device. The infrared emitter of the TCS heated the samples with 23% of the TCS total heating power, which equals approximately  $11.9 \text{ W}_{th}$ , to identify the thermal diffusivity.

## 3.2 Determination of Geothermal Parameters

### 3.2.1 Lambda Measuring Center (LMC)

The LMC device (figure 10), developed by Engineering Office for Environmental and Geotechnical Technology Hamm & Theusner GbR, Erzhausen, Germany, is an instrument measuring the thermal conductivity and diffusivity of solids based on the optical scanning method with a fixed point heat source, a golden evaporated Osram lamp with maximal 150 W<sub>e</sub> performance. Therefore the process is called point measurement. The instrument's dimensions are 0.67 m in length, 0.3 m in width and 0.33 m in height. The weight is 20 kg. The tool is implemented in an aluminum suitcase. For this reason the LMC is portable and allows measurements in the field (Hamm and Theusner, 2010). Pursuant to the operating manual the measured sample should not be smaller than 20·20·10 mm. The measuring range spans from 0.5 to 5.0 W/(m·K) and 0.15 to 3.0 mm<sup>2</sup>/s. The instrument detects the temperature from 4 to 48°C. The samples have to be prepared to goal veridical results by spraying a planar surface with “Acrylic varnish – deep black RAL9005 – matt” so that a similar emissivity for samples and standards is guaranteed. To calculate the geothermal parameters standards are necessary. It is possible to use one or two standards for the determination which are provided with the tool. In the case of utilizing two standards it is not necessary that they have the same properties.



Figure 10: Photo of the LMC instrument

With the aid of standards of known thermal conductivities and diffusivities, the parameters for the measured samples can be calculated. The relation between standard and sample is:

$$\lambda_{sample} = \lambda_{standard} \cdot \frac{\Delta T_{standard}}{\Delta T_{sample}}. \quad \text{Eq. 3.1}$$

The process of measuring the thermal conductivity  $\lambda$  is divided into four parts. The instrument determines the temperature drift at the surface of the sample to ensure steady temperature conditions. The unaffected temperature of the sample surface is detected as the initial temperature before the heating process. Then the surface is heated for 2 seconds with a 150 W infrared emitter. The temperature is quantified during the heating and cooling process of the sample's surface (Hamm and Theusner, 2010). The temperature difference  $\Delta T$  is detected in the third second of the analyzing process which is illustrated by the pink vertical line of figure 11. The analyzing range is displayed by the black dashed vertical lines.

To determine the thermal diffusivity  $\kappa$  the sample is heated for a second time, but now the temperature is measured in a distance  $x$  from the heated spot. After a time  $\tau$  the heating process leads to a temperature maximum in the detecting point. These parameters help to calculate the thermal diffusivity

$$\tau = \frac{x^2}{6\kappa}. \quad \text{Eq. 3.2}$$

As for the thermal conductivity, an analogous relation of time and thermal diffusivity  $\kappa$  is valid

$$\kappa_{sample} = \kappa_{standard} \cdot \frac{\tau_{standard}}{\tau_{sample}}. \quad \text{Eq. 3.3}$$

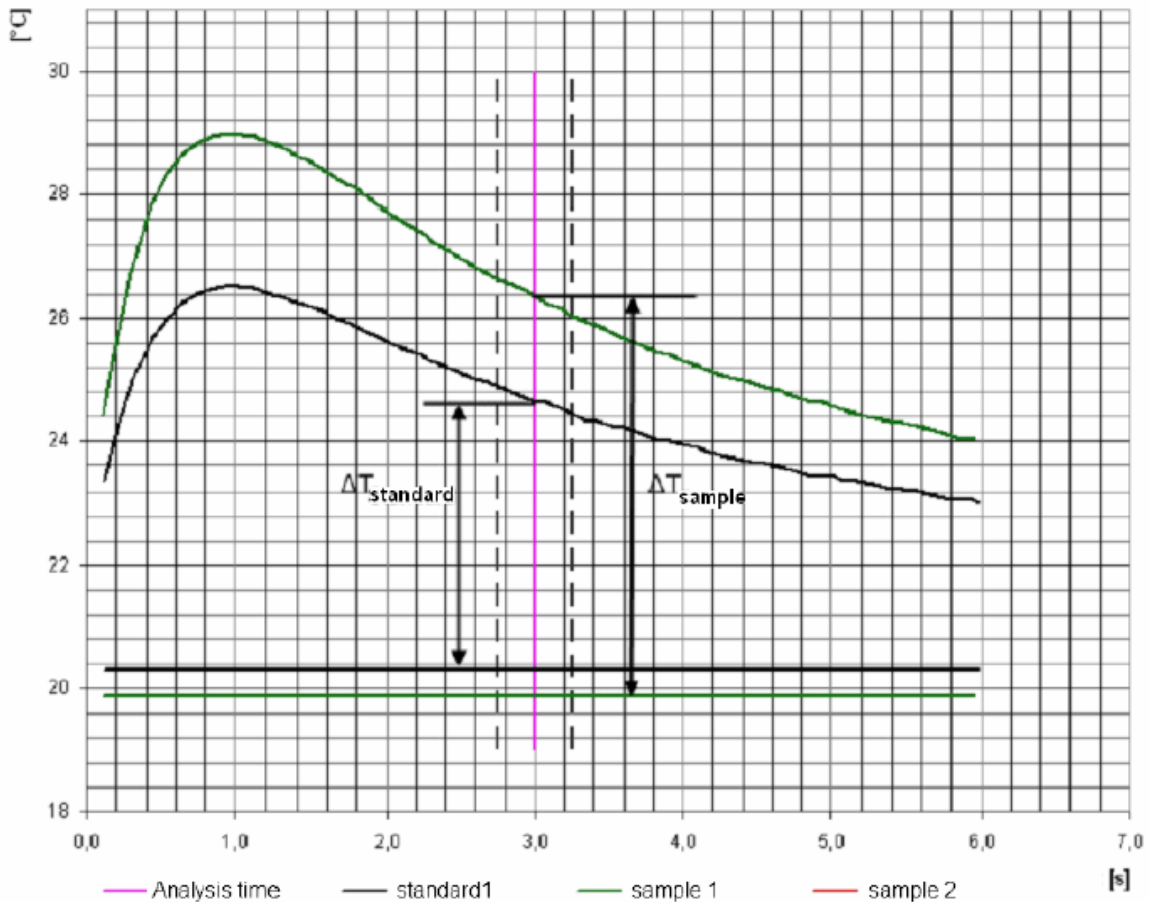


Figure 11: Temporal function of temperature at the sample's surface during a thermal conductivity measurement with the LMC instrument (Hamm and Theusner, 2010)



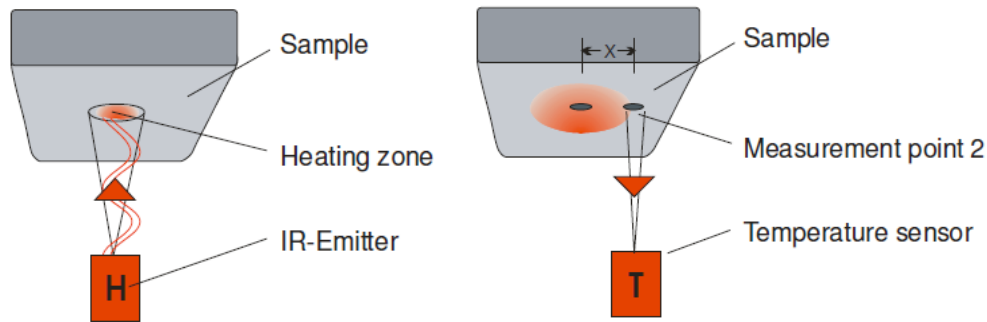


Figure 12: Sketch of the measurement process for the determination of thermal diffusivity by the LMC device (Hamm and Theusner, 2010)

Considering the expected thermal conductivity and diffusivity, one is able to adjust the heating power and heating time of the device. The manual recommends how to arrange the various parameters.

Table 2: Recommended instrument adjustments related to certain thermal conductivities (Hamm and Theusner, 2010)

Temperature differences for bodies with $\lambda$ about 1 W/(m·K):			
Heating period	Heating power	Temperature difference	Samples
2s	8%	Ca. 2K	$\lambda < 1$ W/(m·K)
2s	15%	Ca. 5K	$\lambda$ about 1 W/(m·K)
2s	20%	Ca. 8K	$\lambda > 1$ W/(m·K)
Temperature differences for bodies with $\lambda$ about 3 W/(m·K):			
Heating period	Heating power	Temperature difference	Samples
2s	15%	Ca. 2K	$\lambda < 3$ W/(m·K)
2s	30%	Ca. 5K	$\lambda$ about 3 W/(m·K)
2s	50%	Ca. 8K	$\lambda > 3$ W/(m·K)

### 3.2.2 Thermal Conductivity Scanning (TCS)

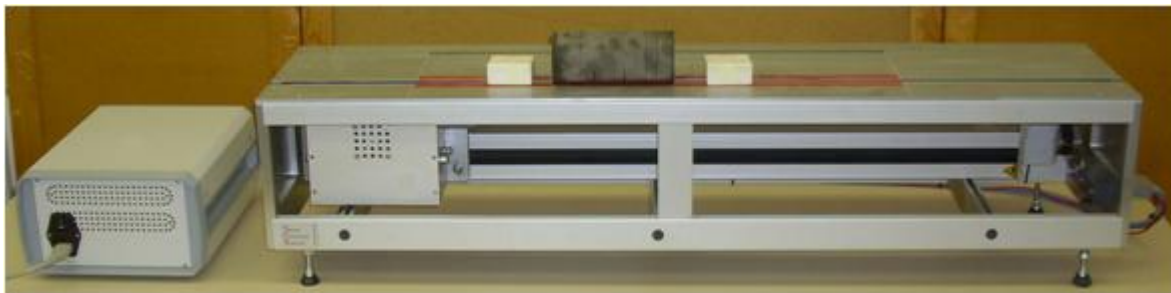


Figure 13: Photo of the TCS instrument (Adapted from Schmidt, 2009)

The TCS instrument quantifies the thermal conductivity and diffusivity of solid samples. The measuring process is based on the optical scanning method derived by Popov in 1983. The 26



kg weighing tool has a length of 1.16 m, a height of 0.21 m and a width of 0.29 m. It is developed by Lippmann & Rauen GbR, Schaufling, Germany, for laboratory experiments. Other than the LMC device the heat source and temperature sensors are not fixed. The unit of the cold temperature sensor, the infrared emitter and two additional hot temperature sensors are moving with a velocity of 5 mm/s along a rail. The standards and samples are positioned above this rail.

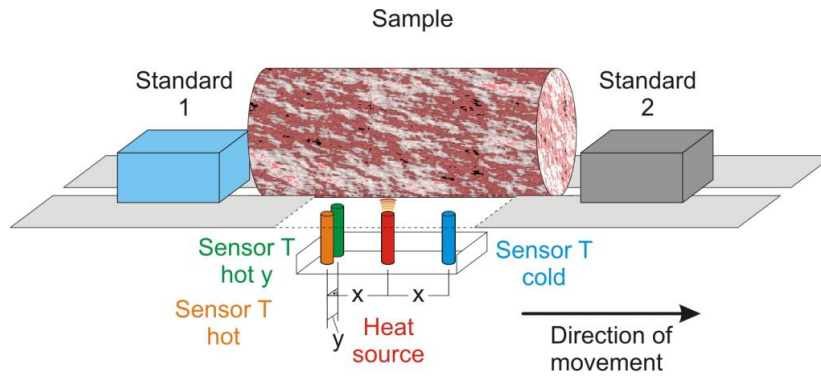


Figure 14: Technical Configuration of the TCS device ([www.geo.tu-darmstadt.de/fg/angeotherm/geotherm\\_forschung/TCS.de.jsp](http://www.geo.tu-darmstadt.de/fg/angeotherm/geotherm_forschung/TCS.de.jsp), 2010)

The different steps of the measuring process are combined to one. The cold sensor of the probe detects the temperature prior to the heating process, then the sample is heated by the emitter and ultimately the temperature of the heated sample is measured. Due to the distance of 5 cm between the heat source and the temperature sensors and the velocity of the probe, the sample is measured ten seconds after initiating the heating process. With the determined temperature difference  $\Delta T$  and the known thermal conductivity of the standard, the thermal conductivity of the sample is calculable by equation 3.1.

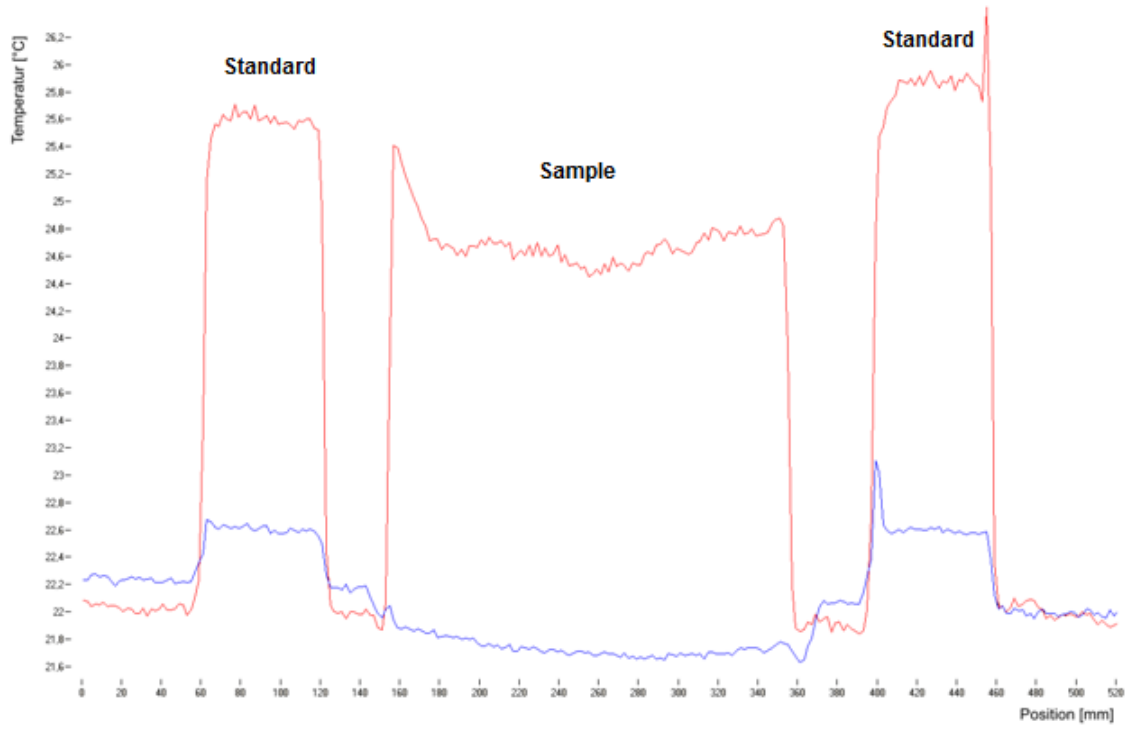


Figure 15: Function of the temperature at the surface of the sample before and after the heating process by the TCS tool. Blue function: Temperature measured prior to heating process, Red function: Temperature measured after heating process (Adapted from Schmidt, 2010)

The second hot temperature sensor y is used to quantify the thermal diffusivity of the sample. It detects the maximal temperature after a time  $\tau$ . The physical parameter is computable by equation 2.10.

In order to obtain valid results some proposed conditions of the manufacturer have to be fulfilled. The measured surface of the sample has to be treated with black polish to achieve the same emissivity as the standards. The measurement has to be supplemented with two standards. On basis of the deviation of the mean temperature difference of both standards, the temperature drift can be compensated. In the case of a conductivity determination both standards have equal properties, but the thermal conductivity of the standard always has to be larger than the thermal conductivity of the sample. For a thermal diffusivity measurement, the first standards' diffusivity is supposed to be lower and the second standards' diffusivity should be larger than the one of the sample. Furthermore, the condition  $\frac{\kappa_{standard\ 2}}{\kappa_{standard\ 1}} < 3$  has to be satisfied.

## 4 GEOLOGICAL INTERPRETATION

### 4.1 Lithologic Interpretation

The Öskjuhlíð outcrop is located in Reykjavík, Iceland, characterized by the coordinates  $N64^{\circ}07'840''$  and  $W012^{\circ}55'475''$  at 48 m above the sea level. The rocks that are exposed belong to a compound olivine tholeiite lava flow. This lava flow originates from the volcano Lykjafell, which is located 20 km southeast of Reykjavík City. Both features are shown in figure 17. The eruption of the flow happened 200 to 300 thousand years ago in the Middle Pleistocene. The interglacial lava flow eroded slightly afterwards (Franzson et al., 2001). According to Einarsson in 1994 the lava flow belongs to the Grey Basalt Formation, called the Reykjavík grágrýti. In a simplified geological map of Reykjavík it is noticeable that this grey basalt builds the base rock of the Icelandic capital. In some places it is covered by younger sediments or lava flows.

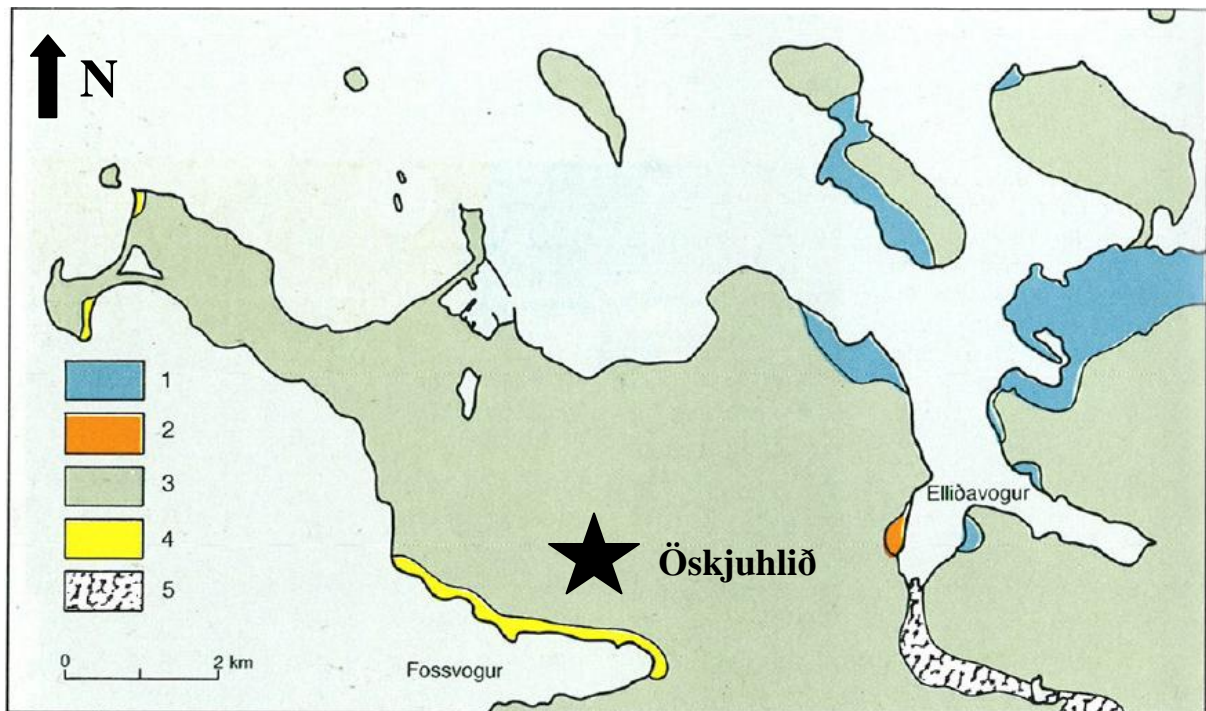


Figure 16: Sketch of the geological map of Reykjavík. 1) early quaternary formations, 2) Elliðavogur sedimentary beds, 3) Reykjavík interglacial grey basalt, 4) Fossvogur sedimentary beds, 5) Elliðárhraun lava (Einarsson, 1994)



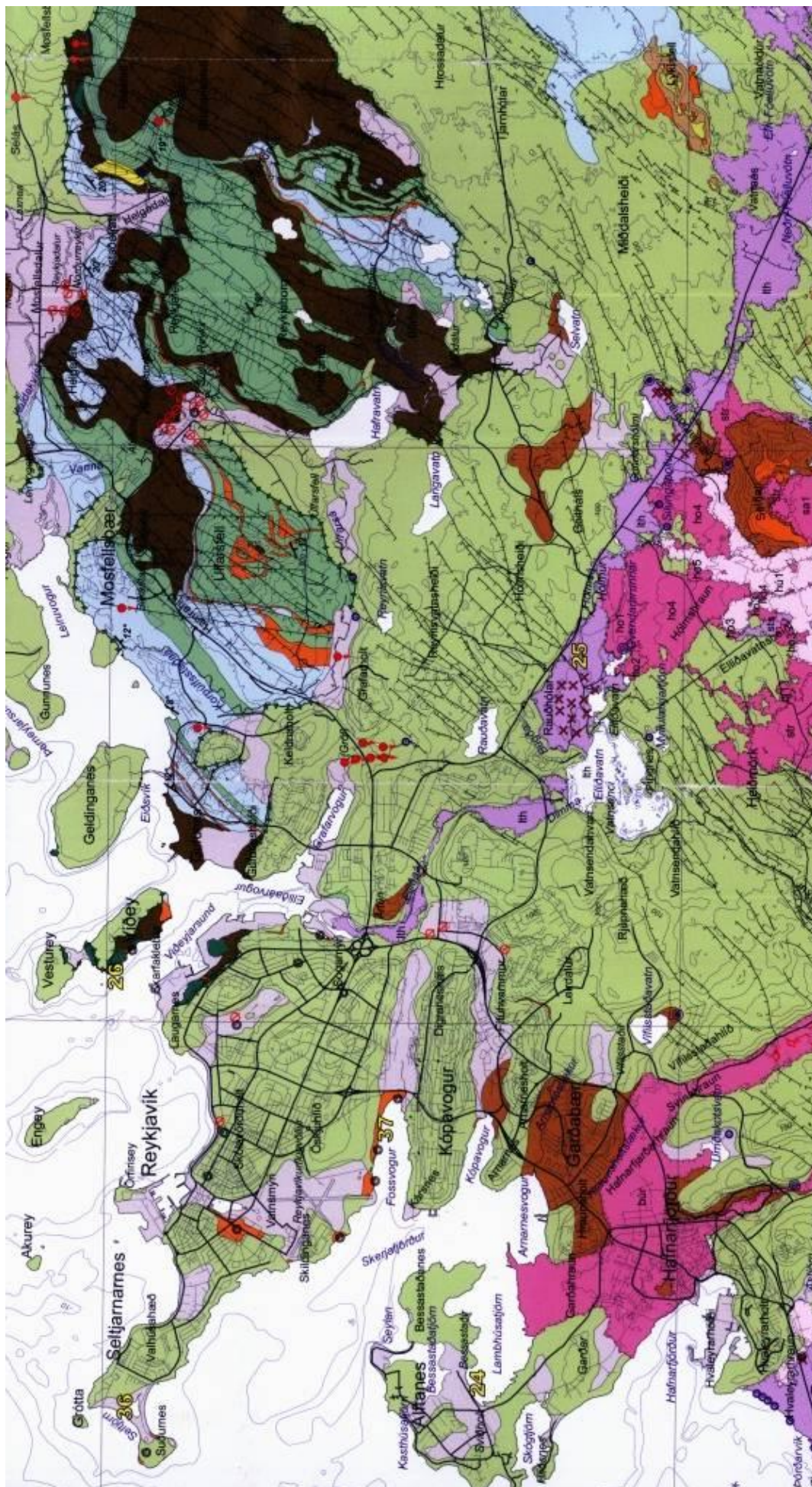




Figure 17: Geological map of southwest Iceland (Adapted from Jóhannesson et al., 2010)



## Skýringar / Legends




### Hraun / Postglacial lavas

-  Söguleg hraun frá 9.-13. öld / Historical lavas from 9th-13th century
-  Hraun frá 8.-9. öld / Lavas from 8th-9th century
-  Forsöguleg hraun 1900-2400 ára / Prehistoric lavas 1900-2400 years old
-  Forsöguleg hraun > 2400 ára / Prehistoric lavas > 2400 years old
-  Pikrithraun / Picrite basalt lavas
-  Dyngja < 7000 ára / Lava shield < 7000 years old
-  Dyngja > 7000 ára / Lava shield > 7000 years old

### Berggrunnur / Bedrock

-  Móberg frá seinni hluta síðasta jökulskeiðs / Subglacial hyaloclastite from late Weischel
-  Móberg frá fyrri hluta síðasta jökulskeiðs / Subglacial hyaloclastite from early Weischel
-  Móberg frá eldri jökulskeiðum Bruhnes / Subglacial Hyaloclastite from early Bruhnes
-  Móberg eldra en Bruhnes / Hyaloclastite older than Bruhnes
-  Grágrýtishettur á móbergi / Compound lava on hyaloclastite
-  Grágrýtisflákar / Compound lava
-  Þóleiit basalt / Tholeiite lavas
-  Ólívínþóleiit í staffa / Olivine tholeiite
-  Andesit / Andesite
-  Liparít / Rhyolite
-  Innskot / Intrusion
-  Setberg / Sedimentary horizons

### Laus jarðlög / Superficial deposits

-  Berghlaup / Rock slide
-  Óskilgreind sethula / Undefined surface deposits
-  Gjóska / Tephra

### Tákn / Symbols

-  Gigar / Postglacial craters
-  Gigaröð / Crater row
-  Gervigigur / Rootless cones
-  a. Dyngjugigur frá isöld / Pleistocene crater  
b. Dyngjugigur frá nútíma / Postglacial crater
-  Hrauntröð / Lava channel
-  Hellir / Cave
-  Fornskeljar / Fossil shells
-  Gufu- eða leirhver / Solfatara, fumarole
-  a. Laug / Warm spring  
b. Horfin laug / Dried up hot spring
-  Ölkelda / Mineral spring
-  Lind 10-100 l/s / Spring 10-100 l/s
-  Lind >100 l/s / Spring >100 l/s
-  Lindasvæði >100 l/s / Spring area >100 l/s
-  Halli jarðlaga / Dip and strata
-  Öskjurími / Caldera rim
-  Framhlaupsskál / Landslide scar
-  Hraunjaðar / Lava margin
-  Óviss hraunjaðar / Inferred lava margin
-  Misgengi / Fault
-  Gjá / Open fissure
-  Mörk milli tertier og kvarter 2,58 M ár / Tertiary and Quaternary boundary 2.58 Ma
-  Mislægi, eyða ~ 1/2 - 2 milljónir ára / Unconformity, hiatus ~ 1/2 - 2 Ma years

Figure 18: Legend of the geological map of southwest Iceland (Adapted from Jóhannesson et al., 2010)

## 4.2 Petrologic and Physical Interpretation

The basalt in situ has a thickness of four to six meters. It can be separated into two layers. This distribution is caused by different types of porosity, not petrology. The cooling and degassing process of the freshly erupted lava indicates different matrixes. At the surface of the lava, where it cools fast, a short crystallization process leads to fine grained minerals and large pores, with diameter more than 1 cm caused by gas bubbles in the lava. Due to the fast cooling process the lava chilled partly to glass around the vesicles. The degassing process takes place in between plagioclase crystals and impedes the pyroxene crystallization. This highly vesicular and rigid layer is shown in figure 19 in red. The layer it is called A. The second layer B, pictured in yellow, is characterized by a medium to coarse grained, dense matrix. The size of the crystals is caused by a slower cooling process which indicates a sub-ophitic texture. Secondly the inhibited late degasification of the lava leads to an intercrystalline porosity with diameters below 1 mm. The long time of cooling and degassing leads to relatively high fluidity, which generally decreases with the progression of the process. The upwards migrating gases are trapped at the zonal boundary, which is extending downwards. Microcracks are detected by analyses of thin sections within crystal grains and boundaries as well as fractures, which are cutting through the matrix of the rock. The cracks are caused by thermal contraction and tectonic movements (Franzson et al., 2001).

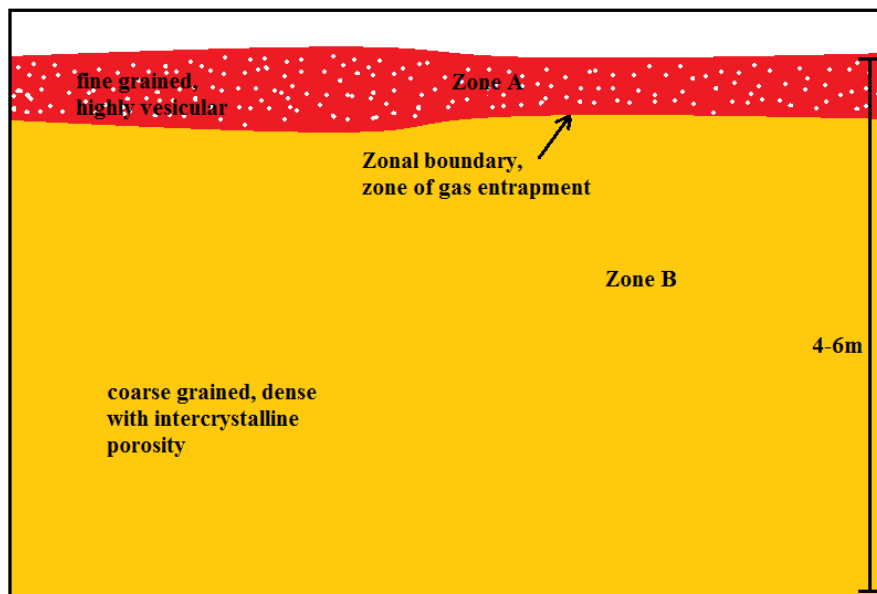


Figure 19: Sketch of the zonation in the Öskjuhlíð lava flow

The national energy authority of Iceland Orkustofnun analyzed the rocks with respect to permeability, porosity, sonic velocity and grain density. The analyses support the model of a twice-layered lava flow.

Table 3: Observed properties of two zones A and B in the Öskjuhlíð (Franzson et al., 2001)

Property	Zone A	Zone B
Permeability [mD]	<1	>1
Sonic velocity [m/s]	>3000	<3000
Grain density [g/cm <sup>3</sup> ]	<3.0595	>3.0595
Porosity [%]	>13.5	<13.5

The vesicular rocks of group A have a high variety in porosity, but compared to the dense basalts of group B, they are less permeable. This uncommon relationship is caused by an insulation of the large vesicles. The pores in the fine grained, vesicular basalts are not connected to each other and consequently the effective porosity is lower in zone A than in zone B dominated by intercrystalline pores.

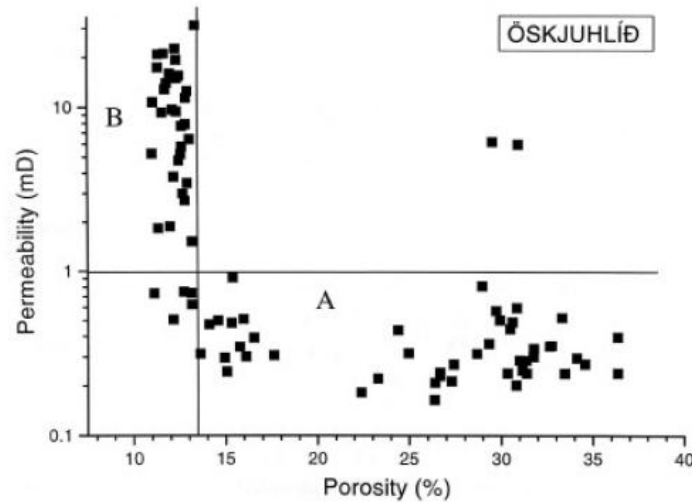


Figure 20: Relation between porosity and permeability in the Öskjuhlíð lava flow (Franzson et al., 2001)

This statement is proved by comparing the determined gas porosity to the type of porosity. The pores are categorized by thin section analyses. It appears that the upper layer A is characterized by isolated vesicular pores, while the lower zone B mainly consists of intercrystalline pores.

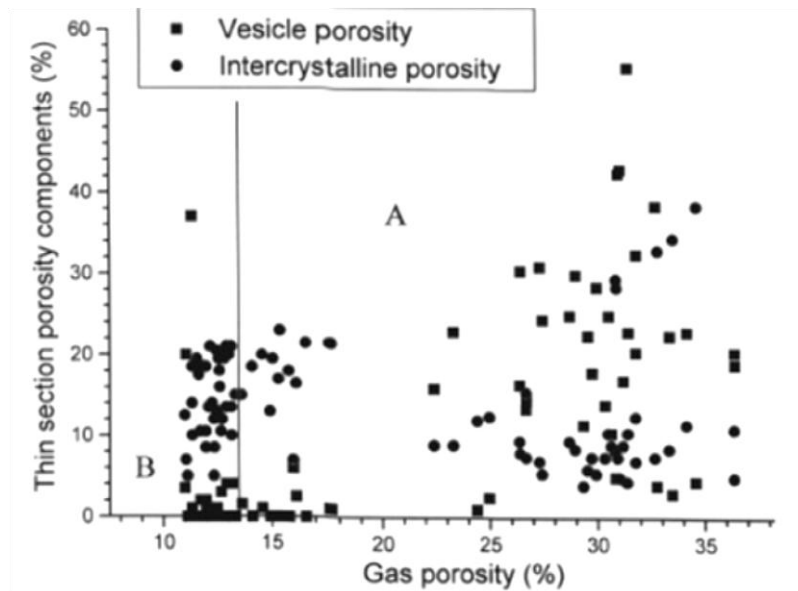


Figure 21: Relation between measured gas porosity and the thin section porosity components in the Öskjuhlíð lava flow (Franzson et al., 2001)

The sonic velocity being an indicator for rigidity of the rocks matrix separates the rocks into two groups. The rocks of group A have a sonic velocity of 3500 to 5000 m/s and in the zone B the sonic velocity amounts to a value between 2000 and 3000 m/s. The different

velocities probably are caused by the occurrence of grain boundary cracks which reduce the sonic P-wave velocity.

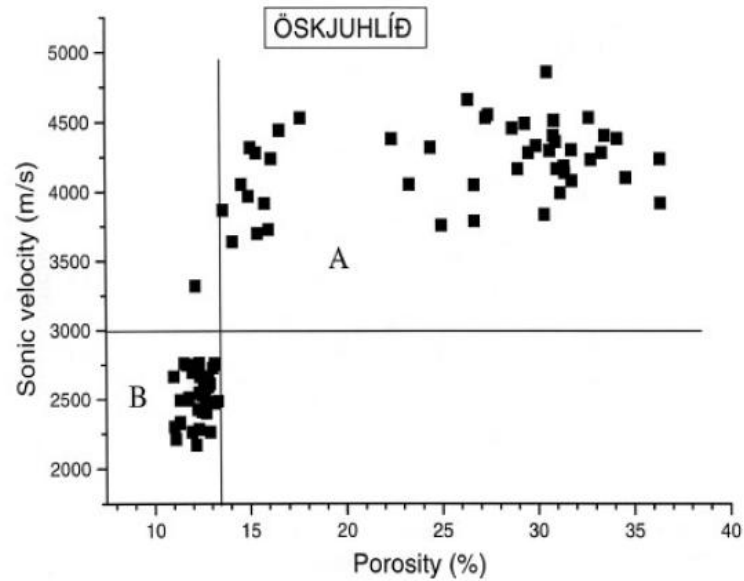


Figure 22: Relation between sonic velocity and porosity in the Öskjuhlíð lava flow (Franzson et al., 2001)

The variety in sonic velocity can also be caused by diverse glass contents in the two zones. High glass content increases the sonic velocity, but reduces the grain density of basalt. The glass rimmed pores occurring in zone A lead to this phenomenon. Otherwise the rocks of layer B do not have a high glass content caused by a slow cooling increasing the grain density and lowering the sonic velocity.

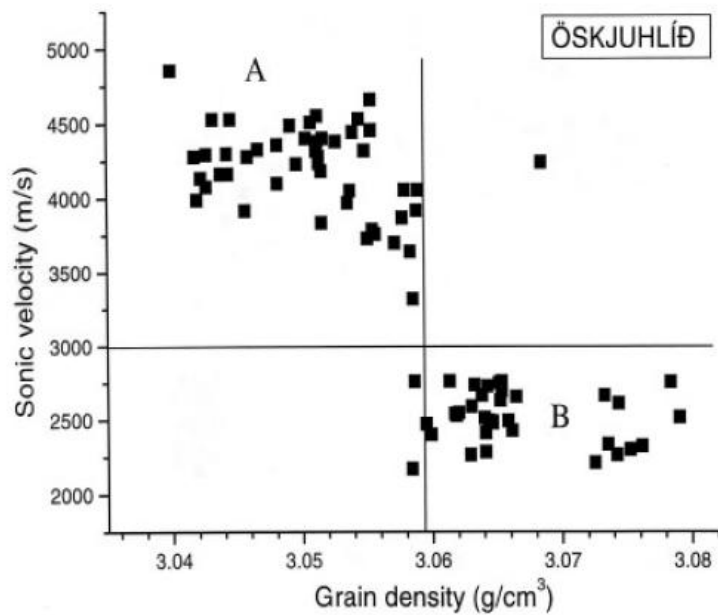


Figure 23: Relation between grain density and sonic velocity in the Öskjuhlíð lava flow (Franzson et al., 2001)



The analyses of four thin sections have been done in Darmstadt by Sanaá Al-Zyoud. Due to the analyses the distribution of the mainly occurring minerals is provided and shown in figure 24 and 25. The comparison of two coarse and two fine grained samples show the mineralogical difference between zone A and B. The content of olivine and altered olivine in all samples is approximately 6%. The Öskjuhlíð basalt is characterized by the sodium rich plagioclase albite, which adds up with a minor portion of bytownite to approximately 40% plagioclase. As earlier mentioned at the surface of the lava degassing takes place in between plagioclase crystals and inhibits pyroxene crystallization. It can be noticed a tendency of reduced pyroxene content in group A compared to group B by totting up the portions of enstatite, augite, altered enstatite and altered augite. There is no relation between the content of the iron rich minerals hematite, magnetite and olivine, which vary from 16 to 23%, and the layering in the lava flow. In the samples QA5 and QB10 minor components of chlorite are observed. Interestingly, the pore space in all samples equals approximately 15% proving the observation of the Orkustofnun thin sections visualized in figure 21.

Orkustofnun analyzed 83 thin sections with respect to mineralogy. The arithmetical mean distributions of the major minerals of group A and B are shown in figure 26. Both zones have an average content of 11% olivine and 39 % pyroxene. The coarse samples are characterized by a higher plagioclase content caused by a slower cooling process. The fast chilling of the upper zone leads to 5% glass rim around the grain pores compared to 2% in the lower part of the lava flow. The loss of water by degassing leads to crystallization of 2% opaline silica in group A.

Julia Jóhannsson analyzed one sample of the Reykjavík grágrýti by XRD and XRF in October 2010. The results of the x-ray fluorescence spectroscopy are shown in figure 27. The XRF analysis verifies that the rock mainly consists of silica representing generally plagioclases, and aluminum oxides indicating pyroxenes. Minor components are calcium oxides, which represent anorthite, magnesium and iron (III) oxides indicating olivine and pyroxene. Accessory minerals are sodium oxide representing albite, titanium oxide, manganese oxide, phosphorus oxides, rhenium, nickel oxides, copper oxide, chromium (III) oxide, potassium oxides, vanadium oxides, zirconium oxides and strontium oxides.

Results of the analysis by x-ray diffraction are shown in figure 28. The intensities of x-ray reflection are displayed depending on the reflection angle. Each crystal plane reflects x-rays in phase at a certain angle of the incident beam. Therefore it is possible to analyze the reflection pattern of the analyzed sample by looking for congruence with certain mineral patterns. The XRD analysis detects the occurrence of plagioclase in general, anorthite and albite, but also the pyroxenes diopside and pigeonite in the Öskjuhlíð sample. The analysis is not very detailed and exact due to an enormous amount of noise in the XRD which is visualized by the black background.

All analyses show that the mineralogical properties of the observed rocks are similar to those of olivine tholeiitic basalts. Basalts are commonly defined by a  $\text{Na}_2\text{O}+\text{K}_2\text{O}$  weight percentage above 2% and a  $\text{SiO}_2$  weight percentage in between 45 and 52 %. The Öskjuhlíð basalt consist of 3%  $\text{Na}_2\text{O}+\text{K}_2\text{O}$  and 47%  $\text{SiO}_2$ . A tholeiitic basalt contains potassium-poor pyroxenes like pigeonite and further orthopyroxenes (Shelley, 1993). The occurrence of these minerals is proved in the XRD and thin section analysis. Additionally a high iron and titanium content is certified by the XRF. The different interpretations of thin sections and the analyses with aid of x-ray result in varying mineralogical and chemical compositions. A comparison of chemical analyses, displayed in table 4, for alkali basalt, olivine tholeiite and tholeiite show that the Öskjuhlíð basalt is a olivine tholeiite. Deciding is the absence of quartz and nepheline minerals and the occurrence of olivine minerals.

Furthermore, the weight percentage of the Öskjuhlíð basalt resembles the most with the exemplary olivine tholeiite.

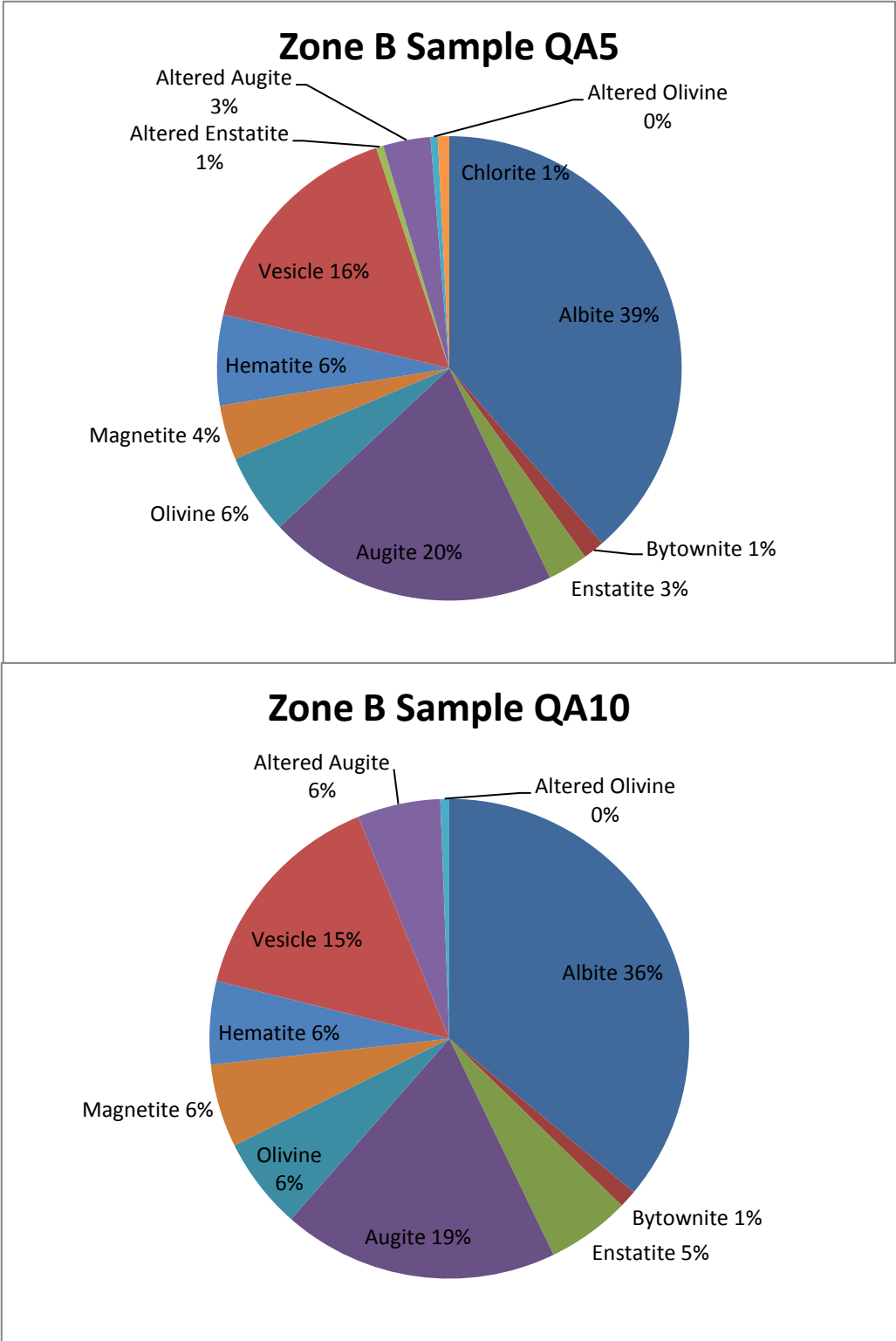
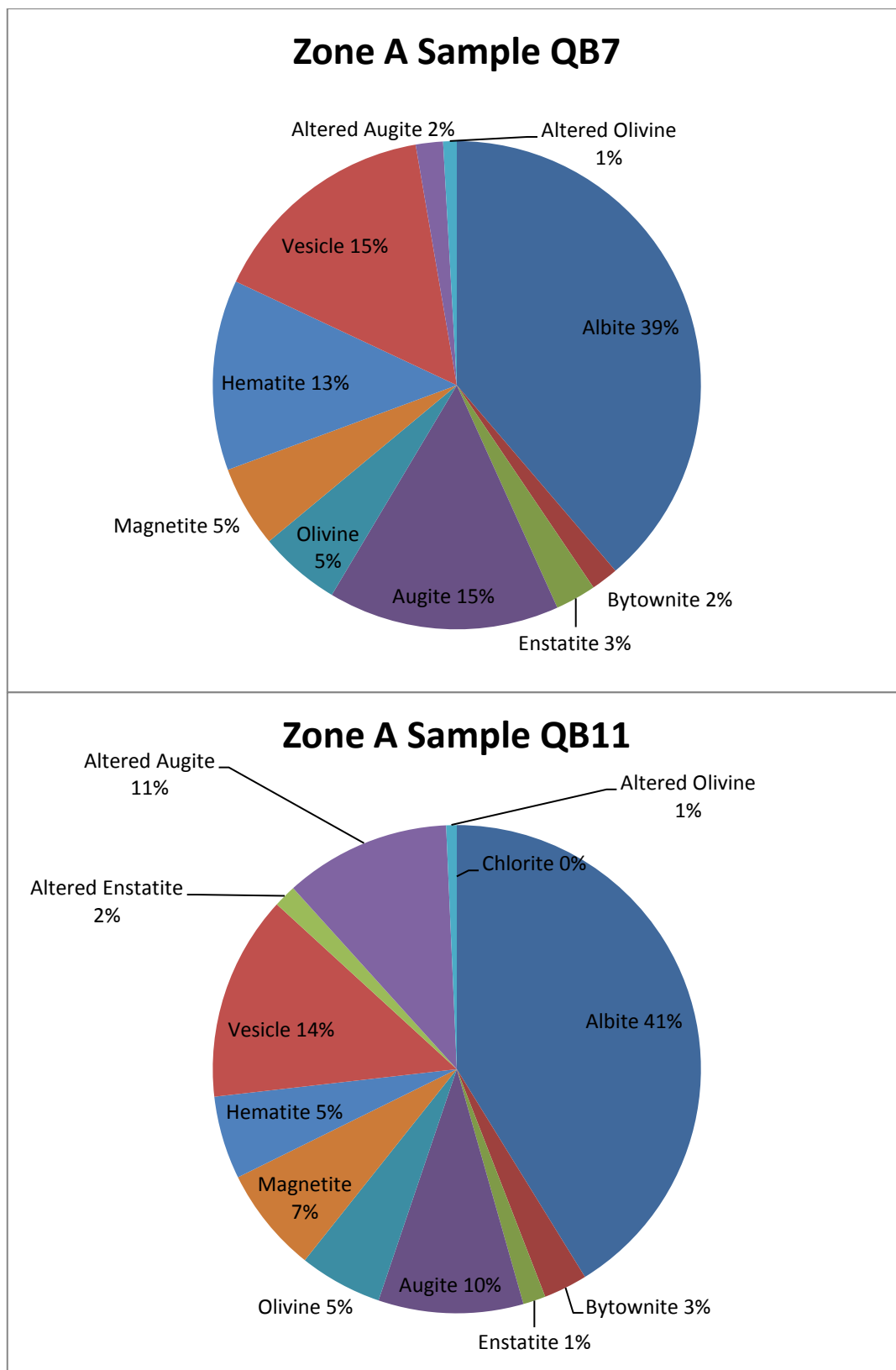


Figure 24: Distribution of mineralogical main components for the zone B in the Öskjuhlíð lava flow



*Figure 25: Distribution of the mineralogical main components for zone A in the Öskjuhlíð lava flow*

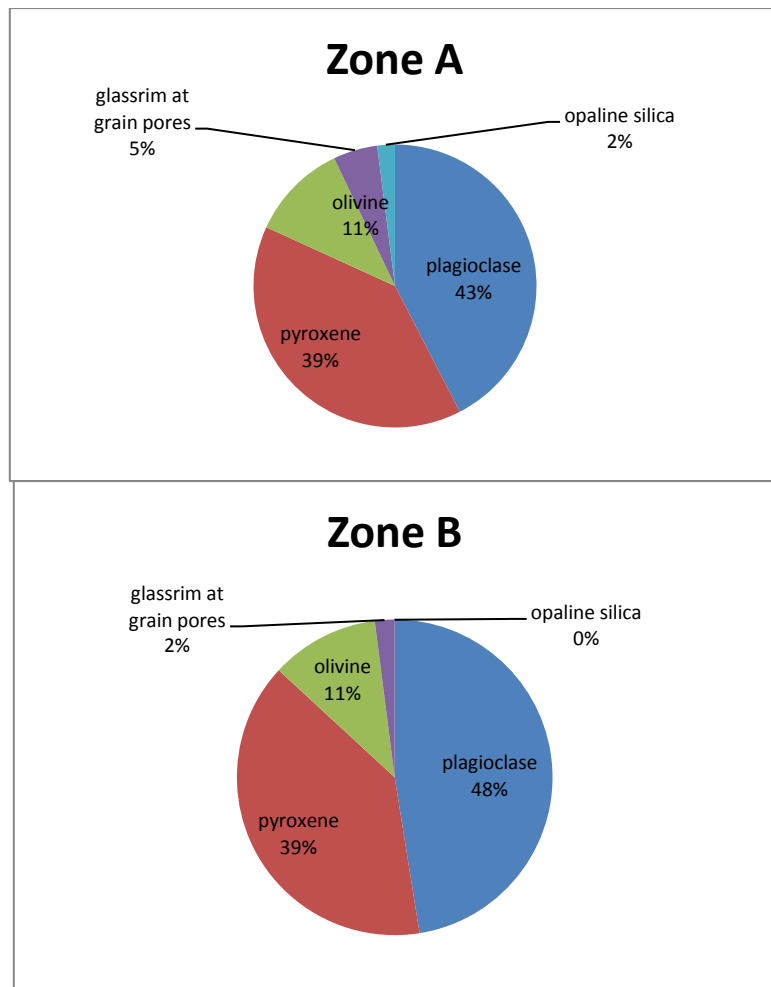


Figure 26: Distribution of the mineralogical main components for the Öskjuhlíð lava flow determined by Orkustofnun

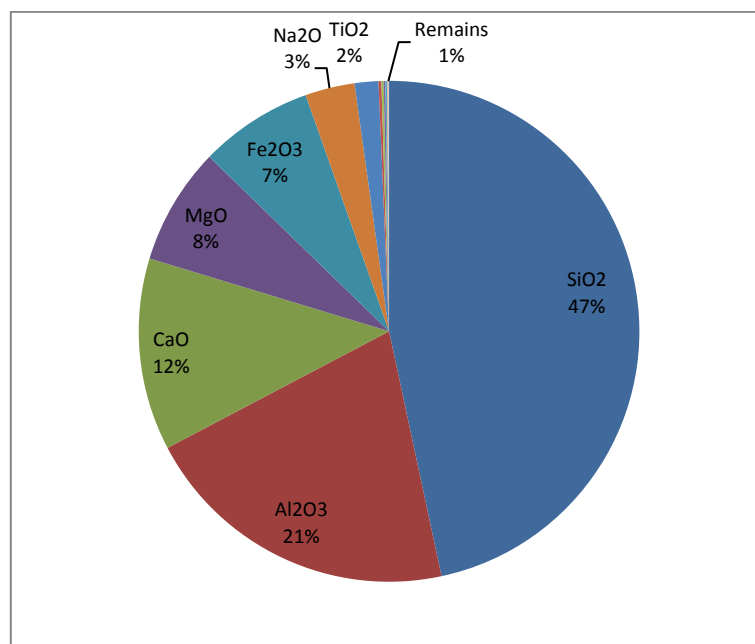


Figure 27: Results of the x-ray fluorescence spectroscopy. Distribution of the chemical components for the Öskjuhlíð lava flow

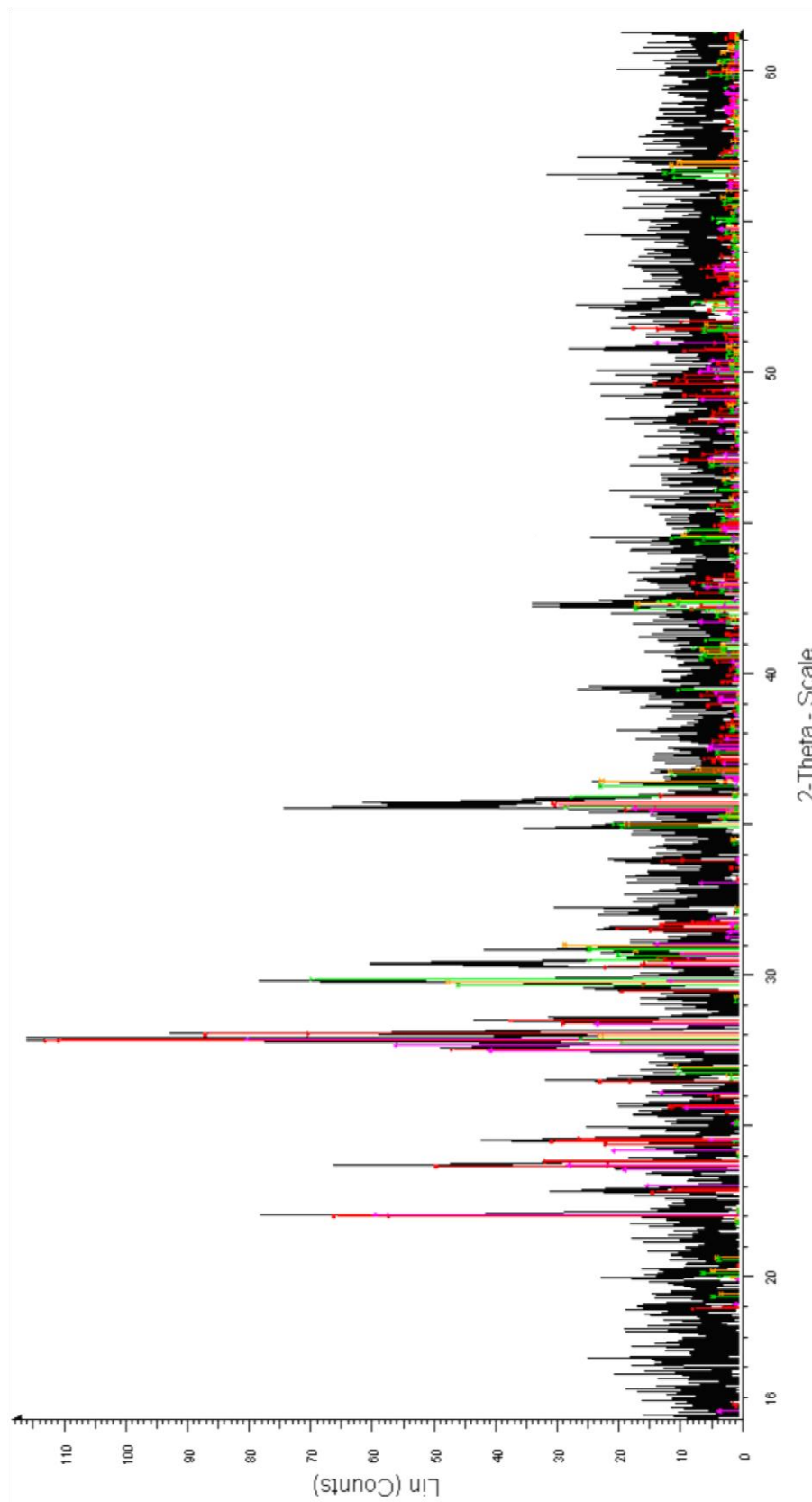


Figure 28: Results of the x-ray diffraction analyses. Relation of the reflected x-ray's intensity to the reflection angle. The colored signals represent the matches to certain minerals. 1) Red: Labradorite, 2) Light green: Aluminium diopside, 3) Dark red: Sodian anorthite, 4) Yellow: Calcium-free Pigeonite, 5) Pink: Albite

*Table 4: Comparison of chemical analyses of alkali basalt, olivine tholeiite and tholeiite from Hawaii. All results are shown in wt % (Hall, 1996)*

	<b>Alkali basalt</b>	<b>Olivine tholeiite</b>	<b>Tholeiite</b>
<b>SiO<sub>2</sub></b>	46.59	49.16	51.02
<b>TiO<sub>2</sub></b>	2.26	2.29	2.03
<b>Al<sub>2</sub>O<sub>3</sub></b>	15.19	13.33	13.49
<b>Fe<sub>2</sub>O<sub>3</sub></b>	2.96	1.31	3.22
<b>FeO</b>	9.89	9.71	8.12
<b>MnO</b>	0.18	0.16	0.17
<b>MgO</b>	8.74	10.41	8.42
<b>CaO</b>	10.02	10.93	10.3
<b>Na<sub>2</sub>O</b>	3.01	2.15	2.1
<b>K<sub>2</sub>O</b>	0.96	0.51	0.4
<b>H<sub>2</sub>O<sup>+</sup></b>	0.05	0.04	0.21
<b>H<sub>2</sub>O<sup>-</sup></b>	0	0.05	0.28
<b>P<sub>2</sub>O<sub>5</sub></b>	0.29	0.16	0.26
<b>Quartz</b>	-	-	4.26
<b>Orthoclase</b>	5.56	2.78	2.22
<b>Albite</b>	20.96	17.82	17.82
<b>Anorthite</b>	25.3	25.3	26.13
<b>Nepheline</b>	2.27	-	-
<b>Diopside</b>	18.51	22.93	18.6
<b>Hypersthene</b>	-	15.35	21.27
<b>Olivine</b>	18.21	9.14	-
<b>Montmorillonite</b>	4.41	2.09	4.64
<b>Ilmenite</b>	4.26	4.41	3.8
<b>Apatite</b>	0.67	0.34	0.67

### 4.3 Geodynamic Interpretation

42 joint measurements give a brief overview of stress impacting on the rock. The majority of joints dip steeply with 70 to 90° in all directions with a trend in direction southeast and northwest. This is typical for basalt commonly characterized by column joints. The joints are generated perpendicular to the cooling surface of the lava flow. Therefore at Öskjuhlíð the joint surfaces are oriented vertically. It is difficult to interpret the results related to paleostress. However, it is eye-catching that the strike of the joints is perpendicular to the

strike of the occurring faults in this region, shown figure 28. Mainly, the basalt is jointed due to thermal contraction. The results are shown in a Schmidt's grid a cleavage rose. Both figures show the lower hemisphere projected on the equatorial plane. The rose diagram proves the statement of not defined strike directions.

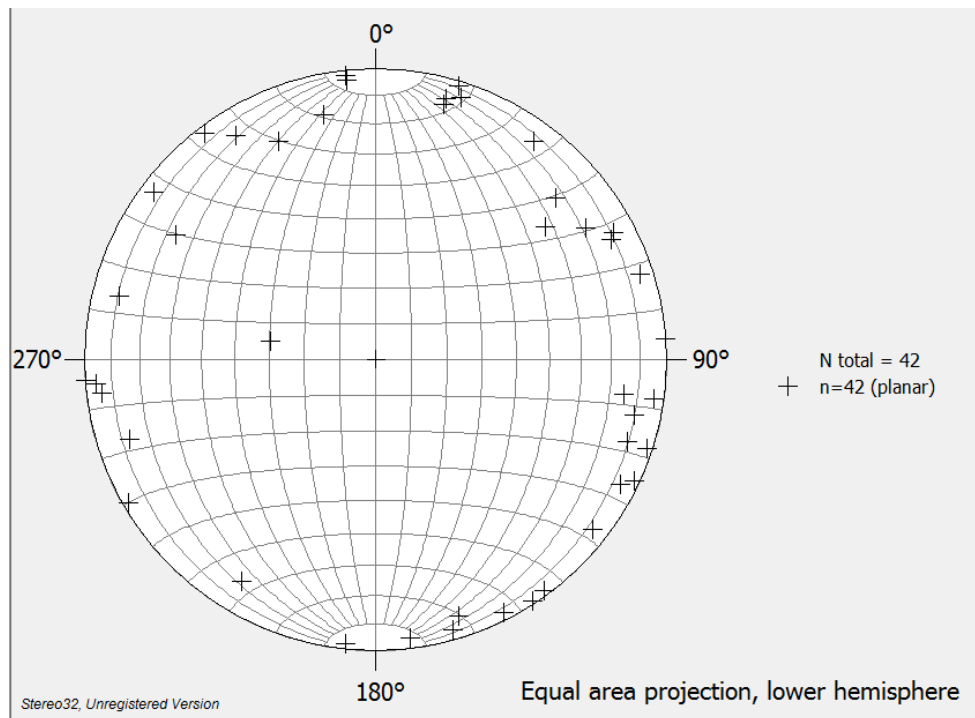


Figure 29: Joint measurements of the Öskjuhlíð lava flow illustrated in the Schmidt's grid

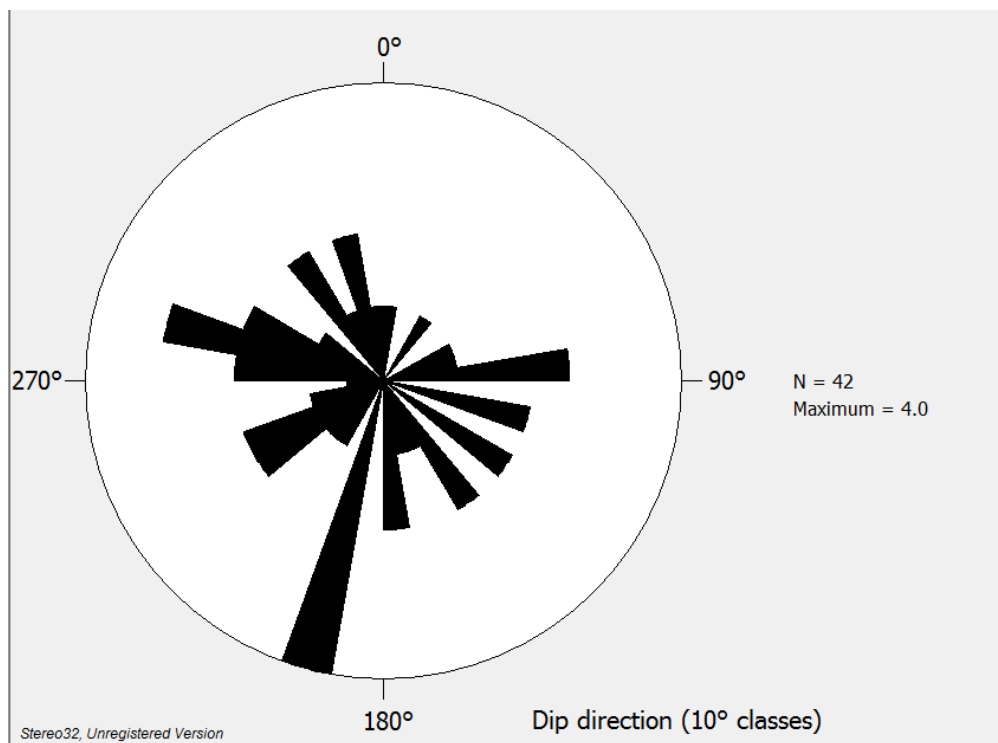


Figure 30: Joint measurements of the Öskjuhlíð lava flow displayed in a rose diagram

## 5 ANALYSIS OF THERMAL CONDUCTIVITY

The different measurements for the various sample types and the treatments of the samples are listed in table 5.

*Table 5: Overview of the analysis program of thermal conductivity*

Analysis of thermal conductivity				
Kind of sample	Preparation of the sample	Number of samples	Measuring Device	Number of measurements
Hand probes	uncut, polished	70	LMC	5
Hand probes	cut, polished	150	LMC	3
Cuboids	cut, polished	99	LMC	3
Cuboids	cut, polished	99	TCS	3
Cores	drilled, polished	21	LMC	3
Cores	drilled, polished	21	TCS	3

### 5.1 Interpretation of the Data

#### 5.1.1 Hand Probes

The thermal conductivity of 150 hand probes of the Öskjuhlíð basalt is defined with the LMC instrument. 70 of these samples are measured in uncut, but treated with black polish and afterwards in cut and varnished conditions. In the course of the analysis an immense spread of results is noticeable. Therefore each uncut sample is determined five times. The cut samples are analyzed three times due to lack of time. The arithmetical means of the three or five results for all 70 samples are shown in figure 31. The distribution of thermal conductivity for the uncut samples ranges from 0.92 to 8.24 W/(m·K). These results are observed due to heating the sample's surface about 0.96 to 4.41 K. The spread of the data is primarily dependent on temperature difference being a result of the heating process. The lower the temperature difference, the larger the observed thermal conductivity. The resulting low temperature difference in these pictured cases is caused by a rough surface of the sample. The samples shown in blue report the results of cut and varnished hand probes. The thermal conductivity of the data ranges from 0.76 to 1.49 W/(m·K) dependent on a temperature difference of the samples from 2.75 to 4.82 K. The decrease of thermal conductivity with an increase of temperature difference is also outstanding, but in contrast to the results of the uncut samples the data of the treated hand probes does not show a scattering in a comparable magnitude.



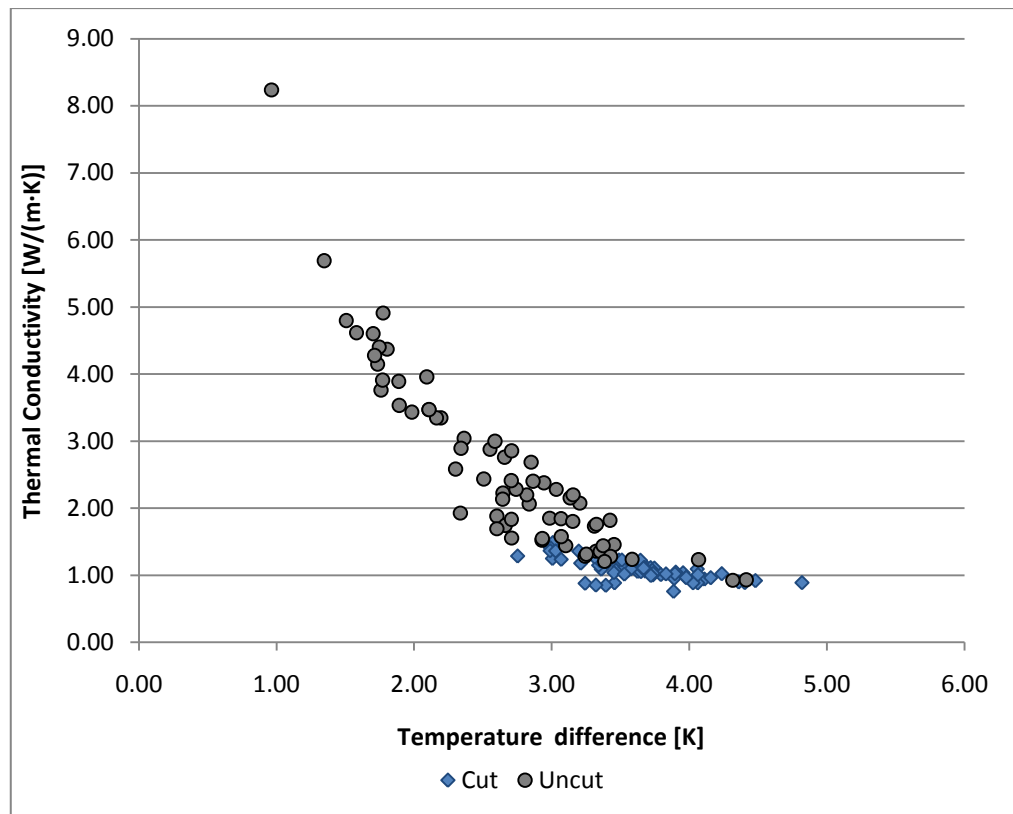


Figure 31: Relation between the thermal conductivity and the temperature difference at uncut and cut hand probes of the Öskjuhlið lava flow observed by the LMC device

The lava flow exposed in Öskjuhlið originates from a volcano called Lyklafell. This volcano is located southeast of Reykjavik. Generally the lava flow streamed from direction southeast to northwest. In the following chart the samples in the outcrop are ordered in four series from southeast to northwest and additionally in upper-vesicular and lower-dense samples. The cut and varnished samples vary from 0.67 to 1.49 W/(m·K) at a temperature difference of minimal 2.75 and maximal 5.75 K. There is no outstanding tendency from the southeastern to the northwestern part of the outcrop noticeable, but for both cases – the southeastern and the northwestern hand probes - the dense lower samples have higher thermal conductivity than the vesicular upper samples. All samples show the relation of a larger thermal conductivity with a decreasing temperature difference.

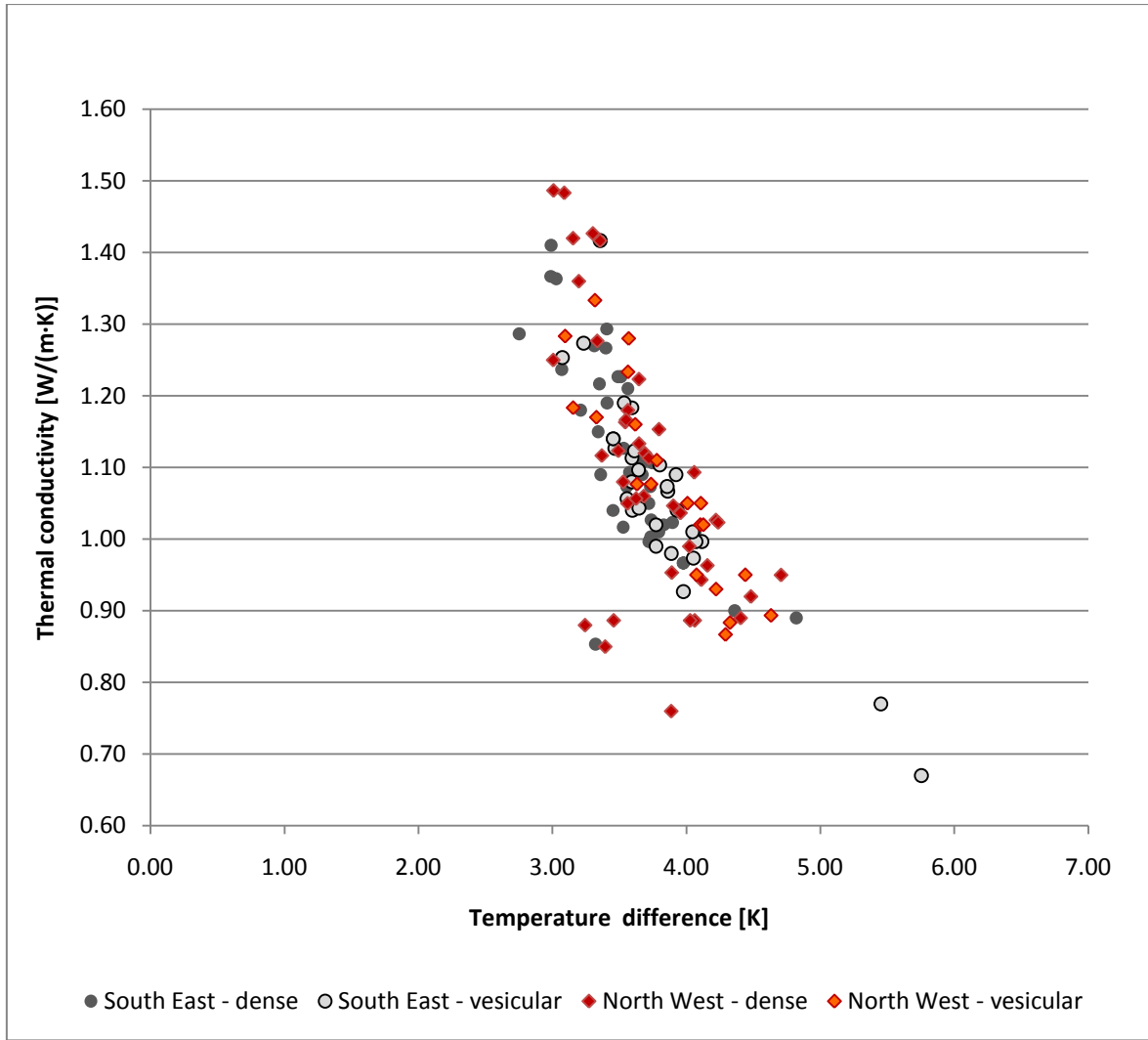


Figure 32: Relation between thermal conductivity and temperature difference for samples classified by their location in the Öskjuhlíð outcrop determined by the LMC device

### 5.1.2 Cuboids

The LMC device is evaluated by measuring samples under the same conditions with a second device. Therefore 33 cuboids with planar surfaces were transported to Germany. The thermal conductivity is determined by the LMC and the TCS instrument in the laboratory of the Institute of Applied Geosciences in Darmstadt, Germany. All 33 cuboids are separated in three parts X.01, X.02 and X.03. Hence 99 measurements are done to observe the thermal conductivity of the rock samples. The cuboids themselves can be divided into two groups characterized by dense and vesicular matrix. There are 17 dense and 16 vesicular samples. Each sample is measured three times. The arithmetical means of the tripled measurements are shown in figure 33. The thermal conductivity measured by the LMC ranges from 0.82 to 1.42 W/(m·K) dependent on a temperature difference of 3.02 to 4.9 K. The TCS device measures a thermal conductivity ranging from 0.93 to 1.42 W/(m·K) and a temperature difference of 3.78 to 5.87 K. Both instruments detect the thermal conductivity in the similar range. It is outstanding that the TCS instrument

determines the comparable thermal conductivity as does the LMC device, but at a higher temperature difference than the LMC. For both instruments it is noticeable, that a higher temperature difference results in a lower thermal conductivity. The results of both instruments seem to belong to a parallel function. The LMC device does not show a relation between the matrix and the thermal conductivity of the sample. Otherwise the TCS instrument gives larger thermal conductivities for the dense samples at lower temperature differences than the vesicular cuboids. This relationship can be explained with air filled pores which operate as insulators, and reduce the thermal conductivity of the rock sample. Hence the vesicular rock is heated more than dense rock conducting the heat.

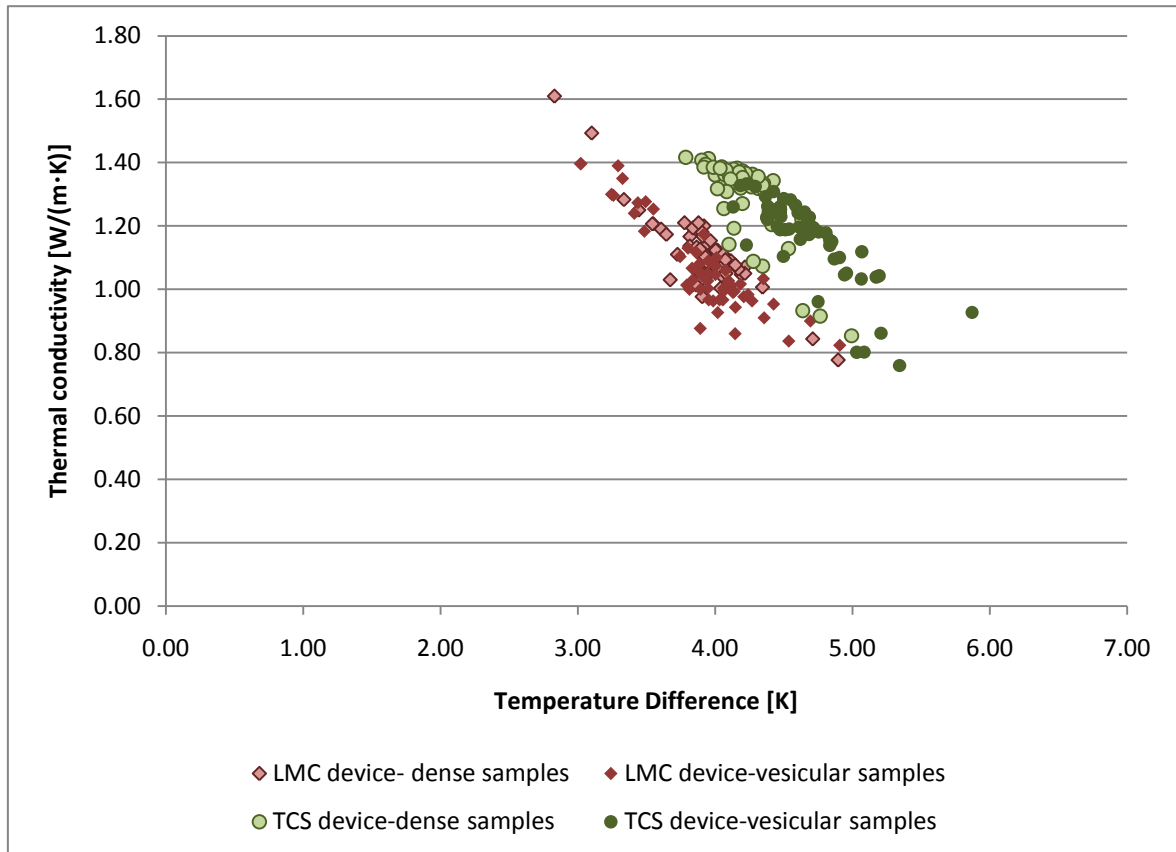


Figure 33: Relation between thermal conductivity and temperature difference of Öskjuhlíð cuboids classified by texture determined by LMC and TCS instruments

### 5.1.3 Cores

10 cores drilled by Orkustofnun were transported to Germany to be analyzed by the LMC and TCS instrument. Depending on the length of the cores some of the samples are subdivided into two or three samples, so that altogether 21 samples were determined. All 21 cores are measured three times with respect to thermal conductivity by both instruments. In figure 34 the results of the measurements and the arithmetical means of the results are shown. The data points plotted in red illustrate the results of the LMC tool. The data observed by the TCS instrument is displayed in green. The LMC detects a thermal conductivity of 0.72 to 1.81 W/(m·K) at a temperature difference of 2.60 to 5.25 K. The

arithmetical means vary from 0.78 to 1.61 W/(m·K) depending on a temperature difference of 2.83 to 4.89 K. The TCS' results range from 0.74 to 1.32 W/(m·K) at a temperature difference of 3.94 to 5.46 K. The derived arithmetical means include a margin of 0.76 to 1.32 W/(m·K) resulting from a temperature difference of 4.02 to 5.34 K. The difference of the results to the arithmetical means of the TCS does not differ as much as the arithmetical means to the results of the LMC device. The large scattering of the LMC device' results supports a threefold measurement of samples to ensure the verification of results. Both devices show the declining dependency of thermal conductivity with an increasing temperature difference.

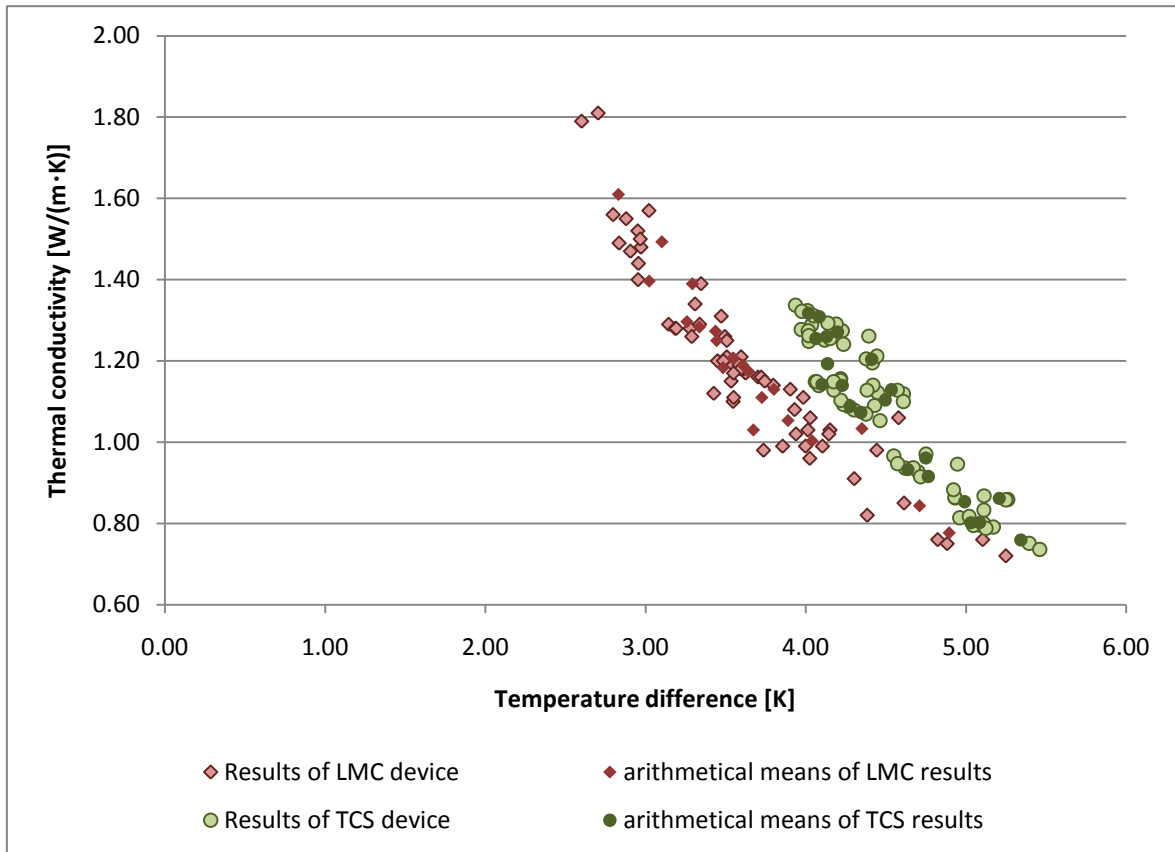


Figure 34: Relation between thermal conductivity and temperature difference of Öskjuhlíð cores determined by the LMC and the TCS device

#### 5.1.4 Entire Sample Base

The relation of thermal conductivity and matrix of the rock samples was determined for altogether 270 cut and varnished samples by the LMC device. Each measurement is done three times to minimize the scattering of the values. The maximal derived thermal conductivity and temperature difference is 1.61 W/(m·K) and 5.75 K. The LMC device observes a minimal thermal conductivity and temperature difference of 0.67 W/(m·K) and 2.75 K. The results do not demonstrate a dependency of thermal conductivity on the variety of the matrix. However, all samples show a functional drop of thermal conductivity with increasing temperature difference.

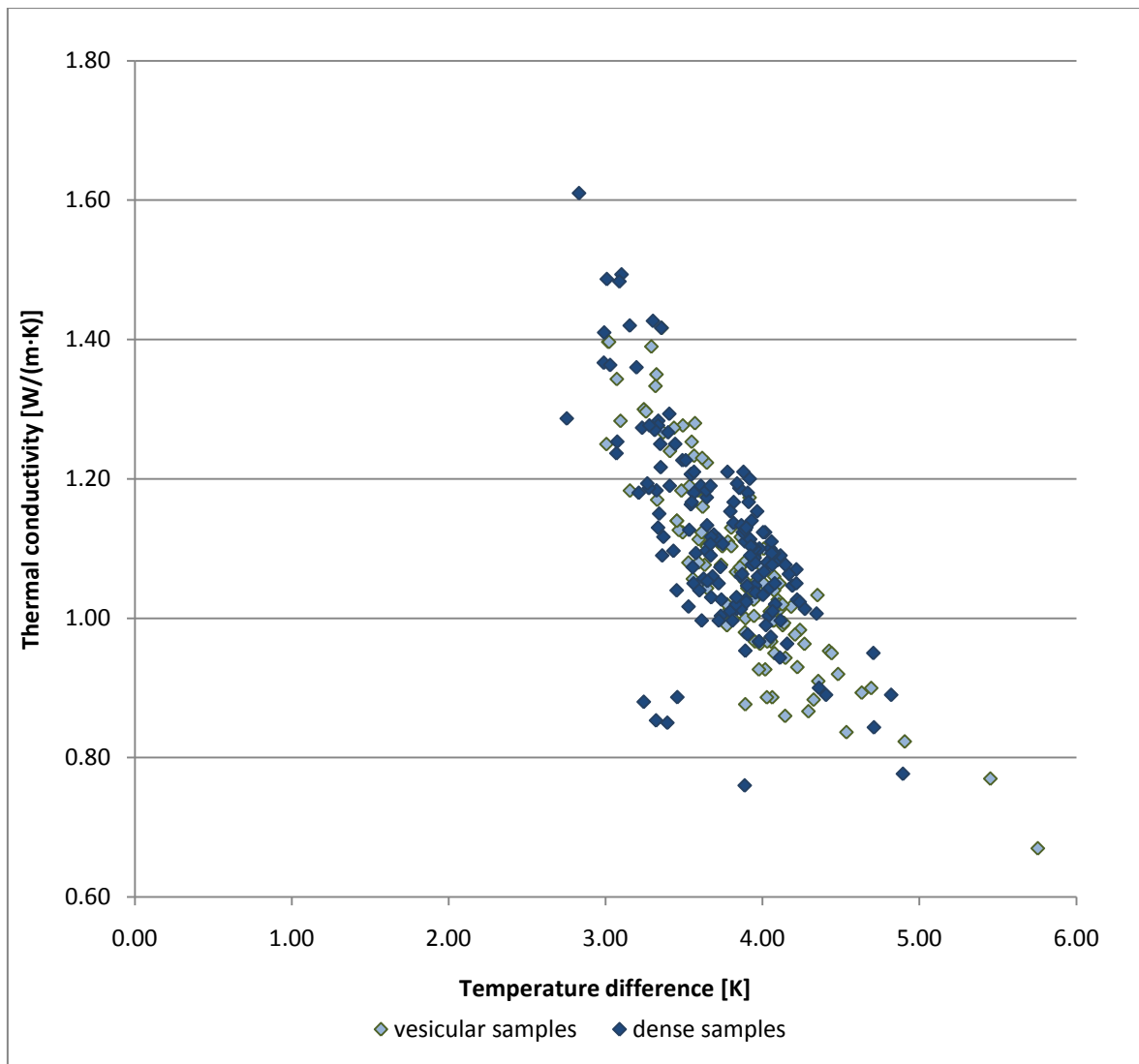


Figure 35: Relation between the thermal conductivity and temperature difference of Öskjuhlíð samples determined by the LMC tool

## 5.2 Statistical Analysis

### 5.2.1 Entire Sample Base Determined by the LMC Device

The distribution of 810 thermal conductivity measurements by the LMC is shown in figure 36. The data is classified in 27 bins, which contain a width of 0.05 W/(m·K). The histogram displays bins varying from 0.55 to more than 1.90 W/(m·K). The maximal frequency with 140 data points is observed for a thermal conductivity of 1.00 to 1.05 W/(m·K).

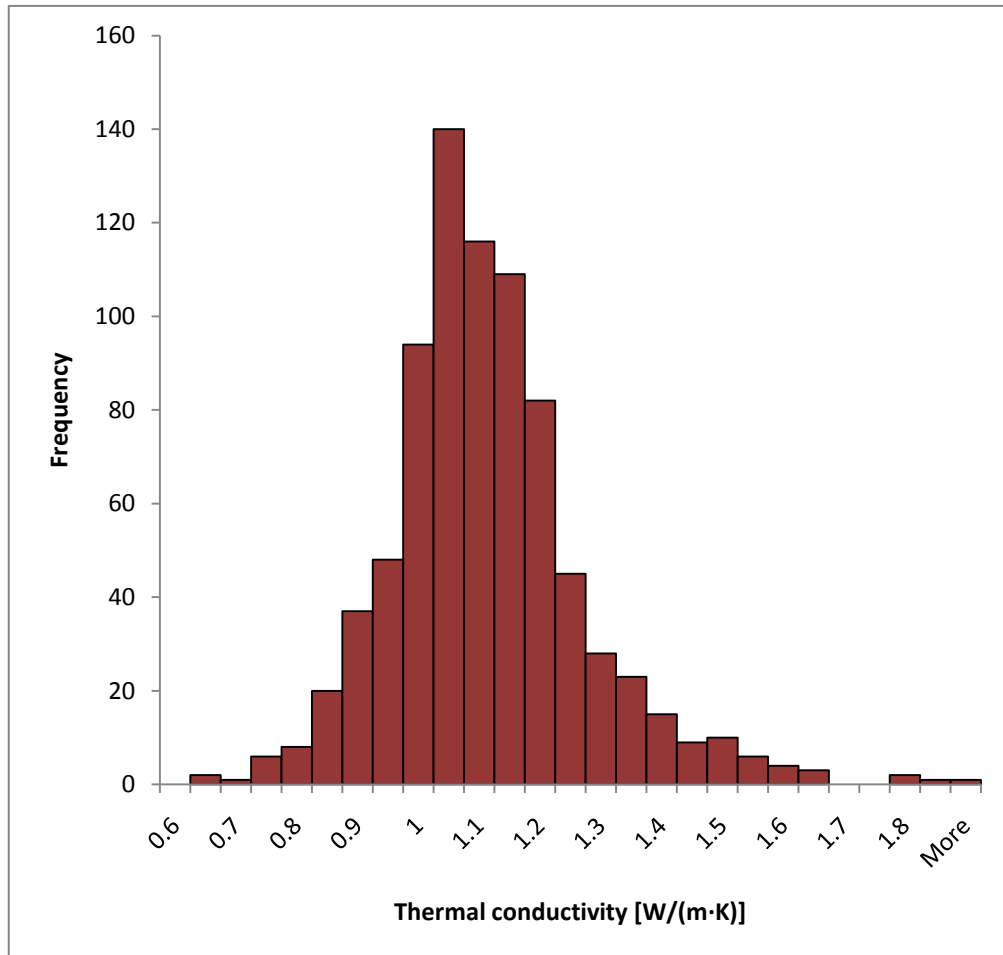


Figure 36: Histogram of the thermal conductivity Öskjuhlíð data series determined by the LMC device

In table 5 the descriptive parameters of the 810 thermal conductivity determinations are presented. The data is characterized by a right-skewed distribution based on the valid condition  $\bar{x} > \tilde{x} > x_{mod}$ . This assumption matches with a skewness of 0.86. The kurtosis of 2.30 reflects a larger maximum of the distribution than the related normal distribution. The measures of dispersion show an absolute measuring error of 0.16 W/(m·K) and a relative error of almost 15 %, represented by the standard deviation and the coefficient of variation.

Table 6: Statistical descriptive parameters of the Öskjuhlíð data series determined by the LMC instrument

Arithmetical mean	1.09	0.75-quartile	1.17	Harmean mean	1.07	Range	1.25
Median	1.08	Minimum	0.62	Variance	0.03	Interquartile range	0.17
Mode	1.04	Maximum	1.87	Standard deviation	0.16	Skewness	0.86
0.25-quartile	1.00	Geometric mean	1.08	Coefficient of variation	0.15	Kurtosis	2.30

The cumulative frequency of the data is shown in figure 37. The data varies from -0.49 to 0.76 W/(m·K) apart from the arithmetical mean  $\mu$  of the data series. The frequency distribution is compared to the normal cumulative distribution with the parameters  $\mu = 1.09$  and  $\sigma = 0.16$ . Both distributions are displayed relative to the deviation of the data point to the arithmetical mean  $\mu$ . The functions approximate asymptotically to their limiting values of zero and one relative frequency or probability. The frequency distribution only differs marginally from the normal cumulative distribution. The deviation of the distribution from the normal distribution is based on the positive skewness of the function.

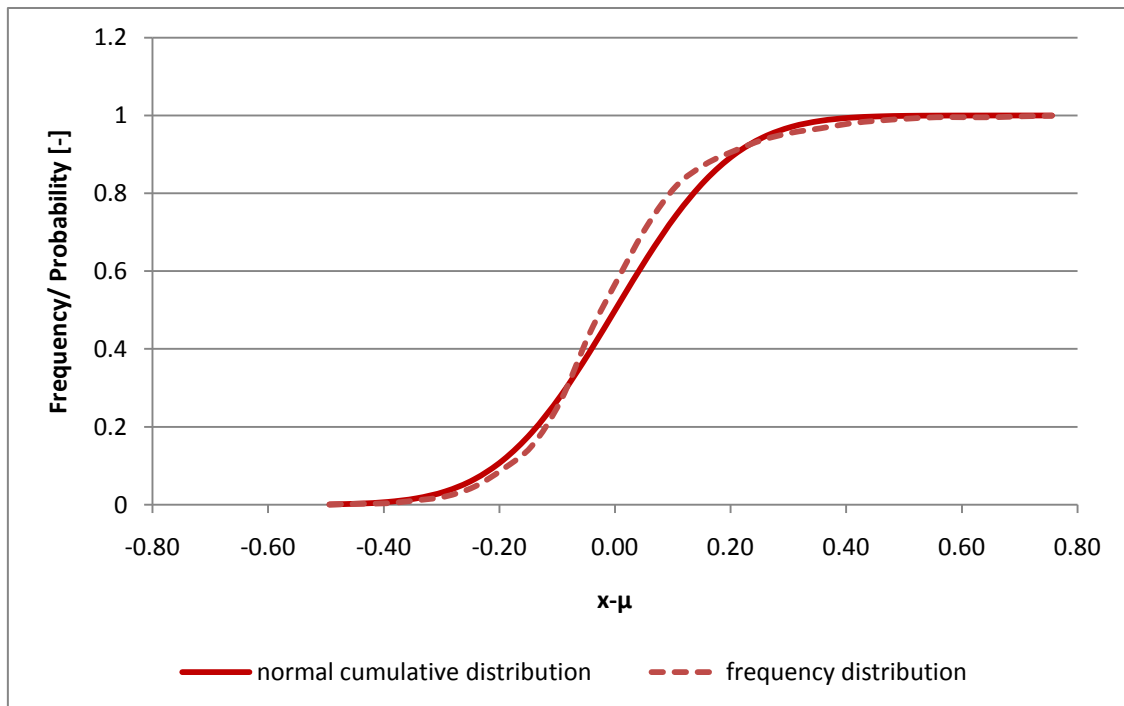
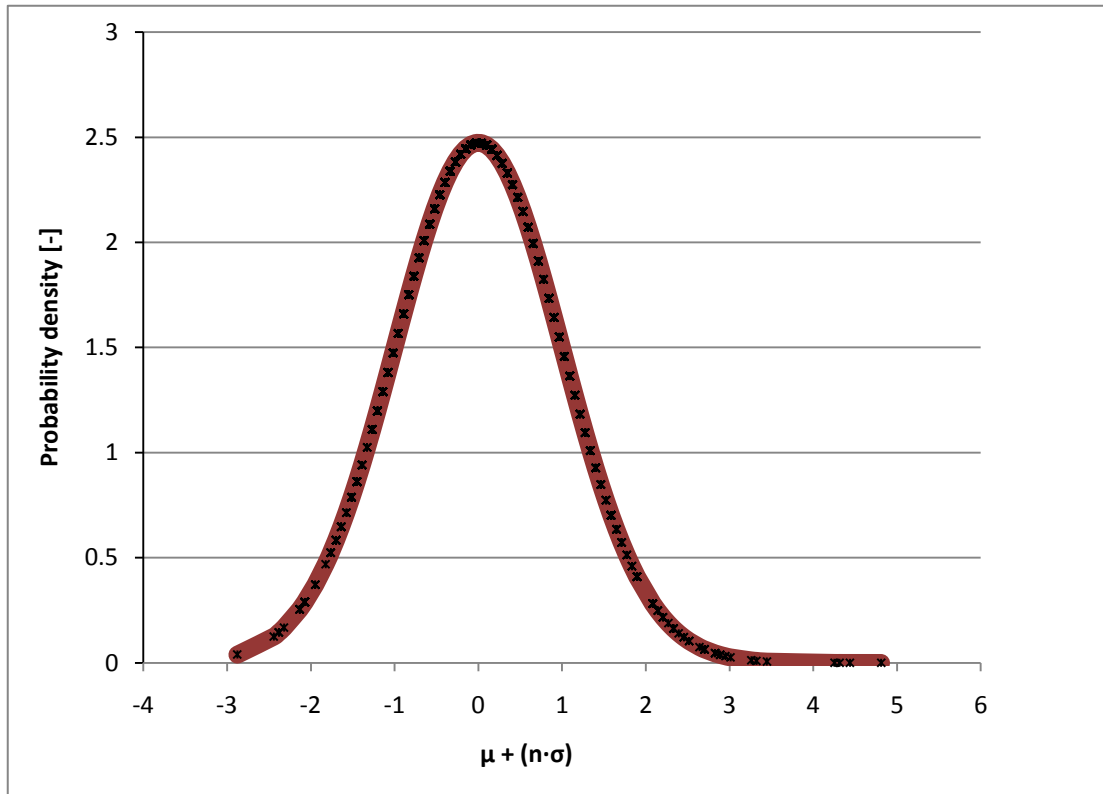


Figure 37: Frequency and cumulative normal distribution of the thermal conductivity Öskjuhlíð data series determined by the LMC instrument

The probability density distribution of the data is shown in figure 38. The maximum of the symmetrical distribution is reached at arithmetical mean with a probability density of 2.50. The function approximates both-sided asymptotically to the limited values zero. The distribution ranges from the negative threefold to the positive fivefold standard deviation. It is noticeable that only a minor number of values deviate more than three times of the standard deviation from the arithmetical mean of the data set.



*Figure 38: Probability density distribution of the thermal conductivity Öskjuhlíð data series determined by LMC instrument*

The box plot of the series visualizes that the majority of values range in between 1.00 to 1.17 W/(m·K). Some outliers characterize the wide range of 0.62 to 1.87 W/(m·K) of the data set. These outliers explain the large deviation in the probability density distribution.



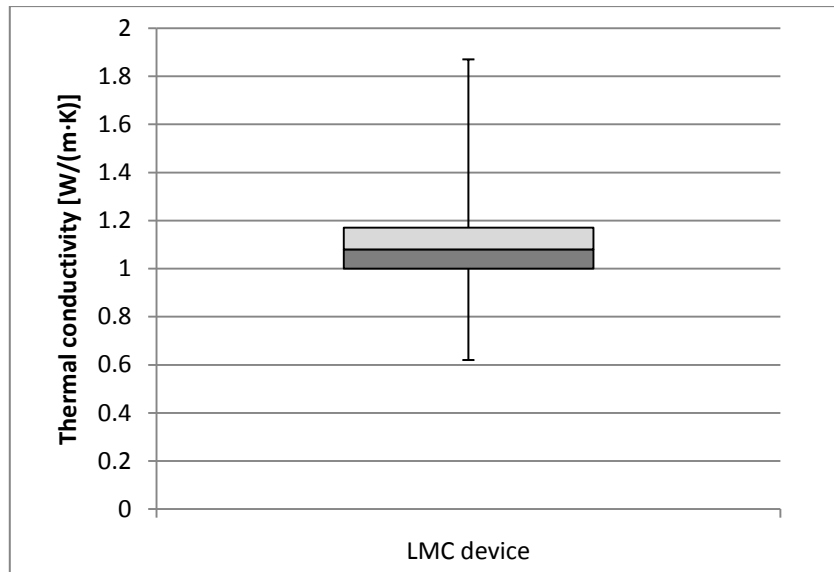


Figure 39: Box plot of the thermal conductivity Öskjuhlið data series determined by the LMC device

### 5.2.2 Comparison of LMC and TCS Instruments

120 samples from the Öskjuhlið outcrop are determined with respect to the thermal conductivity by the LMC and TCS instrument. The distributions of data sets are shown in the histograms below. These histograms are characterized by 10 bins with ranges of 0.10 W/(m·K) varying from 0.70 to 1.70 W/(m·K). The LMC distribution has its maximum in the range of 1.00 to 1.10 W/(m·K) with an absolute frequency of 49 values. The highest frequency with 53 values is observed in between 1.30 and 1.40 W/(m·K) by the TCs device.

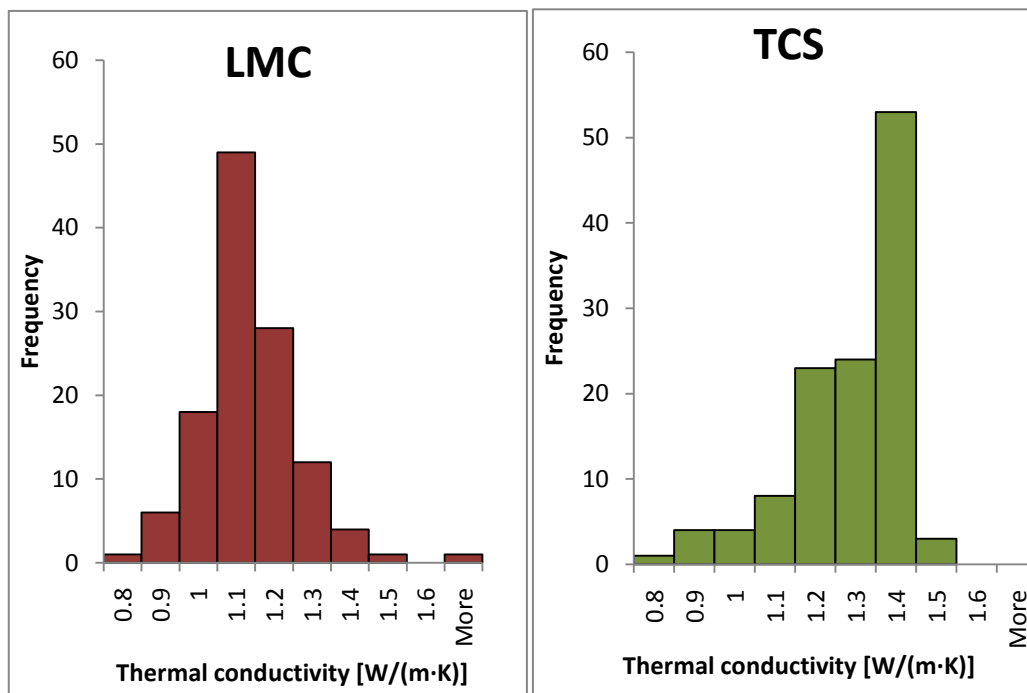


Figure 40: Histograms of the thermal conductivity Öskjuhlið data series determined by the LMC and the TCS devices

The statistical measures of the data series analyzed by both devices are shown in table 7. The parameter of location can not characterize the distribution of the LMC data as symmetrical, right – skewed nor left – skewed. The distribution is approximately symmetrical due to the valid condition of  $\bar{x} \approx \tilde{x} \approx x_{mod}$ . The skewness of the function is positive and the kurtosis indicates that the maximum of the distribution is larger than the maximum of the related normal distribution. The statistical parameters of distribution suggest an absolute measuring error of 0.13 W/(m·K) and a relative measuring error of 12% for the LMC distribution. The TCS data series is a left-skewed distribution, characterized by the condition  $\bar{x} < \tilde{x} < x_{mod}$ . A second evidence of a left – skewed distribution is the negative skewness. The kurtosis is similar as for the LMC positive. The standard deviation, an indicator for the measuring error is 0.16 W/(m·K) and the relative coefficient of variation amounts to 12%. The statistical analysis of the location measures shows larger values for the TCS than for the LMC. Even if the range of the LMC data set is higher than the range of the TCS series, the parameters of dispersion show that the measuring error of the LMC device is smaller than the error of the TCS.

*Table 7: Statistical descriptive parameters of the thermal conductivity Öskjuhlíð data series determined by the LMC and the TCS devices*

Instru ment	Arithmeti cal mean	Median	Mode	0.25- quartile	0.75- quartile	Minimum	Maximum	Geometric mean	Harmean mean
LMC	1.09	1.08	1.1	1.01	1.14	0.78	1.61	1.08	1.07
TCS	1.24	1.27	1.36	1.18	1.36	0.76	1.42	1.23	1.22
Instru ment	Variance	Standard deviation	Coefficient of variation	Range	Inter- quartile range	Absolute deviation	Median absolute deviation	Skewness	Kurtosis
LMC	0.017	0.13	0.12	0.83	0.13	0.09	0.07	0.90	2.35
TCS	0.021	0.16	0.12	0.66	0.18	0.11	0.09	-1.34	1.56

In figure 41 the frequency distributions of the data series for both instruments are displayed. Additionally the related normal cumulative distributions are shown. The distributions are pictured relatively to the distance of their arithmetical mean. All four functions approximate asymptotically to their limit values zero and one. The distribution of the LMC device ranges from 0.33 W/(m·K) less the arithmetical mean to 0.56 W/(m·K) above the measure of location. The distributions of the TCS data set vary relatively to the arithmetical mean value from -0.49 W/(m·K) up to 0.4 W/(m·K). The two normal cumulative distributions do not differ rapidly from each other. However both frequency distributions deviate from their normal cumulative distributions in a similar magnitude.

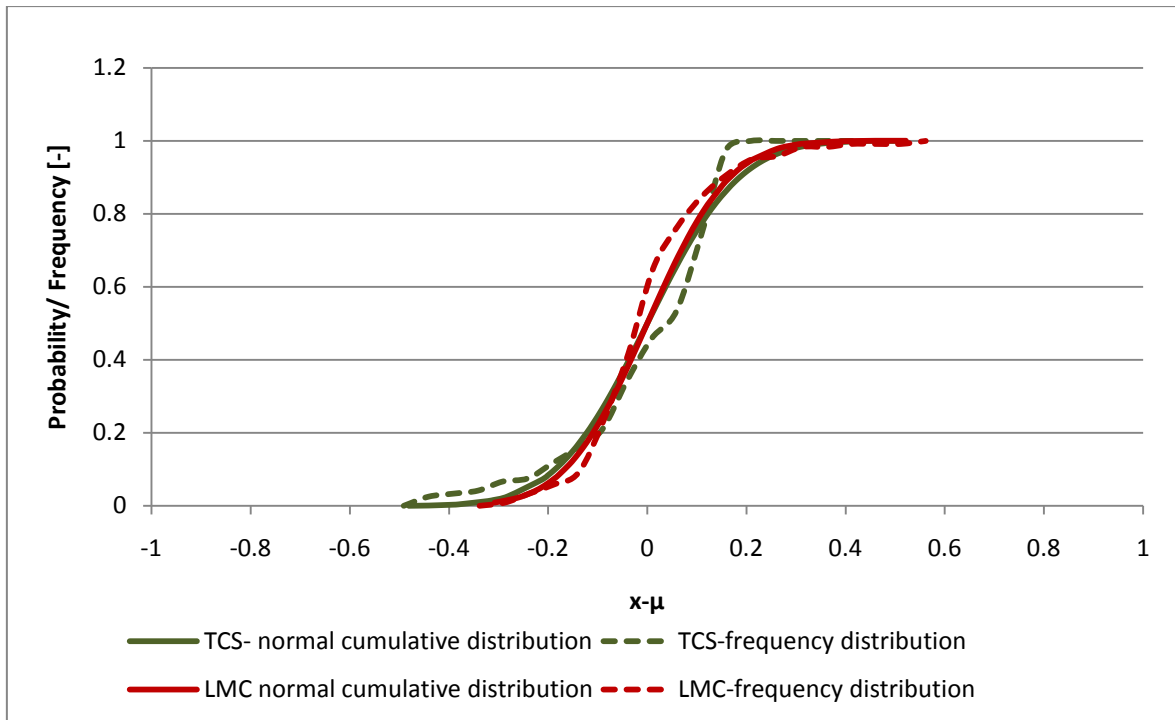


Figure 41: Frequency and cumulative normal distributions of the thermal conductivity Öskjuhlið data series determined by the LMC and the TCS instruments

The probability density distributions of the data sets determined by the LMC and TCS device are presented in figure 42. Both symmetrical distributions are characterized by a maximum at the arithmetical mean. The arithmetical mean of the LMC data set has a larger probability density than the arithmetical mean of the TCS series. The distributions' probability density approximate on both side asymptotically to zero. The data determined by the LMC tool ranges from a negative 2.36-fold to a positive fourfold standard deviation apart from the arithmetical mean. Otherwise the data of the thermal conductivity analyzed by the TCS instrument contains a negative 3.3-fold standard deviation up to a positive 1.2 fold standard deviation from the arithmetical mean. The TCS data distribution underlines the character of its negative skewness and asymmetric character compared to its related probability density distribution.

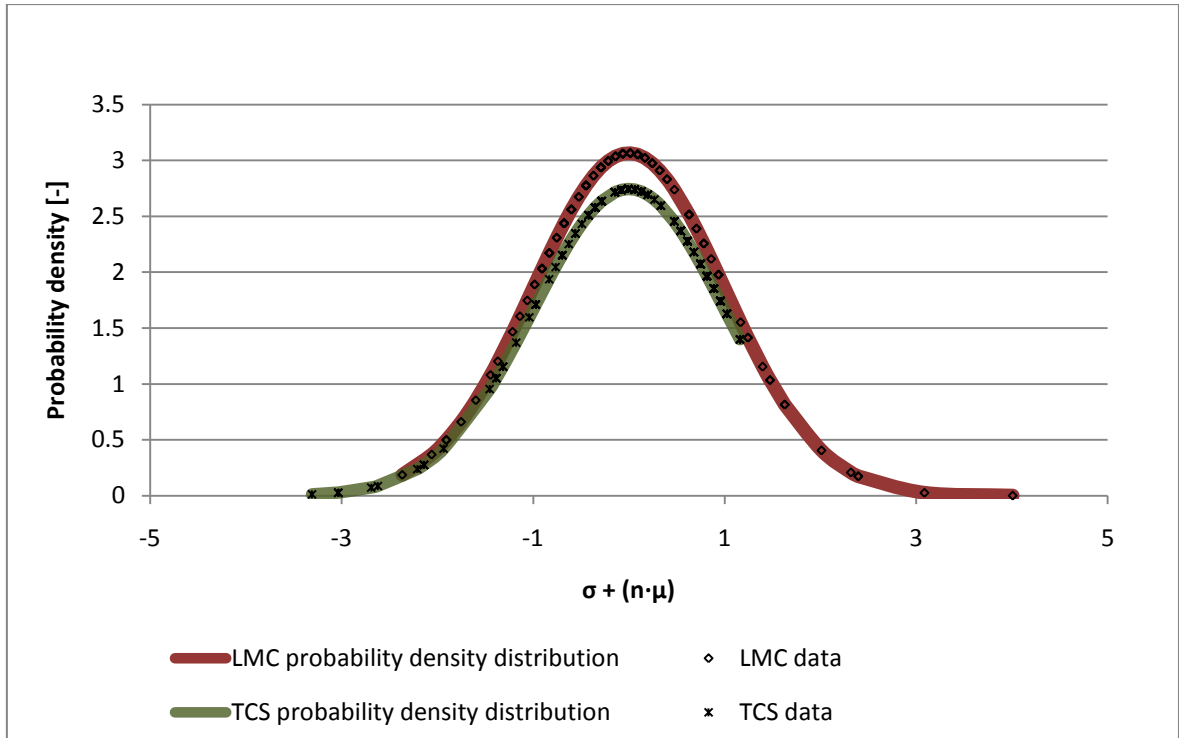


Figure 42: Probability density distributions of the thermal conductivity Öskjuhlíð data series determined by the LMC and the TCS devices

In figure 43 the box plots for the thermal conductivity analysis are shown. The LMC interquartile range contains a thermal conductivity from 1.01 to 1.14 W/(m·K). The data set varies from 0.68 to 1.61 W/(m·K). The data determined by the TCS ranges from 0.76 to 1.42 W/(m·K), including an interquartile range from 1.18 to 1.36 W/(m·K). Both box plots indicate that the ranges as well as the interquartile ranges are of similar magnitude. Furthermore, the character of a negative skewness for the TCS series is once more visualized.

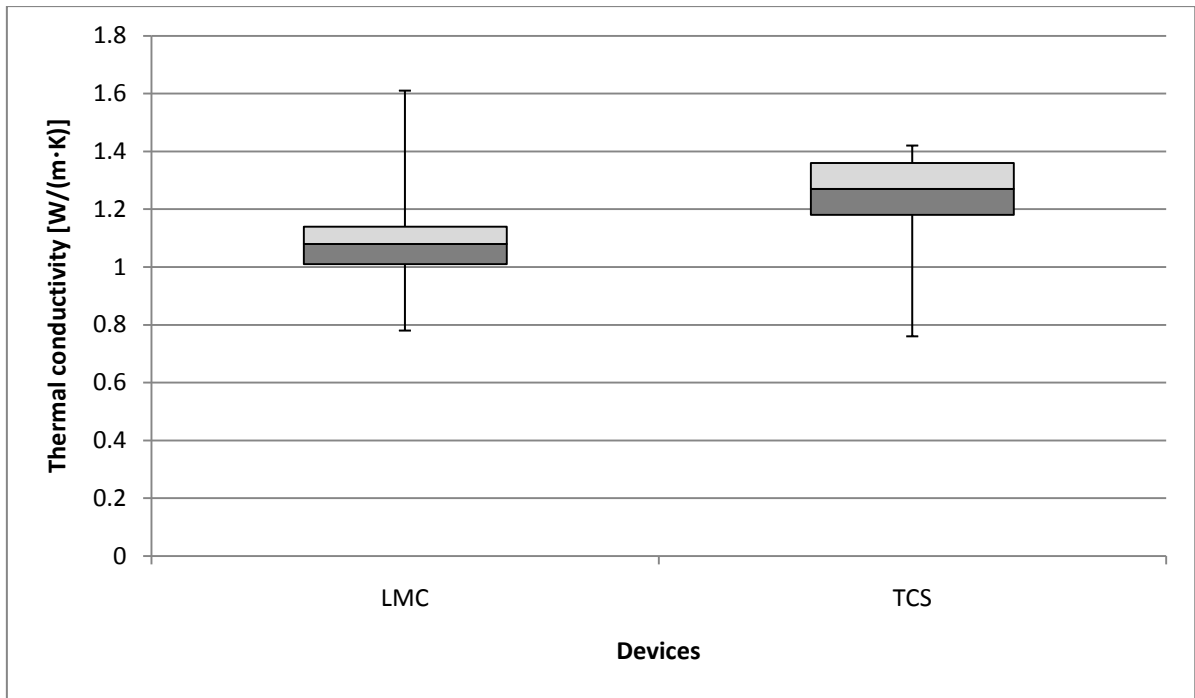


Figure 43: Box plot of the thermal conductivity Öskjuhlíð data series determined by the LMC and the TCS instruments

The analysis of regression with respect to the data observed by the different measuring devices is pictured in figure 44. The linear regression results in the linear function  $y = -0.15x + 1.27$ . The regression is characterized by a Pearson product-moment coefficient of correlation  $r$  of -0.17. This indicates no correlation between the two data sets.

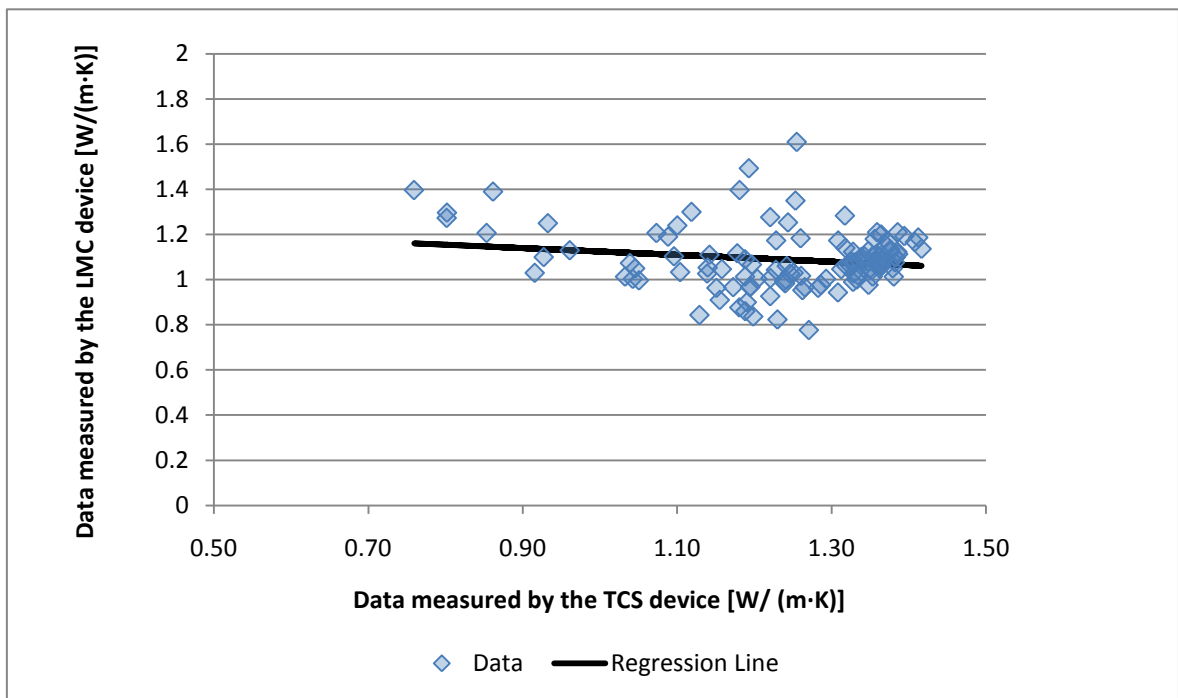


Figure 44: Linear regression of the thermal conductivity of the Öskjuhlíð data series determined by the LMC and the TCS tool

The logarithmic regression leads to a regression line with the logarithmic function  $\log y = -0.15 \log x + 0.05$ . There is no logarithmic correlation between the two data series. This statement is proved by a Pearson product-moment coefficient of correlation of -0.18.

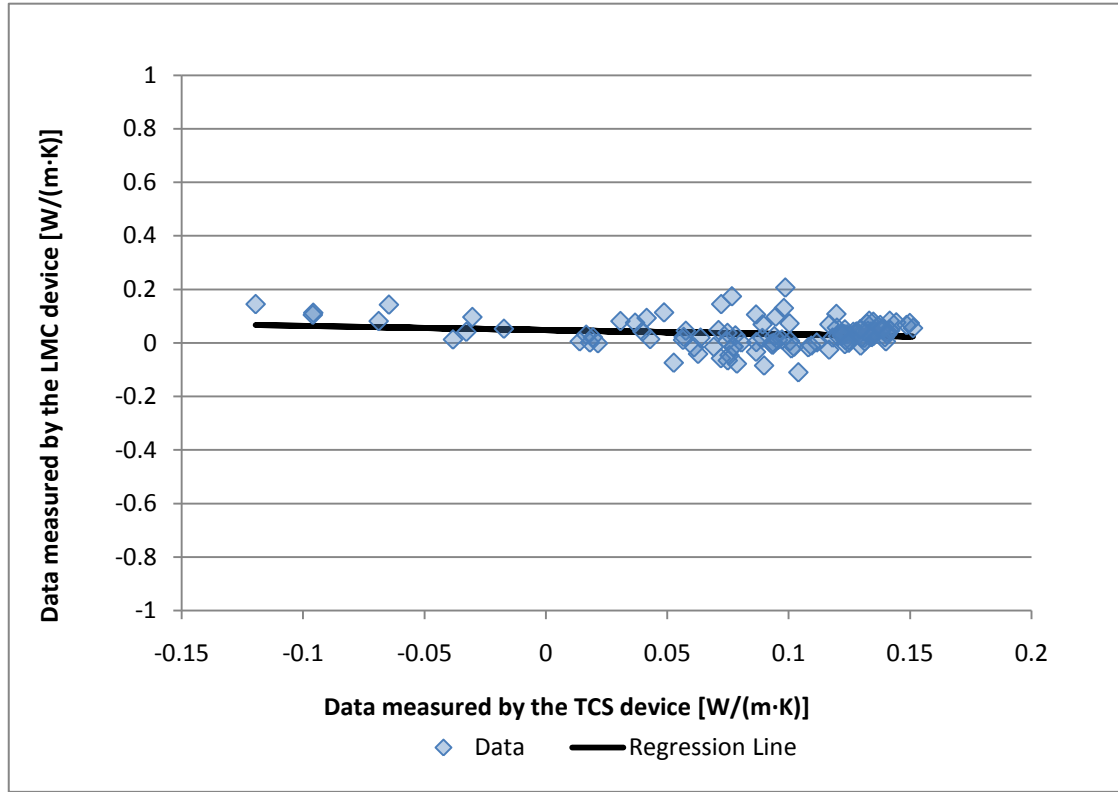


Figure 45: Logarithmic Regression of the thermal conductivity Öskjuhlíð data series determined by the LMC and the TCS tools

## 5.3 Calibration

### 5.3.1 Basic Concept

The correlation of the thermal conductivity determined by the LMC instrument to the physical parameter analyzed by the TCS device requires a model. This model is based on the variables that are used to determine the thermal conductivity. Both devices utilize the temperature difference occurring on the sample surface to derive the physical property. The principle is based on a simple equation

$$\lambda_{sample} = \lambda_{standard} \cdot \frac{\Delta T_{standard}}{\Delta T_{sample}}. \quad \text{Eq. 5.1}$$

The thermal conductivity and the temperature difference of the standard are fixed variables. Therefore the temperature difference which is detected on the surface of the sample should be the only parameter characterizing the derived thermal conductivity. It is in question which further variables can influence the determination of the thermal conductivity. The analyses of the derived data shows that the thermal conductivity is a

function of the reciprocal temperature difference occurring on the sample's surface. This observation matches with equation 5.1. The assumption for the model is:

$$\lambda_{sample} = \frac{x}{\Delta T_{sample}}. \quad \text{Eq. 5.2}$$

In order to understand the reason for varying results with different instruments the thermal conductivity of five samples has been analyzed under changing conditions by the LMC instrument.

### 5.3.2 Validation of Measurement Conditions

The first measurement tends to clarify the relation of the standards' thermal conductivity to the observed thermal conductivity by using five different standards. In figure 46 the fivefold determined thermal conductivity of five dense, ashlar-formed Öskjuhlíð samples is shown relatively to the thermal conductivity of the chosen standards. A fixed heating power of 15% is used to determine the samples. The standards are characterized by thermal conductivities ranging from 0.85 to 6.05 W/(m·K). The determined thermal conductivity of five basaltic, dense samples varies from 0.85 to 1.40 W/(m·K). The maximal thermal conductivity is observed with the standard of 1.35 W/(m·K). The standard with the highest thermal conductivity results in the lowest determined thermal conductivity. The series analyzed with the 0.85 W/(m·K) standard and the 2.75 W/(m·K) yield a thermal conductivity for the basaltic samples which is closest to the arithmetical mean of all results. The arithmetical mean is displayed with a black dashed line in the chart.

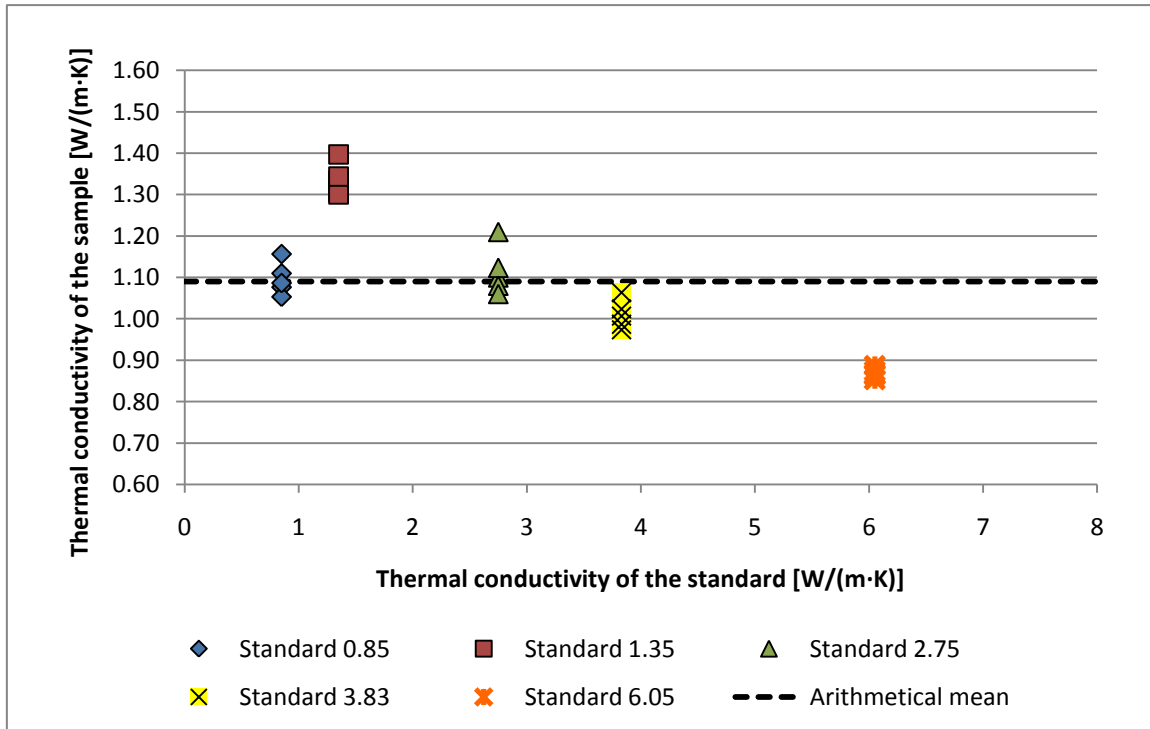


Figure 46: Thermal conductivities as observed by the LMC device with respect to the thermal conductivity of the deployed standard

A second variable that involves the heating process is the heat intensity. Therefore a second measurement is done to identify the dependency of the observed thermal conductivity of the sample with respect to a varying heating power. The five dense, ashlar-formed Öskjuhlíð samples are determined fivefold with a fixed 2.75 W/(m·K) standard but changing heat intensity. The results are shown in figure 47. The relative heat intensity of

the infrared emitter varies from 7 to 50 % of the total heating power. The determined thermal conductivity varies from 0.99 to 1.21 W/(m·K). The results for all different heating intensities approximate the arithmetical mean. It seems that the observed thermal conductivity is changed only slightly by varying the heating intensity.

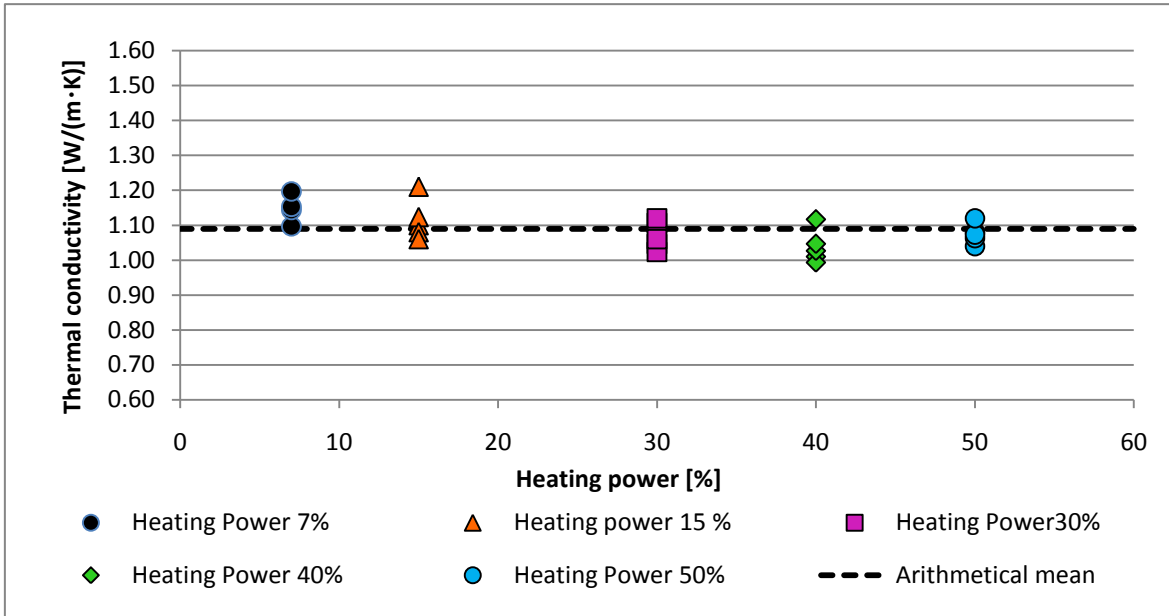


Figure 47: Thermal conductivities as observed by the LMC device with respect to the deployed heating power

### 5.3.3 Derivation

In order to derive the relation between the two analyzed variables with respect to the thermal conductivity it is necessary to display the results with respect to the occurring temperature difference at the sample's surface. In figure 48 the results of the measurement with the varying standards are shown.



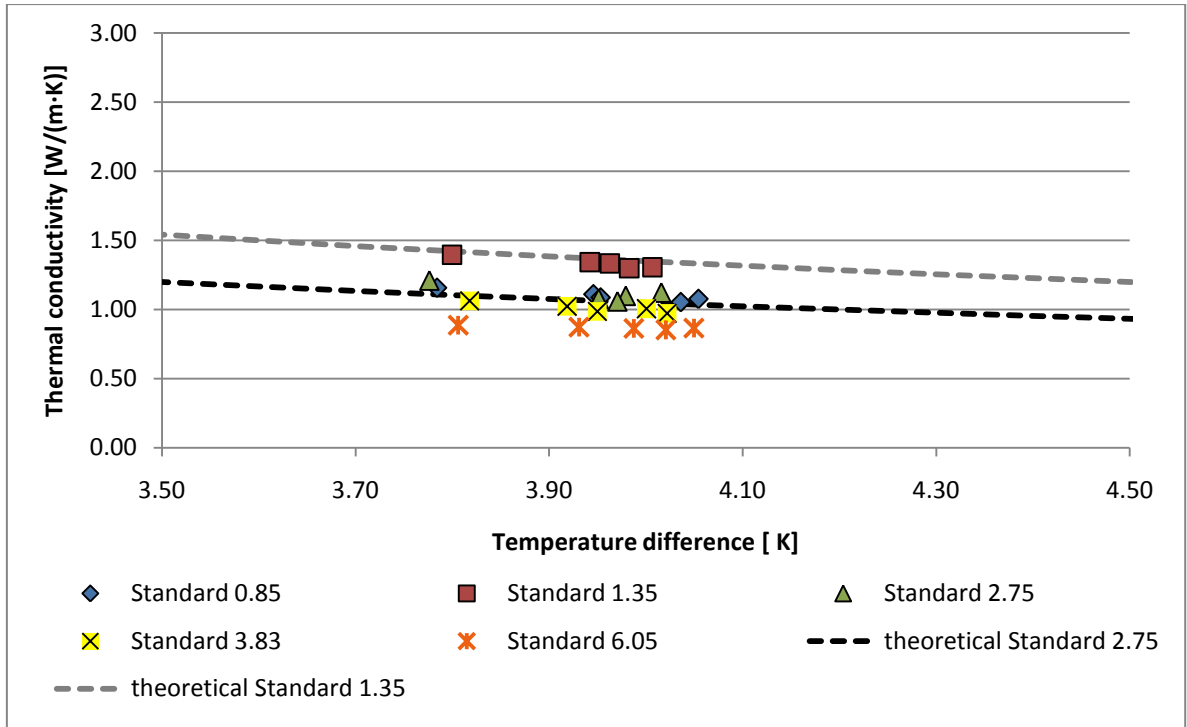


Figure 48: Thermal conductivities as observed by the LMC device with respect to the temperature difference for different deployed standards

It is noticeable that the results determined by different standards belong to different functions, which are parallel to each other. The two dashed lines symbolize the functions belonging to certain standards. They are derived from equation 5.2. The variable  $x$  equals 5.4 for the standard with a thermal conductivity of 1.35 W/(m·K). The function belonging to the standards 0.85, 2.75 and 3.83 W/(m·K) is characterized by a value of  $x=4.2$ .

The results of the second measurement with the differing heating intensity are shown in figure 49. The data is displayed relatively to the temperature difference. In this chart the influence of the heating power is visible. The heating intensity does not change the observed thermal conductivity, but it shifts the temperature difference. Once more the results can be derived by equation 5.2. The dashed lines in this chart symbolize different heating power functions. The heating power of 15% is characterized by a variable  $x=4.2$ . For the heating power of 30 % the value  $x$  equals 10.2. For LMC measurements it can be assumed that an increase of the heating power by 1% results in a rise of 0.4 K at the sample's surface.

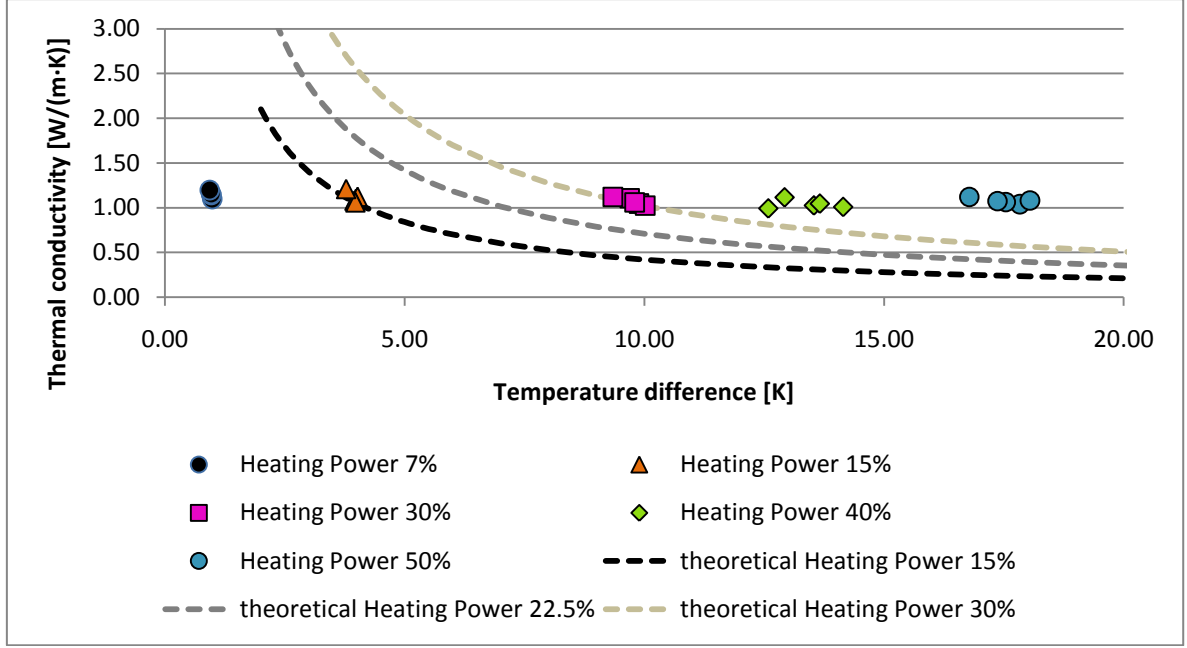


Figure 49: Thermal conductivities as observed by the LMC device with respect to the temperature difference for different deployed heating power

The newly obtained knowledge applied to the determined data sets leads to figure 50. The measurements done by the LMC, displayed in red, were characterized by an used standard of 2.75 W/(m·K) and a heating power of 15% of the LMC emitter. Therefore the data matches to the subsequent function

$$\lambda_{data,LMC} = \frac{4.2}{\Delta T_{data,LMC}} \cdot \quad \text{Eq. 5.3}$$

The measurements done by the TCS instrument, pictured in green, are characterized by a standard of 1.35 W/(m·K). The TCS provides absolute and relative heating intensities, whereas the LMC provides relative electrical heating intensities, therefore it is difficult to compare the heat power of the two instruments, but the arithmetical temperature shift of 0.50 K indicates a 1.25% higher LMC heating power than the heating power used by the LMC instrument. Therefore data observed by the TCS tool belongs to the subsequent equation

$$\lambda_{data,TCS} = \frac{5.4}{\Delta T_{data,TCS}} \cdot \quad \text{Eq. 5.4}$$

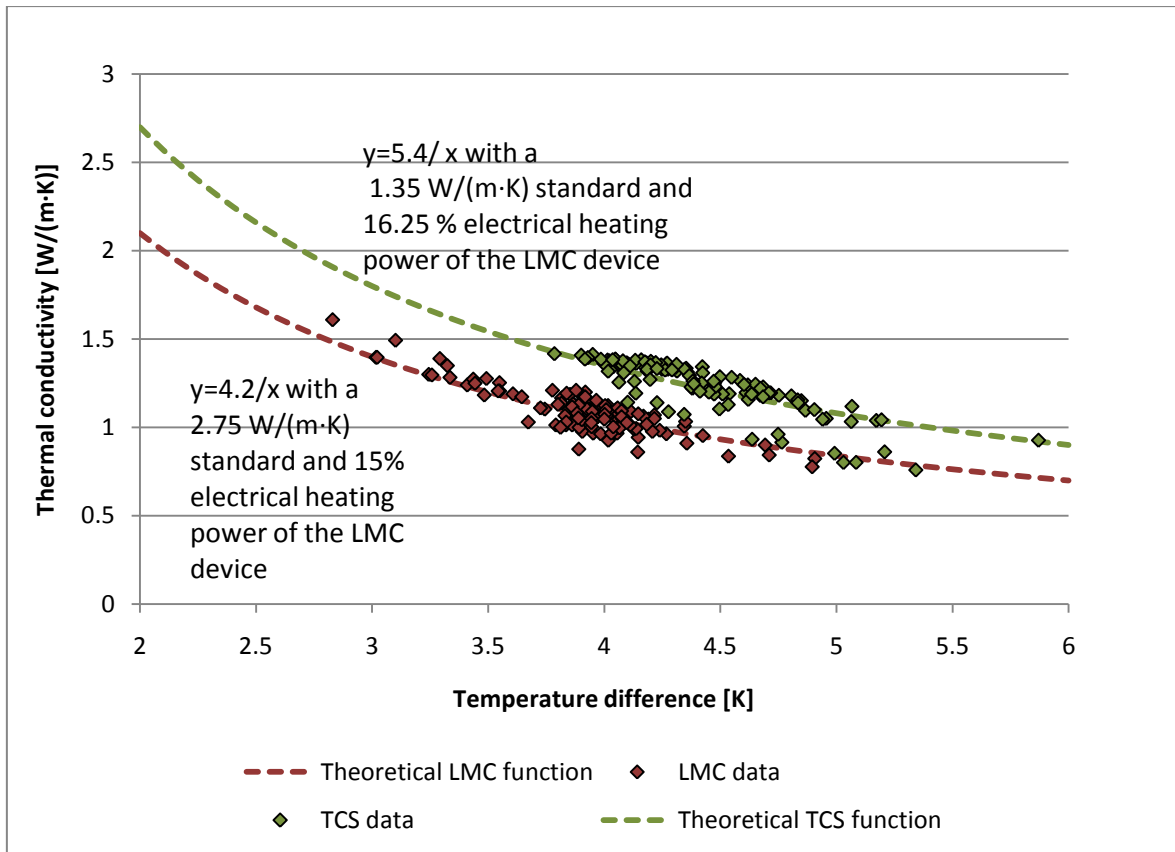


Figure 50: Relation between the thermal conductivity Öskjuhlíð data series and the temperature difference. Displayed are the results for both instruments and their theoretical functions.

## 6 ANALYSIS OF THERMAL DIFFUSIVITY

Table 8 shows an overview of sample type, conducted measurements and preparation of the sample related to the analysis of thermal diffusivity.

*Table 8: Overview of the analysis program of the thermal diffusivity*

Analysis of thermal diffusivity				
Kind of sample	Preparation of the sample	Number of samples	Measuring Device	Number of measurements
Hand probes	uncut, polished	70	LMC	5
Hand probes	cut, polished	150	LMC	3
Cuboids	cut, polished	99	LMC	3
Cuboids	cut, polished	99	TCS	3
Cores	drilled, polished	21	LMC	3
Cores	drilled, polished	21	TCS	3

### 6.1 Interpretation of Data

#### 6.1.1 Hand Probes

70 uncut of 150 hand probes are measured by the LMC device with respect to thermal diffusivity. After cutting these samples they are detected by the LMC device again. The results of both series are shown in figure 51. The thermal diffusivity of the uncut hand probes varies from 0.59 to 5.87 mm<sup>2</sup>/s derived from a temperature difference of 0.96 to 4.41 K. For the cut samples the LMC detected a thermal diffusivity of 0.76 to 1.49 mm<sup>2</sup>/s at a temperature difference of 1.49 to 2.75 K. The large scattering and low temperature difference for the uncut sample's data is caused by the rough surfaces of the samples. A planar cut sample surface however results in a minor scattering of temperature difference and resulting thermal diffusivity. This comparison of the data series shows that it is necessary not only to varnish but also cut the samples to ensure planar sample surfaces.

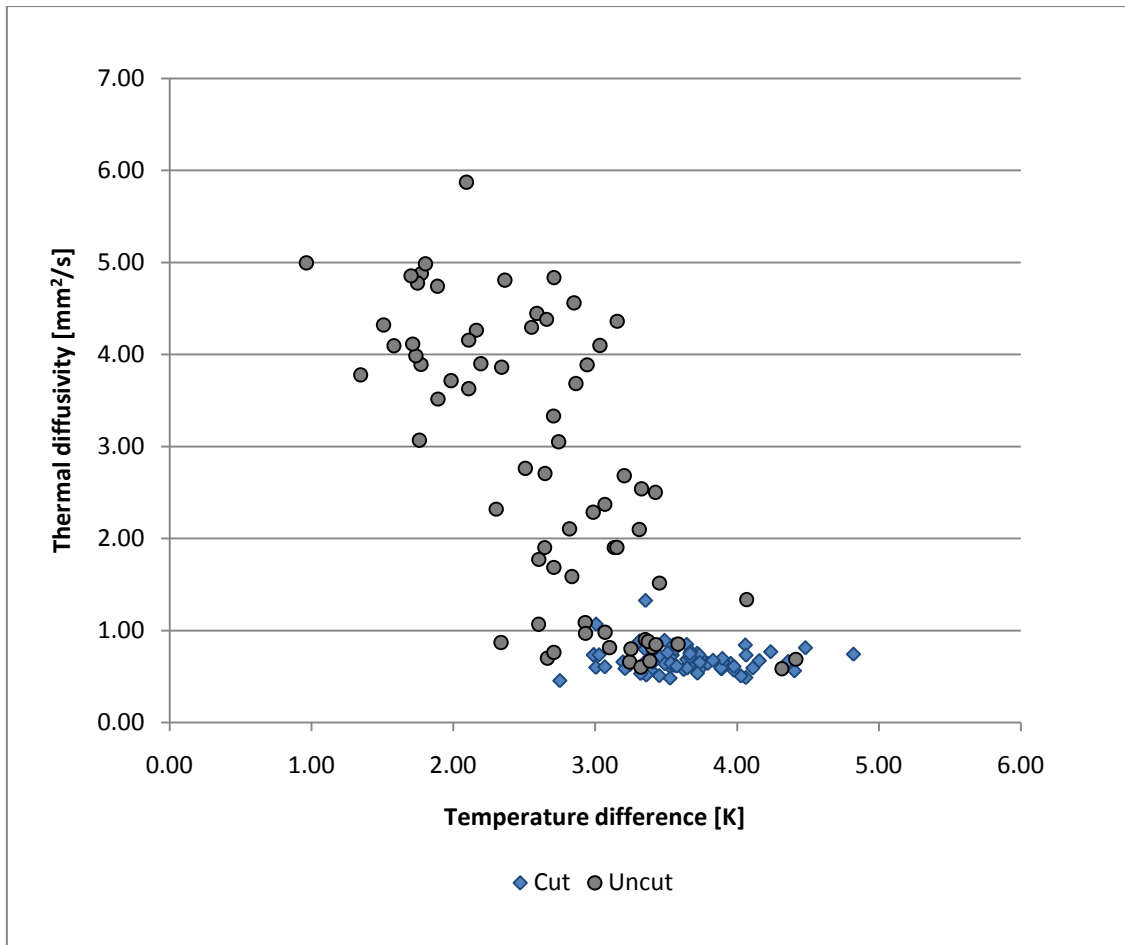


Figure 51: Relation between the thermal diffusivity Öskjuhlíð data series and the temperature difference classified by uncut and cut samples

All 150 cut hand probes are determined with respect to thermal diffusivity by the LMC. They are separated into 15 sample groups based on the location in the outcrop. By this differentiation it is possible to analyze the physical property in relation to the flow direction of the lava stream. The lava has been flowing from southeast to northwest. Therefore the samples are divided in a dense and a vesicular southeastern group and a dense and a vesicular northwestern group. The dense samples originate from the lower bed of the lava flow, whereas the vesicular samples belong to the upper bed of the lava flow. Each sample is measured threefold. The arithmetical means of the measurements are displayed in figure 52. The LMC observes a thermal diffusivity of 0.46 to 1.33 mm<sup>2</sup>/s and a temperature difference range of 2.75 to 5.75 K. All four groups range in a similar magnitude. There is a recognizable minor tendency of decreasing thermal diffusivity with increasing pore size. A dependence on the flow direction is neither in the upper nor the lower layer detectable.

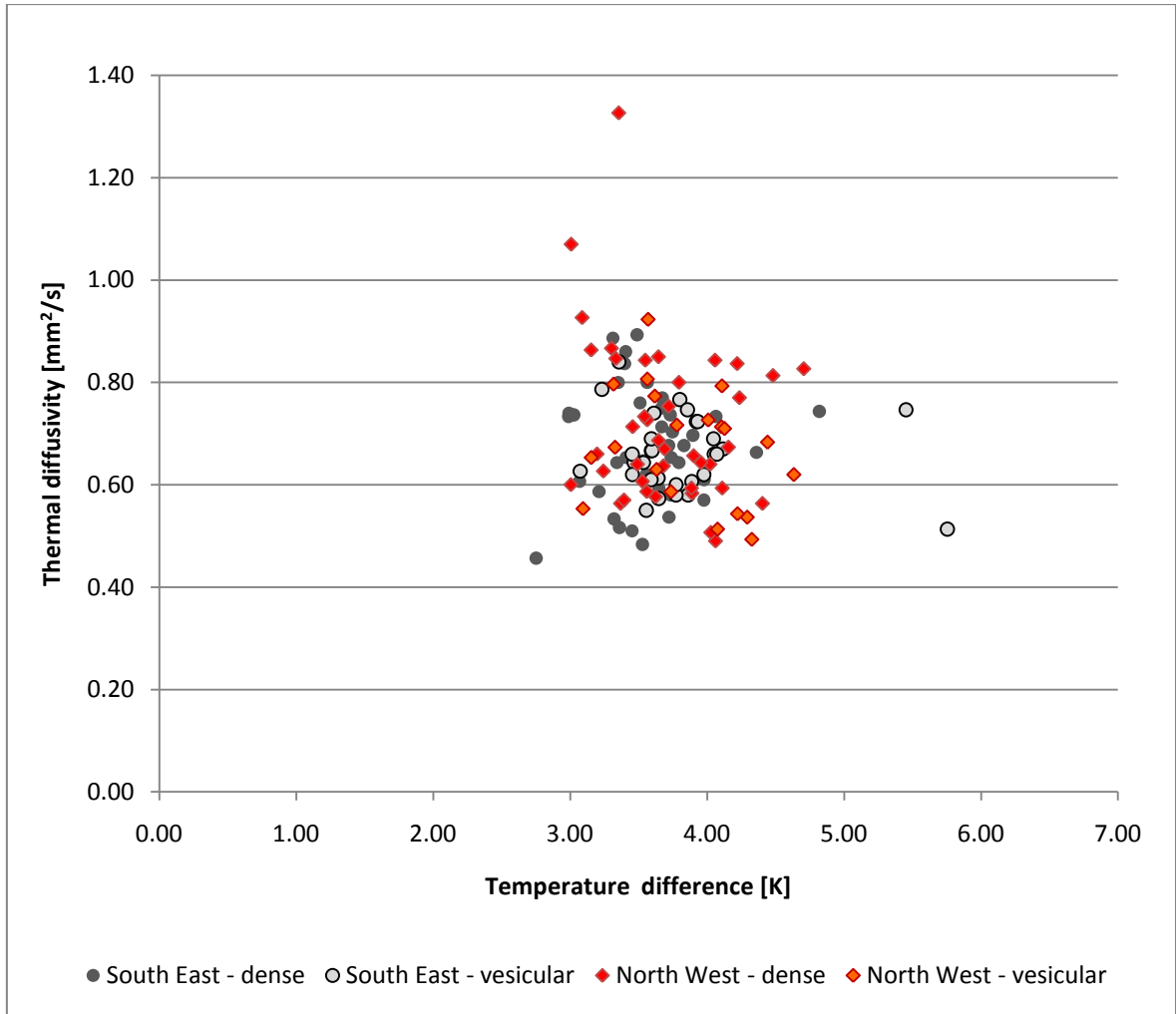


Figure 52: Relation between the thermal diffusivity Öskjuhlíð data series and temperature difference classified by the location in the outcrop

### 6.1.2 Cuboids

17 dense and 16 vesicular cuboids, each divided into three samples, have been analyzed with respect to thermal diffusivity with the LMC and TCS instrument. The comparison of the results enables the validation of the parameter derived by the LMC. The LMC observes a thermal diffusivity of 0.47 to 0.85 mm<sup>2</sup>/s at a temperature difference of 3.02 to 4.91 K. The thermal diffusivity, which is defined by the TCS, ranges from 0.52 to 0.79 mm<sup>2</sup>/s and a temperature difference of 2.06 to 3.18 K. The LMC device gives a generally higher temperature difference than the TCS instrument. Furthermore, the thermal diffusivity, measured by LMC, varies more than the comparing instrument. Both measurements do not show any relation between the matrix variety and thermal diffusivity, though the TCS heats the vesicular samples more than the dense ones.

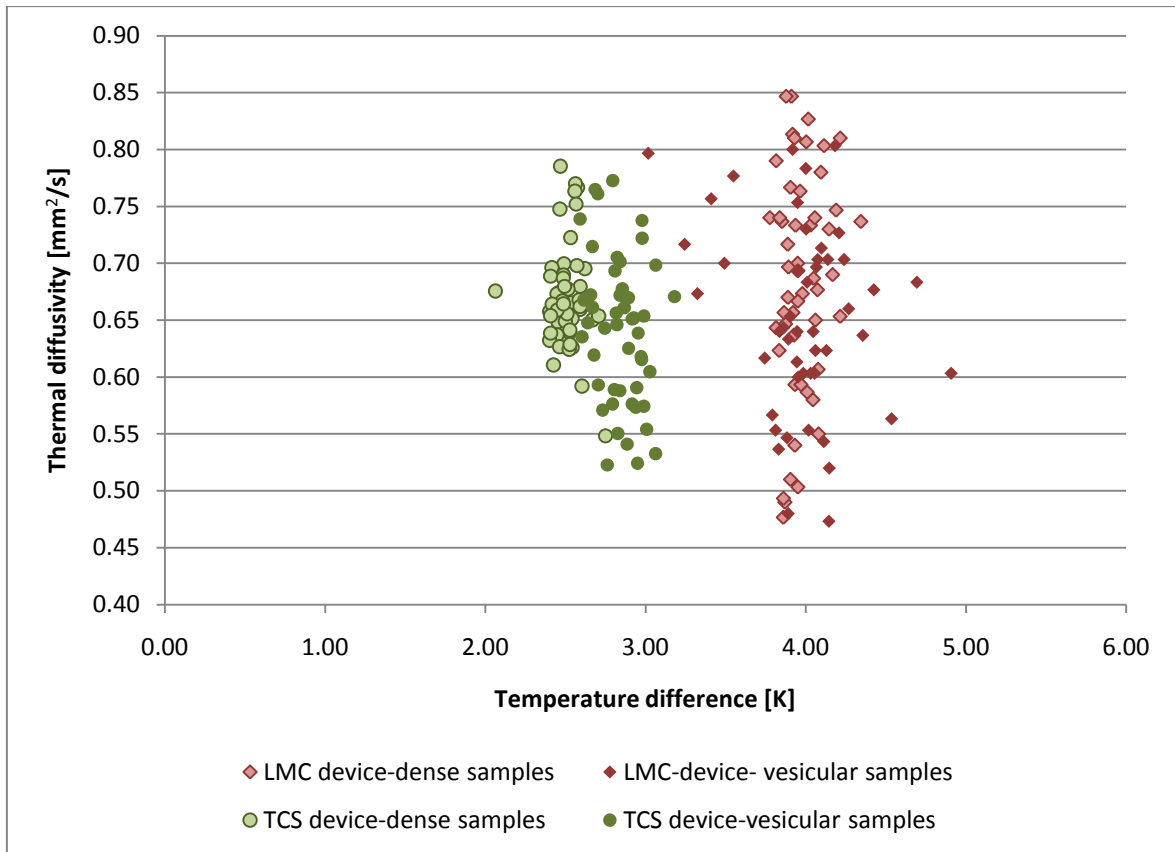


Figure 53: Relation between the thermal diffusivity of the Öskjuhlíð cuboids and the temperature difference determined by the LMC and the TCS devices

### 6.1.3 Cores

The comparison of 21 core samples from Orkustofnun measured with both optical scanning devices is pictured in figure 54. Presented are the results of the triple measurements and the calculated arithmetical means. The thermal diffusivity is analyzed with the LMC and TCS device. The measurements conducted with LMC show a mean thermal diffusivity varying from 0.53 to 0.89  $\text{mm}^2/\text{s}$  at a temperature difference from 2.83 to 4.89 K. The 63 measurements of the LMC contain thermal diffusivities of 0.40 to 1.02  $\text{mm}^2/\text{s}$  at temperature differences from 2.60 to 5.25 K. The mean results of the TCS range from 0.54 to 0.91  $\text{mm}^2/\text{s}$  resulting of a temperature difference from 2.45 to 3.33 K. All results, observed with the TCS device, include thermal diffusivities from 0.54 to 0.95  $\text{mm}^2/\text{s}$ . The results from the LMC device compared to the TCS instrument spread more, so that it is recommended for the new tool to measure samples three times. The arithmetical mean of the thermal diffusivity derived by both devices is similar, but the samples are heated more by the LMC.

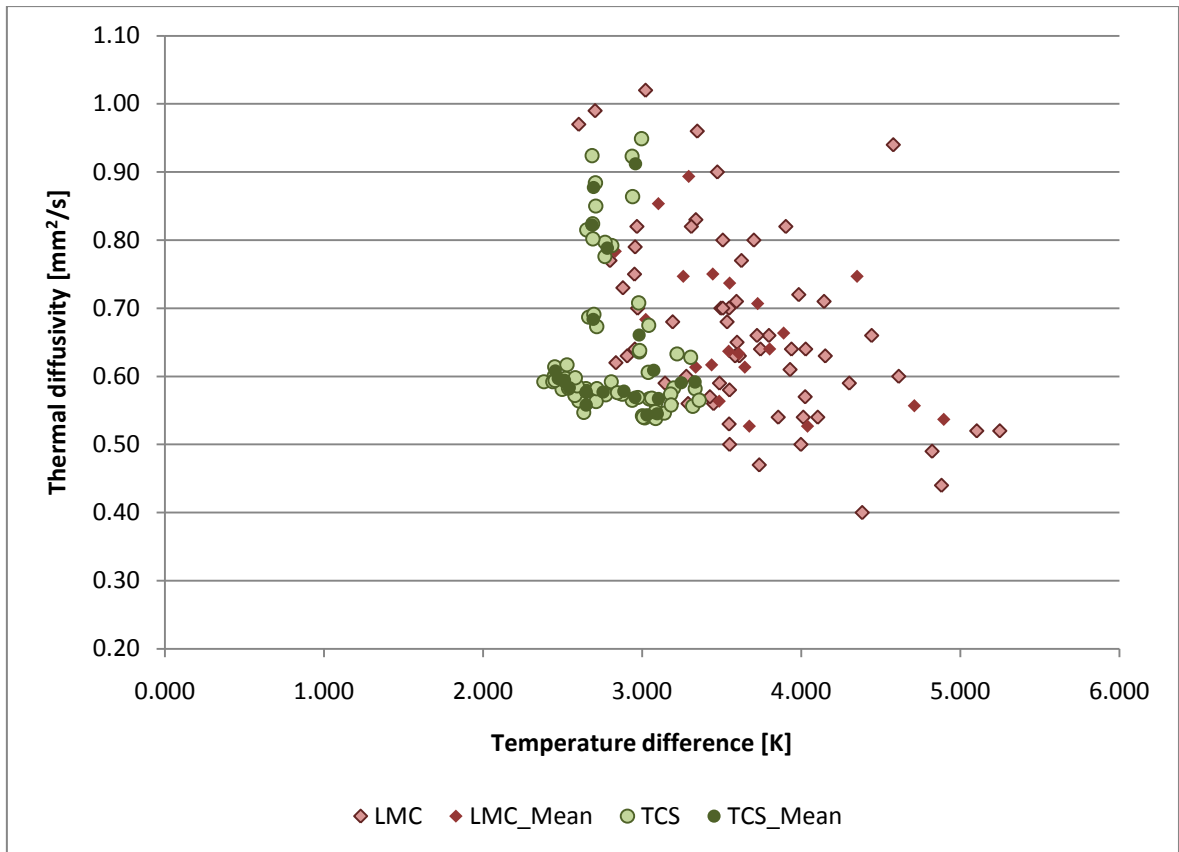


Figure 54: Relation between the thermal diffusivity Öskjuhlíð cores and the temperature difference determined by the LMC



#### 6.1.4 Entire Sample Base

The results of 150 cut hand probes, 99 cuboids and 21 cores which are analyzed with respect to thermal diffusivity by the LMC device are shown in figure 55. The data is separated into two series characterized by the matrix of the rock sample. The physical property is determined three times for each sample and the arithmetical mean of these measurements is displayed. The thermal diffusivity varies from 0.44 to 1.33  $\text{mm}^2/\text{s}$  resulting from a temperature difference of 2.75 to 5.75 K. Both series show similar results. There is no correlation between texture of the rock and thermal diffusivity based on these two observed series.

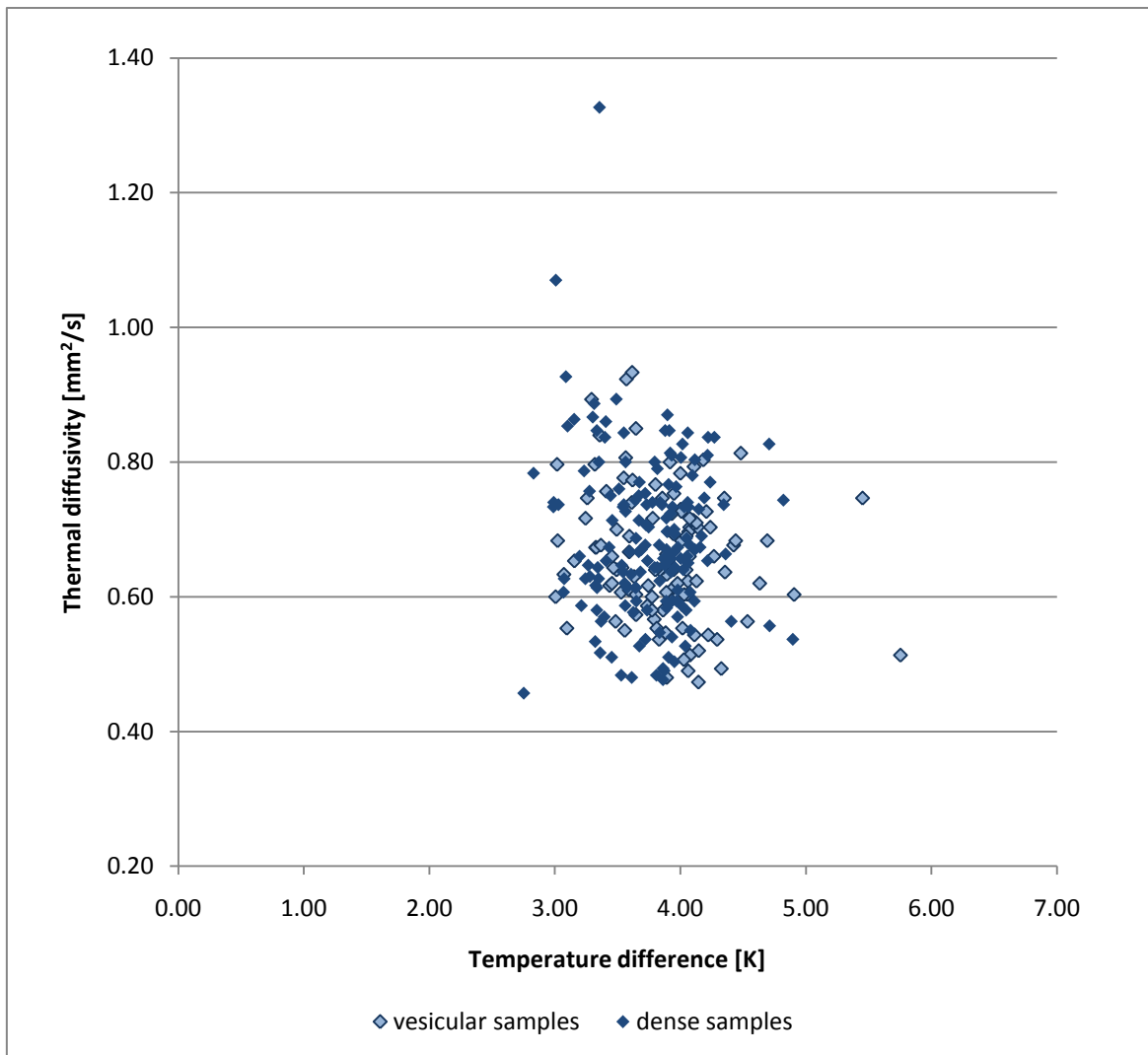


Figure 55: Relation between the thermal diffusivity Öskjuhlíð data series and the temperature difference determined by the LMC classified by the texture of the samples

## 6.2 Statistical Analysis

### 6.2.1 Entire Sample Base Determined by the LMC Device

270 collected samples in Iceland have been analyzed 810 times by the LMC device with respect to thermal diffusivity. The statistical analysis evaluates the quality of this determination. The series is displayed in a histogram to visualize the distribution of values. The data set varies from 0.30 to 1.80 mm<sup>2</sup>/s. The histogram is characterized by 30 bins, which range 0.05 mm<sup>2</sup>/s. The maximal frequency of 133 counts is observed in a range of 0.60 to 0.65 mm<sup>2</sup>/s.

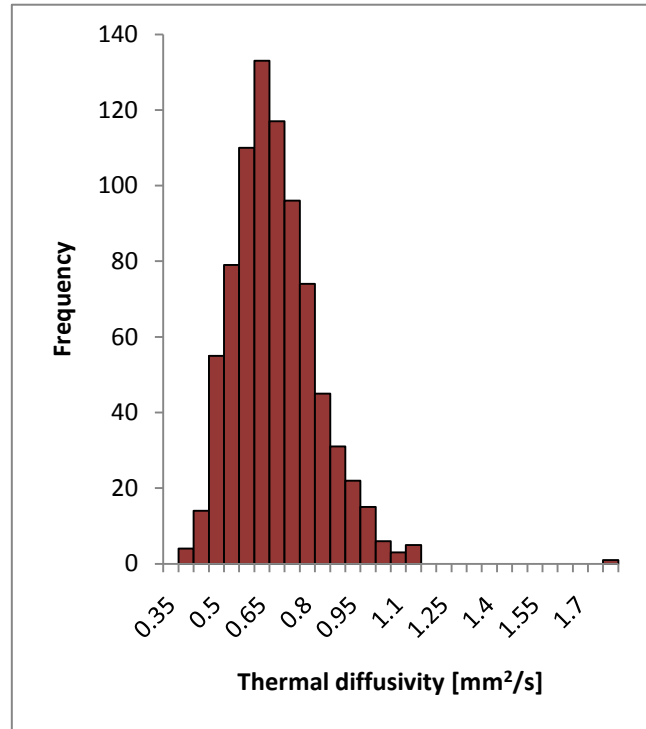


Figure 56: Histogram of the thermal diffusivity Öskjuhlíð data series determined by the LMC

The statistical measures of the series characterize the distribution. The results are represented in table 9. As proven by the location parameters the data set is a right – skewed distribution, based on the valid condition  $\bar{x} > \tilde{x} > x_{mod}$ . This statement is verified by a skewness of 1.13. The positive excess indicates a steep unimodal distribution. The dispersion of the distribution is visualized by a standard deviation of 0.14 mm<sup>2</sup>/s and a coefficient of variation of 21% of the arithmetical mean.

Table 9: Statistical descriptive parameters of the thermal diffusivity Öskjuhlíð data series determined by the LMC instrument

Arithmetical mean	Median	Mode	0.25-quartile	0.75-quartile	Minimum	Maximum	Geometric mean
0.68	0.66	0.65	0.58	0.75	0.39	1.77	0.66
Harmean mean	Variance	Standard deviation	Coefficient of variation	Range	Interquartile range	Skewness	Kurtosis
0.65	0.02	0.14	0.21	1.38	0.17	1.13	4.52

The frequency and related normal cumulative distribution of the LMC analysis is shown in figure 57. The distributions approximate asymptotically from a probability or frequency of zero to one. The functions range in relative distance to the arithmetical mean of the distribution from -0.29 to 1.09 mm<sup>2</sup>/s. The frequency distribution almost matches the normal cumulative distribution indicating the high quality of the data.

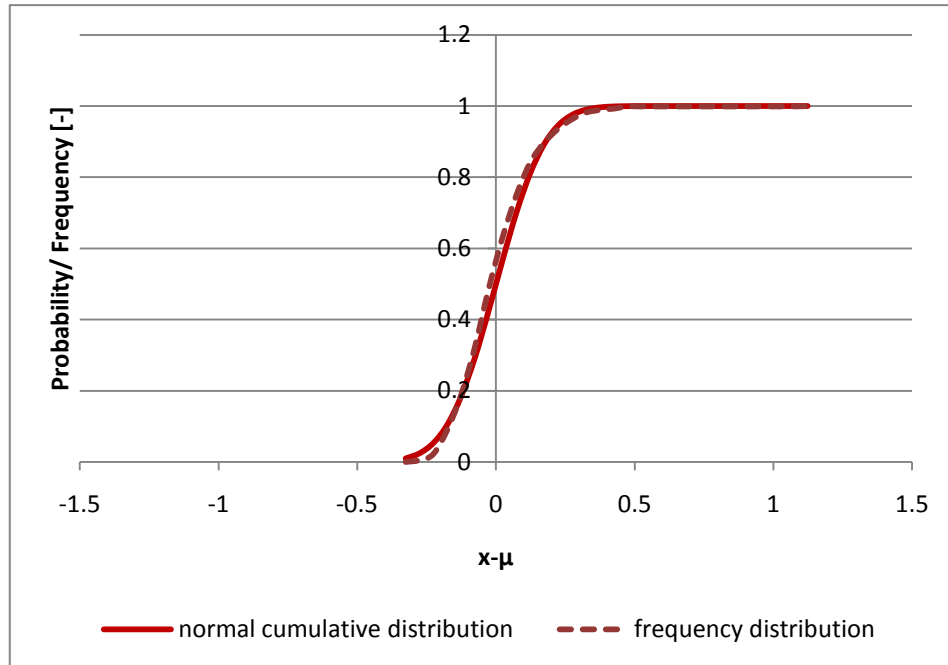


Figure 57: Frequency and cumulative normal distribution of the thermal diffusivity Öskjuhlíð data series determined by the LMC device

In figure 58 the related normal distribution of the data is displayed. The maximum of the function is situated at the arithmetical mean with a probability density of 2.84. The data ranges from a distance of the negative doubled standard deviation to a distance of the positive 7.8 fold standard deviation apart from the arithmetical mean. The probability density distribution visualizes the majority of the data varying in a distance of three standard deviations from the arithmetical mean, and a singular outlier being responsible for the wide range.

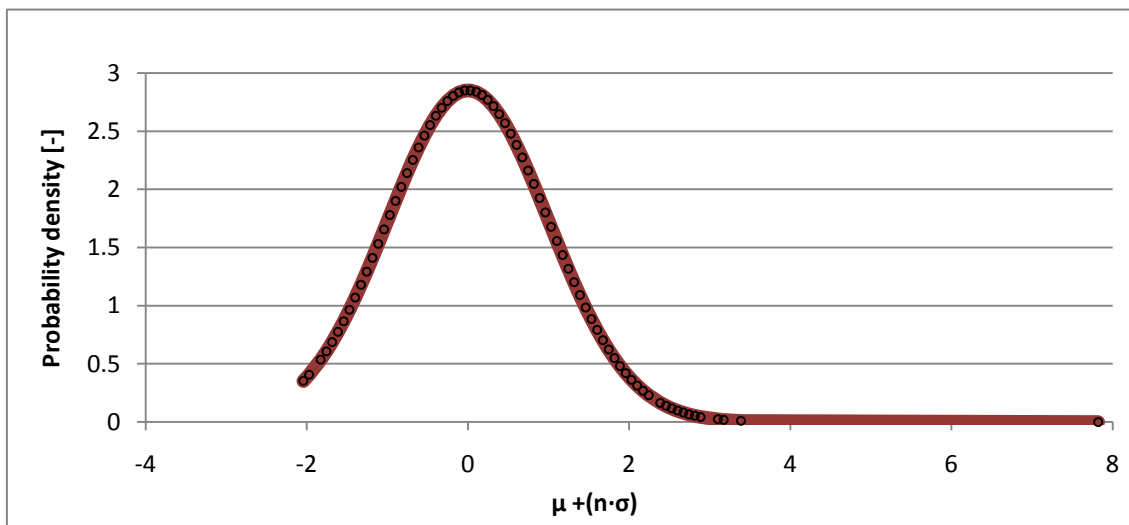


Figure 58: Probability density distribution of the thermal diffusivity Öskjuhlíð data series determined by the LMC instrument

The box plot of the data set ranging from a minimum of  $0.39\text{mm}^2/\text{s}$  to a maximum of  $1.77\text{mm}^2/\text{s}$  underlines the assumption of outliers. The majority of data represented by the interquartile range varies from  $0.58$  to  $0.75\text{mm}^2/\text{s}$ .

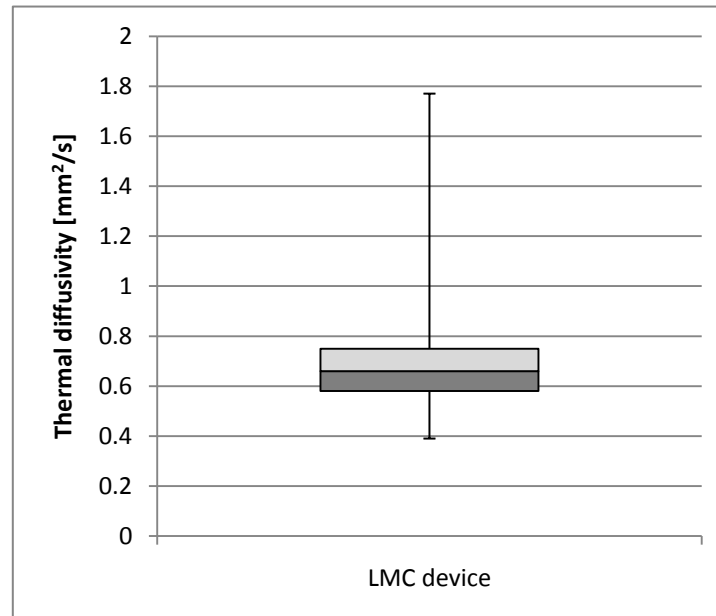


Figure 59: Box plot of the thermal diffusivity Öskjuhlíð data series determined by the LMC device

### 6.2.2 Comparison of LMC and TCS Instrument

The statistical comparison of both optical scanning devices is continued by the data sets of the determination of the thermal diffusivity. The 120 samples which have been analyzed provide the main unit for the analysis. The distributions of the two data sets are shown subsequently. The histograms are characterized by unimodal distributions classified by 13 bins with a range of  $0.05\text{ mm}^2/\text{s}$ . They range from  $0.40$  to  $1.00\text{ mm}^2/\text{s}$ . The maximal frequency values determined by the LMC vary from  $0.55$  to  $0.65\text{ mm}^2/\text{s}$  with a quantity of 48 counts. The TCS most determined thermal diffusivity varies from  $0.65$  to  $0.70\text{ mm}^2/\text{s}$  with 23 counts.

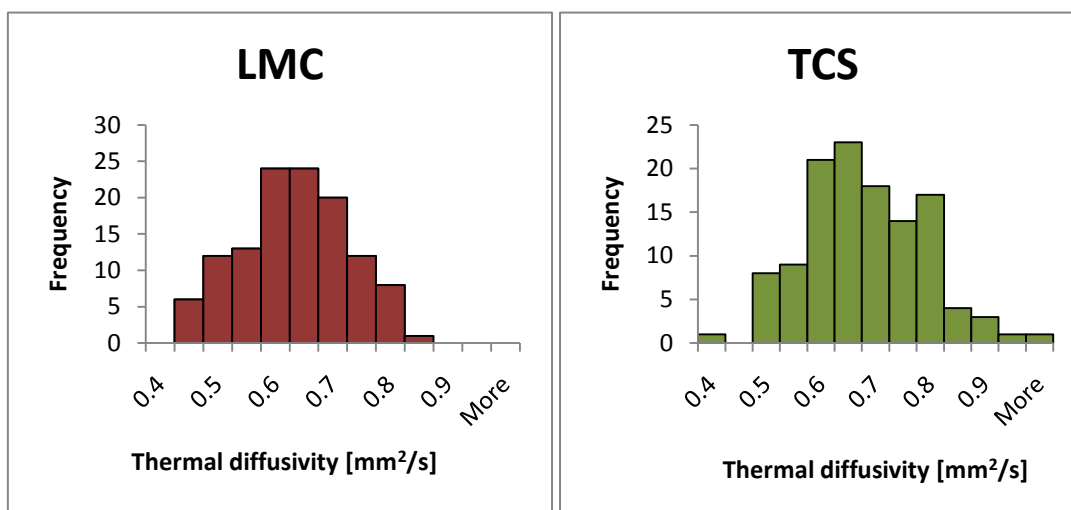


Figure 60: Histograms of the thermal diffusivity Öskjuhlíð data series determined by the LMC and the TCS

The statistical measures of both data sets are compared in table 10. The location parameters of both series satisfy the condition  $\bar{x} \approx \tilde{x} \approx x_{mod}$ , therefore the distributions analyzed by both instruments are approximately symmetrical. The nearly neutral skewness of the LMC series indicates once more a symmetrical distribution. The negative kurtosis describes a shallow unimodal distribution. The parameters of dispersion, characterized by standard deviation and coefficient of variation, of the LMC series are 0.09 mm<sup>2</sup>/s and 14% of the arithmetical mean. The positive skewness of the TCS data series represents a right-skewed distribution. The kurtosis suggests an approximate standard distribution. The measures of dispersion characterize the TCS with an absolute measuring error of 0.11 mm<sup>2</sup>/s and a relative error of 17%. The location measures of both data sets are similar. Caused by a larger range, the dispersion measures of the TCS exceed the dispersion parameters of the LMC instrument.

*Table 10: Statistical descriptive parameters of the thermal diffusivity Öskjuhlíð data series determined by the LMC and the TCS*

Instrument	Arithmetical mean	Median	Mode	0.25-quartile	0.75-quartile	Minimum	Maximum	Geometric mean	Harmean mean
LMC	0.67	0.67	0.64	0.6	0.74	0.47	0.89	0.66	0.65
TCS	0.66	0.65	0.65	0.57	0.74	0.39	0.97	0.65	0.64
Instrument	Variance	Standard deviation	Coefficient of variation	Range	Interquartile range	Absolute deviation	Median absolute deviation	Skewness	Kurtosis
LMC	0.01	0.09	0.14	0.42	0.14	0.08	0.07	-0.02	-0.59
TCS	0.0	0.11	0.17	0.58	0.16	0.09	0.00	0.29	-0.09

The frequency and normal cumulative distributions of both data series are pictured in figure 61. The displayed frequencies and probabilities range from zero to one. The inflection point of the functions is located at the arithmetical mean. The distributions are shown relatively to the distance of the data point to the arithmetical mean. The samples measured by the LMC have a thermal diffusivity with a range from 0.21 mm<sup>2</sup>/s less up to 0.23 mm<sup>2</sup>/s larger than the arithmetical mean. The distributions related to the TCS data set vary from 0.26 mm<sup>2</sup>/s below and 0.29 mm<sup>2</sup>/s above the arithmetical mean. Both frequency distributions almost match their related normal cumulative distribution indicating a high quality of the analyses.

The probability density distributions, which are related to the thermal diffusivity data sets determined by the LMC and the TCS device are shown in figure 62. The largest probability density for both symmetrical distributions is reached at their arithmetical mean. The distribution of the LMC instrument is characterized by a larger maximal probability density than the TCS' distribution. The data series of the LMC varies with twice standard deviation from the arithmetical mean. The deviation of the TCS' data ranges -2.5 fold up to 2.8 fold of the standard deviation from the arithmetical mean. The chart shows that the data being observed by the TCS is characterized by outliers compared to the LMC data.

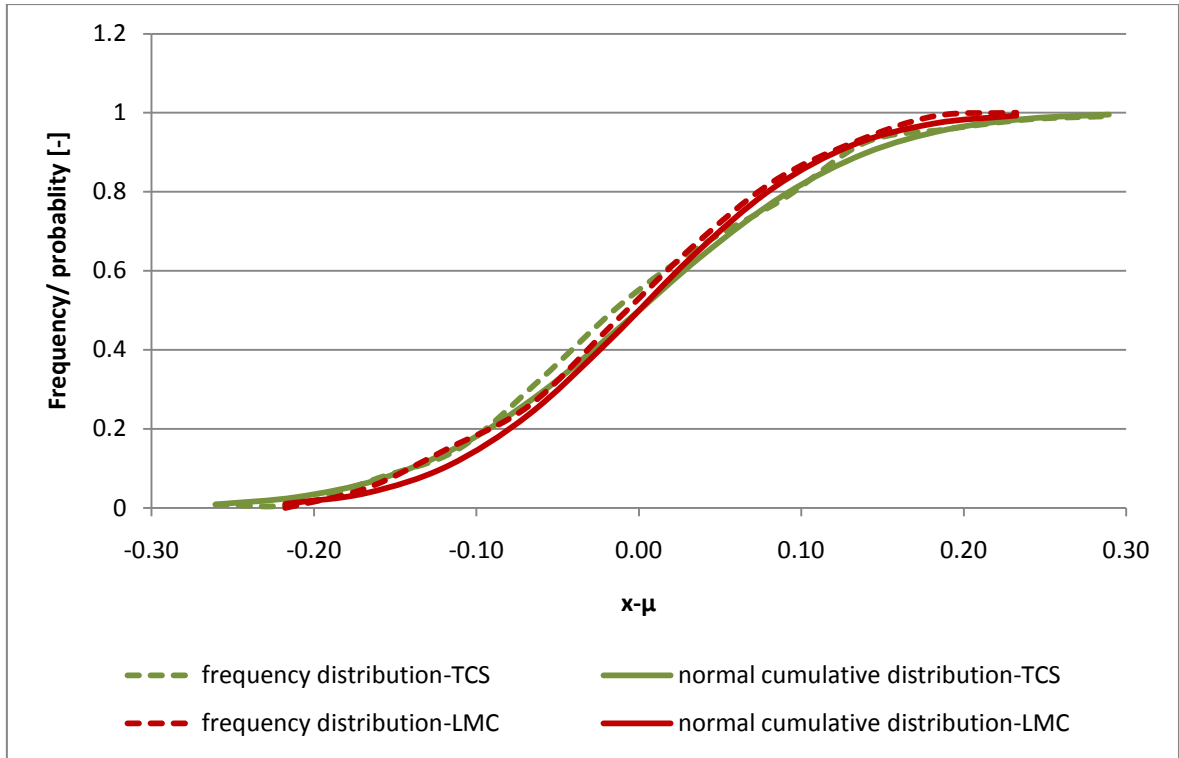


Figure 61: Frequency and cumulative distribution of the thermal diffusivity *Öskjuhlíð* data series determined by the LMC and the TCS devices

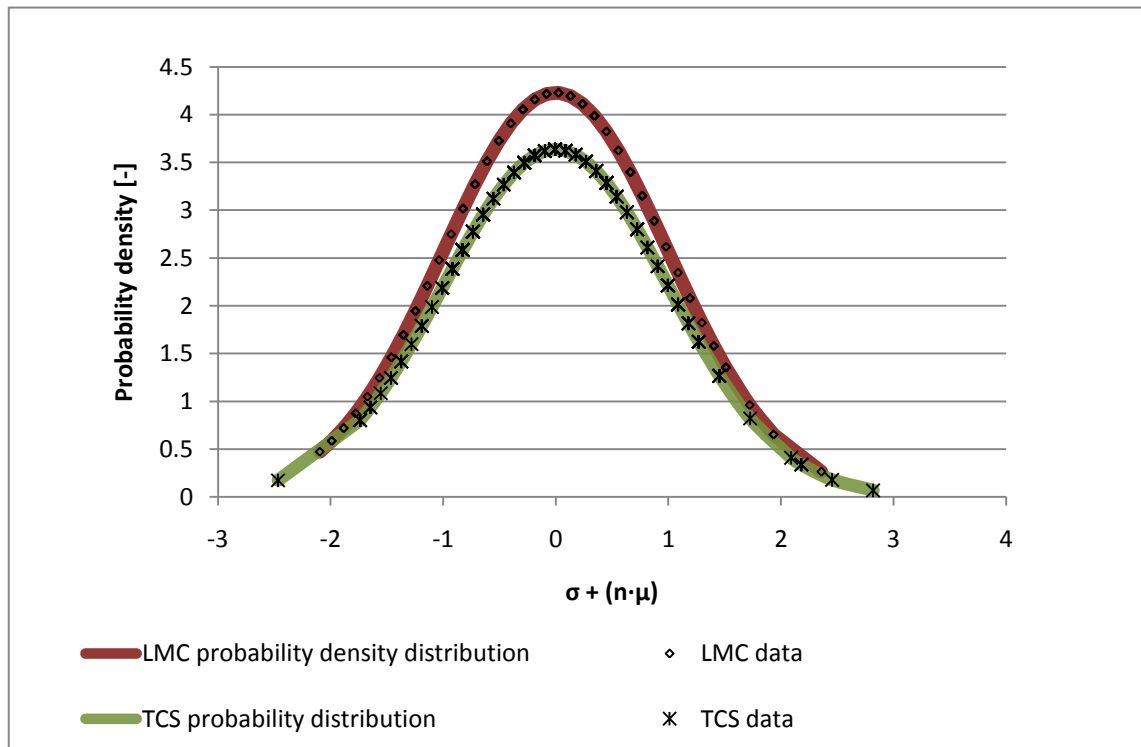


Figure 62: Probability density distributions of the thermal diffusivity *Öskjuhlíð* data series determined by the LMC and the TCS

In figure 63 the box plots of both data series are displayed. The LMC device is characterized by a minimum of  $0.47 \text{ mm}^2/\text{s}$  and a maximum of  $0.89 \text{ mm}^2/\text{s}$ . The interquartile range contains  $0.14 \text{ mm}^2/\text{s}$ . The data set of the TCS instrument belongs to a range of  $0.58 \text{ mm}^2/\text{s}$  from  $0.39$  to  $0.97 \text{ mm}^2/\text{s}$ , including an interquartile range of  $0.16 \text{ mm}^2/\text{s}$ . The box plot clarifies the lower quality of the TCS data set compared to the LMC data series.

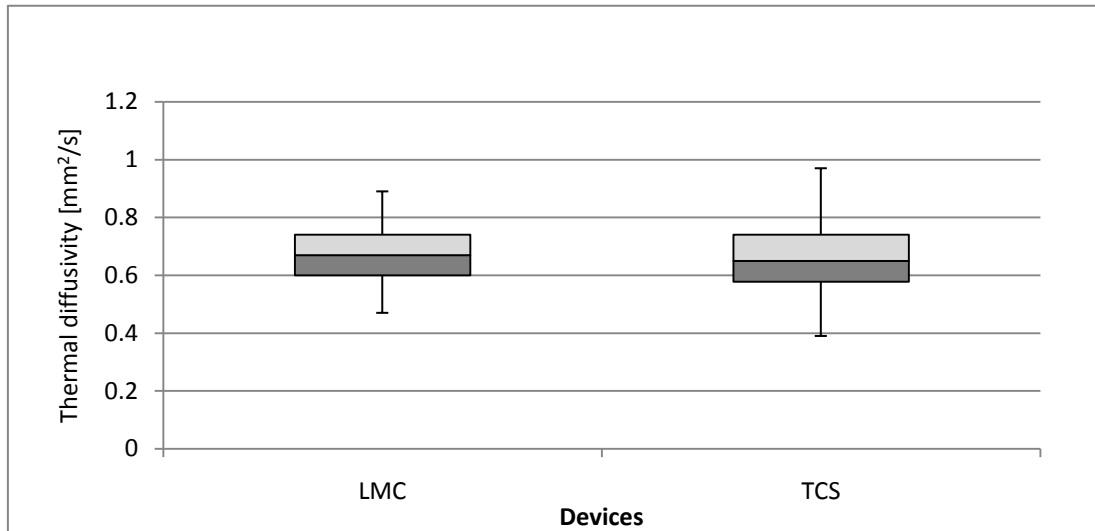


Figure 63: Box plots of the thermal diffusivity Öskjuhlíð data series determined by the LMC and the TCS instrument

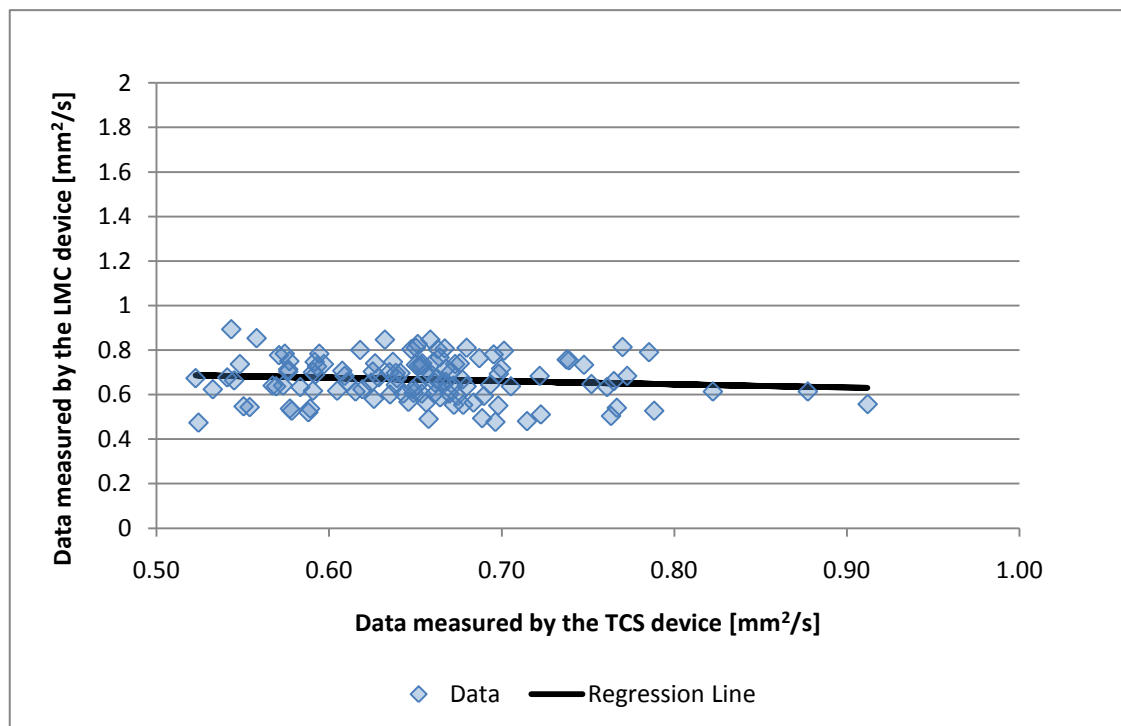


Figure 64: Linear regression of the thermal diffusivity Öskjuhlíð data series determined by the LMC and the TCS device

The analysis of regression for both data sets is pictured in figure 64. The linear regression results in a regression line described by the function  $y = -0.15x + 0.76$ . The Pearson product-moment coefficient of correlation of -0.11 indicates that there is no linear correlation.

The logarithmic regression is diagrammed in figure 65. The regression line belongs to the logarithmic function  $\log y = -0.13 \log x - 0.21$ . The regression is characterized by a Pearson product-moment coefficient of correlation of -0.10. Consequently there is no logarithmic correlation between the data set of the LMC and the TCS.

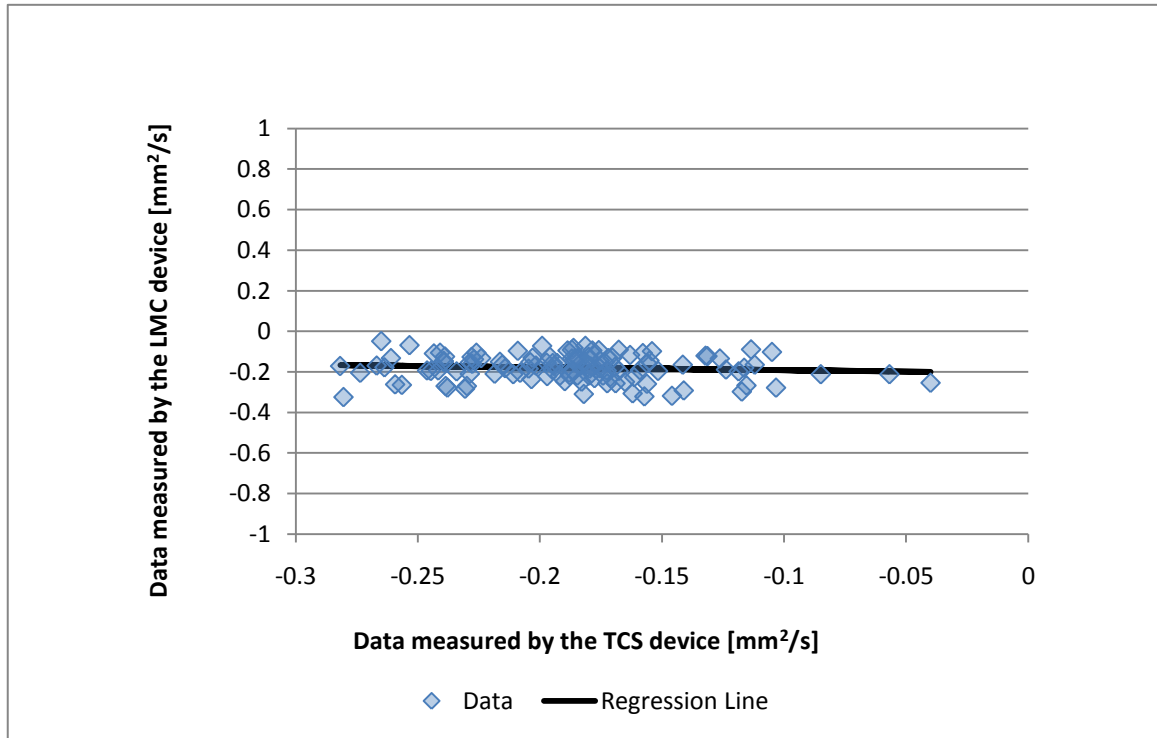


Figure 65: Logarithmic regression of the thermal diffusivity Öskjuhlíð data series determined by the LMC and the TCS

## 6.3 Calibration

### 6.3.1 Basic Concept

The determination of the thermal diffusivity based on the optical scanning method is dependent on the time  $\tau$  at which the temperature maximum is reached at a certain point. The dependency of the physical property is expressed in equation 2.10 and 3.3. Unfortunately both devices do not provide this time  $\tau$  in their interpreted data. However, there is a difference in the results observed by the LMC instrument and the TCS. Caused by the influence the standard's properties and the deployed heating power on the observed thermal conductivity, the same program with the LMC has been done with respect to thermal diffusivity.



### 6.3.2 Validation of Measurement Conditions

The five Öskjuhlíð samples have been determined fivefold with varying standards. The standards' thermal conductivity ranges from 0.85 to 6.05 W/(m·K). In figure 66 the results of the experiment are shown. The black dashed line symbolizes the arithmetical mean of all determined thermal diffusivities. The largest thermal diffusivity is detected with the 2.75 W/(m·K) standard. The 1.35 W/(m·K) achieves thermal diffusivities above average, however the with aid of the 3.83 and 6.05 W/(m·K) standards analyzed samples have thermal diffusivities below the arithmetical mean. The physical property ranges from 0.48 to 0.83 mm<sup>2</sup>/s.

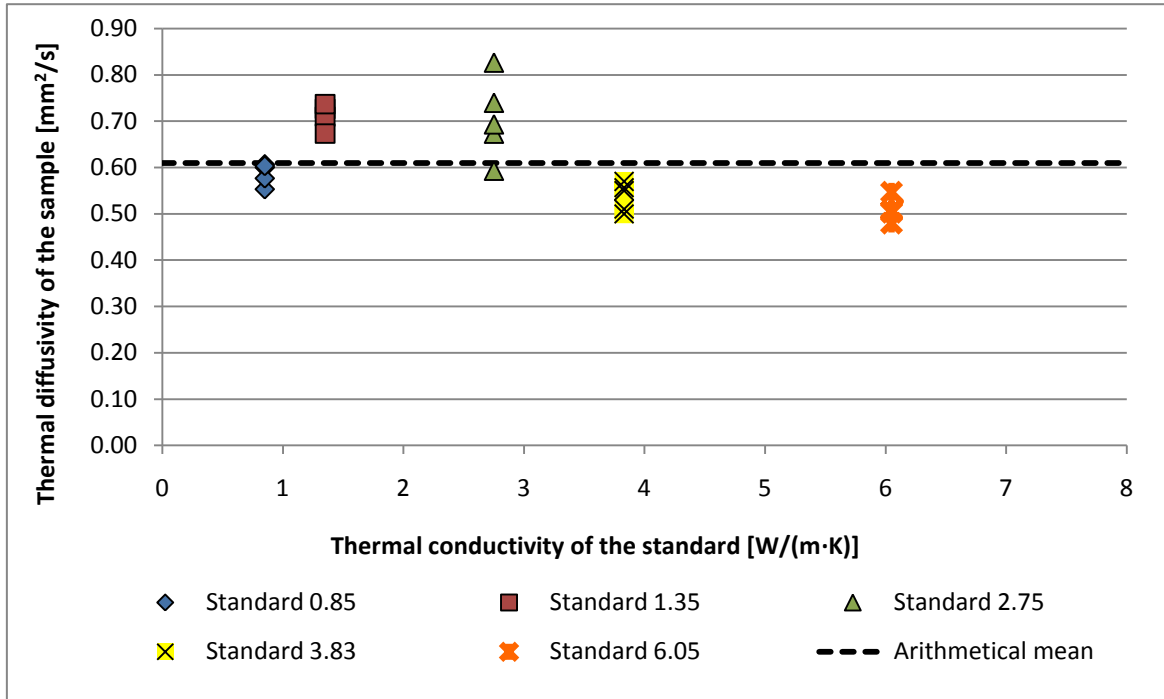


Figure 66: Thermal diffusivities as observed by the LMC device with respect to the thermal conductivity of the deployed standard

The results of the second experiment, in which the heating power is varied, are pictured in figure 67. The five samples are five folds heated with heating intensities ranging from 7 to 50%. The average determined thermal diffusivity amounts to 0.6 mm<sup>2</sup>/s and is shown by a black dashed line. The detected thermal diffusivity ranges from 0.58 to 0.83 mm<sup>2</sup>/s. The variation of heating intensity does not have an effect on the determined thermal diffusivity. All results approximate to the arithmetical mean.

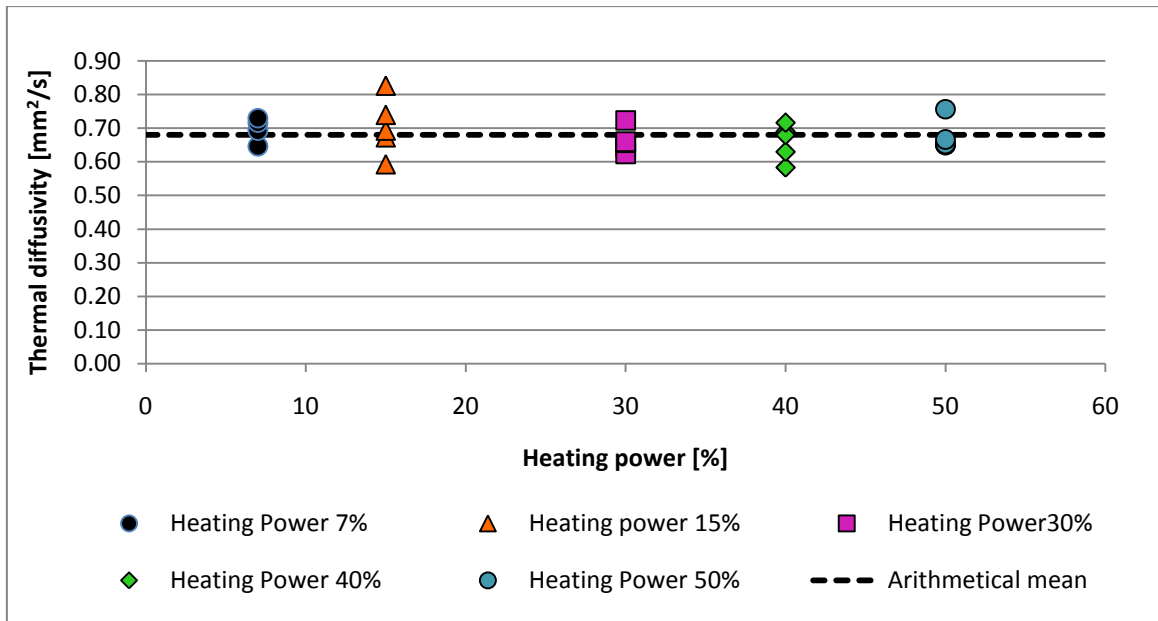


Figure 67: Thermal diffusivities as observed by the LMC device with respect to the deployed heating power

### 6.3.3 Derivation

The illustration of results from the first experiment shows that there is no correlation between observed thermal diffusivity and temperature difference on the sample's surface with respect to the thermal conductivity of the standard. The cluster of data is not derivable to any function.

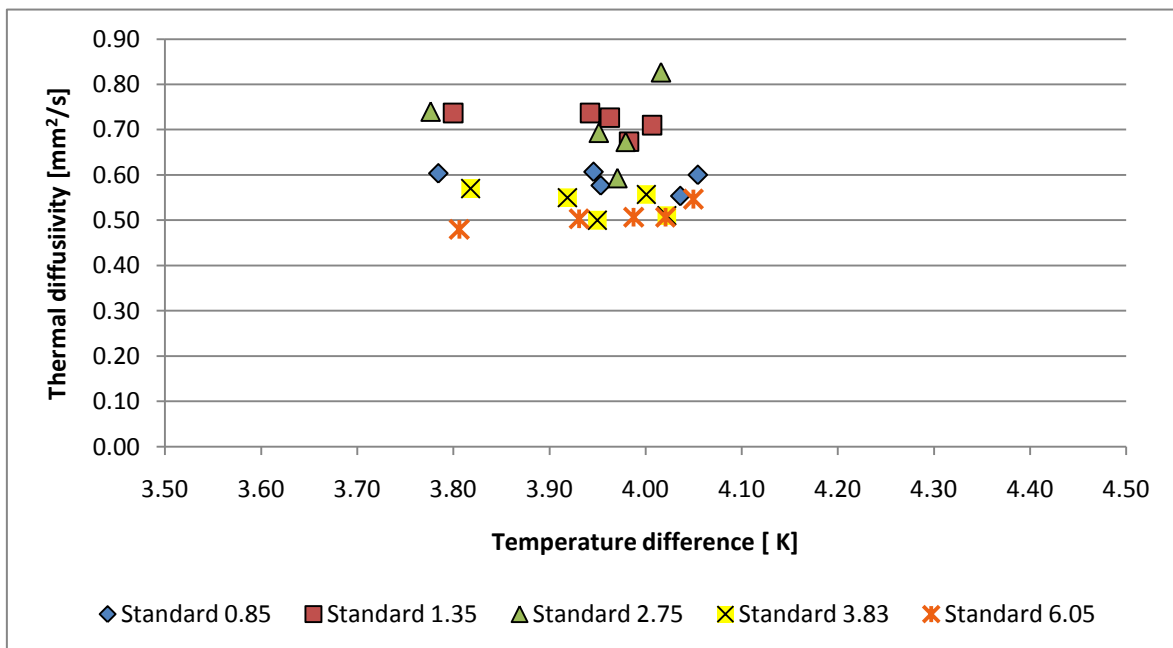


Figure 68: Thermal diffusivities as observed by the LMC device with respect to the temperature difference for different deployed standards

The results of the second experiment explain the relation of heating power to the resulting temperature difference on the sample's surface. In figure 69 the data of the measurements is pictured with respect to the temperature difference. Additionally theoretical functions for diverse heating power are displayed. The observed thermal diffusivity, not being affected by a variation of the heating intensity, is detected at a higher temperature with increasing heating power. In general a change of 0.4 K per 1% variation of the electrical heating power of the LMC can be expected.

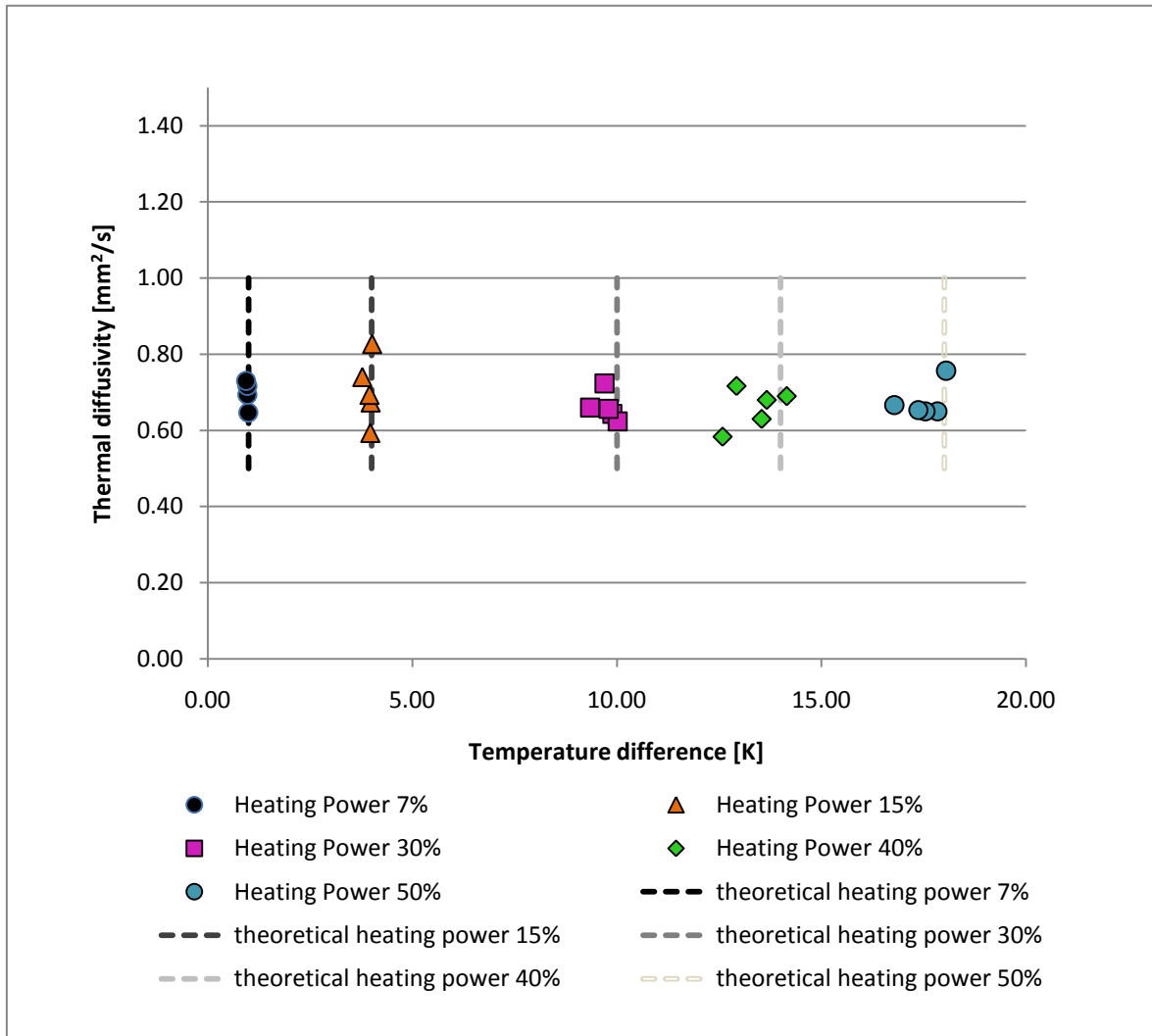


Figure 69: Thermal diffusivities as observed by the LMC device with respect to the temperature difference for different deployed heating power

Transferred to the data set of 120 analyzed samples, the observed temperature shift of the data according to the instrument can be explained by a different heating intensity of both devices. Figure 70 visualizes that the thermal diffusivity analyzed by the LMC belongs to an electrical heating power of 15%. The average difference of the temperature difference between LMC and TCS instrument amounts to 1.2 K. This indicates that the TCS heats the sample with 12% of the total LMC electrical heating power. The described theoretical functions are illustrated by dashed lines and the data by diamonds in the chart. The variation of thermal diffusivity with respect to the occurring temperature difference on the surface of the sample cannot be explained on the basis of this plot.

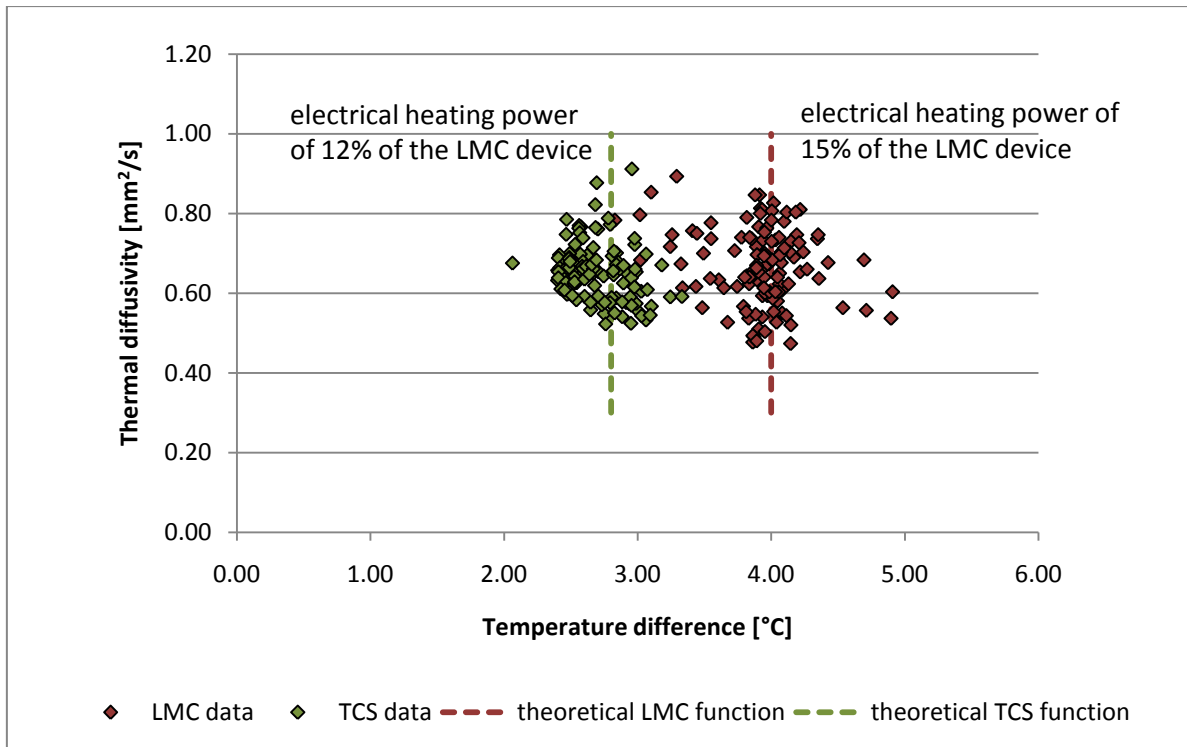


Figure 70: Relation between the thermal diffusivity Öskjuhlíð data series and the temperature difference. Displayed are the results for both instruments and their theoretical functions

## 7 CONCLUSION

### 7.1 Results

The analysis program and the results develop a validation of the LMC device. The instrument cannot be recommended for field measurements for two reasons. First, the adjustment for the temperature drift before the measurements takes several minutes in the laboratory, where generally stable conditions prevail. This adjustment would probably take even longer and may prove very difficult during outside measurements due to temperature fluctuations. The second reason why field measurements by the LMC tool are impracticable is shown by the comparison of uncut and cut samples. The observed data of uncut samples spread immensely for thermal conductivity and diffusivity, thus the results are not veridical. Therefore it is unavoidable to cut and varnish samples and determine them in windless, stable temperature conditions. Although the device is mobile and hence measurements can be done in the field, it is necessary to provide laboratory conditions to ensure high quality results.

The measurements of cores show that rounded surfaces have to be determined at least three times by the LMC to maintain veridical results.

The study shows that the LMC determines the thermal conductivity depending on the occurring temperature difference. The temperature difference on the other hand is related to the deployed heating power of the instrument. Furthermore the analyzed thermal conductivity is dependent on the used standard. Interestingly, the observed thermal diffusivity is independent on the properties of the used standard and even if the deployed heating power has an effect on the temperature difference this does not influence the determined thermal diffusivity.

The LMC can barely distinguish results from samples with large vesicles from samples characterized by intercrystalline porosity. Furthermore the LMC does not detect a variation of the physical properties in flow direction of the analyzed lava stream.

The comparison of the LMC device with the TCS instrument shows several differences between the two tools. The determination of the thermal conductivity by the LMC device is characterized by a positive skewness indicating a minor overestimation of the measurement, whereas the TCS instrument generally marginally underestimates the physical property. The absolute error of the new tool is lower than the one of the TCS, but both tools are characterized by the same relative measuring error of 12%. The statistical analysis of the thermal diffusivity determination shows that the data of the LMC being approximately symmetrical, in contrast to the results of the TCS device slightly underestimating the thermal diffusivity. Both tools have a relatively high measuring error of 14% (LMC) and 17% (TCS). But again the LMC device is featured by a lower absolute measuring error of  $0.09 \text{ mm}^2/\text{s}$  compared to  $0.11 \text{ mm}^2/\text{s}$ . Due to different measuring conditions of the instruments the results of thermal conductivity and diffusivity neither show a linear nor a logarithmic regression.

## **7.2 Outlook**

The validation of the LMC device is an important task to enhance the applied methods in the geothermal laboratory at the Technical University of Darmstadt in Germany. Due to the analysis of the new tool the quality of measurements can be improved. On the one hand the results of the study show the importance of sample preparation and steady temperature conditions for laboratory measurements. On the other hand the quality of geothermal property analysis can be enhanced by the LMC, because it is characterized by lower measuring error than the TCS. Secondly the analysis of basalt has been included into the thesis. With the help of the new results the data base of analyzed basalts, being useful to characterize geothermal reservoirs, is enlarged. Additionally the data will be used to confirm the analysis of the relation between thermal conductivity and the content of ferriferous basalts. The study of the LMC validation will be proceeded with further studies of different basalts in Germany.

## REFERENCES

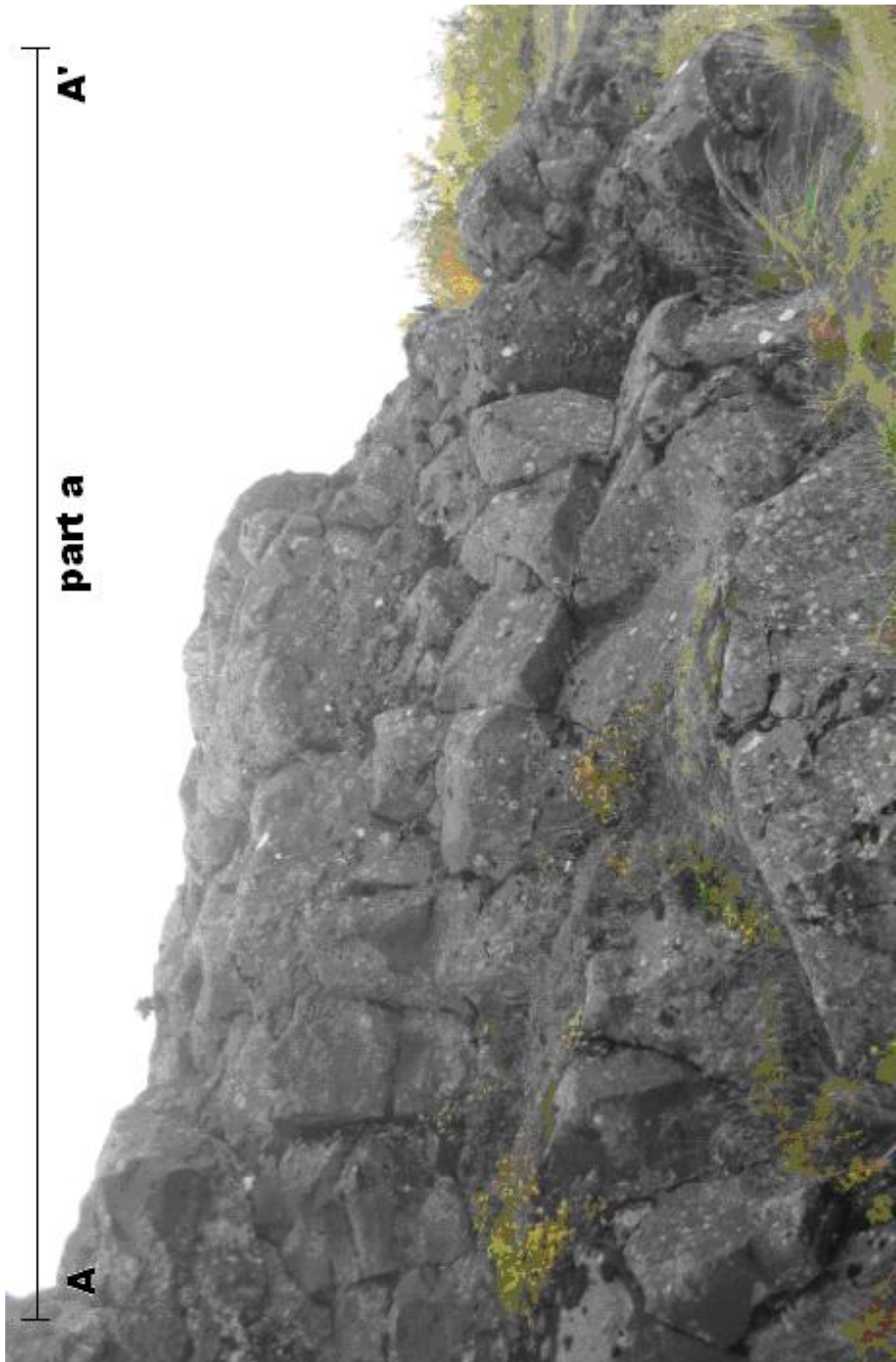
- Abramowitz, Milton and Stegun, Irene A. (Eds.) (1972) *Handbook of Mathematical Functions with Formulas, Graphs, and Mathematical Tables*. 9th edition. New York, Dover, 931-933.
- Bergmann, Ludwig and Schäfer, Clemens (2008) *Lehrbuch der Experimentalphysik. Band I. Mechanik, Akustik, Wärme*. 12th edition. Berlin, de Gruyter.
- Bertani, Ruggero (2009) *Geothermal energy: An overview on resources and potential*. Proceedings of the International Conference on National Development of Geothermal energy use 2009, Slovakia.
- Björnsson, Axel et al. (2007) *Geothermal Projects in NE Iceland at Krafla, Bjarnarflag, Gjástykki and Theistareykir*. Landsvirkjun, LV-2007/075.
- Björnsson, Axel (2010) *Geophysical Exploration for geothermal resources*. University of Akureyri, Iceland (manuscript in print).
- Clauser, Christoph and Huenges, Ernst (1995) Thermal conductivity of rocks and minerals. In: T. J. Ahrens (ed.), *Rock Physics and Phase Relations - a Handbook of Physical Constants, AGU Reference Shelf*, 3, American Geophysical Union, Washington, 105-126.
- Dickson, Mary H. and Fanelli, Mario (2004) *What is geothermal energy?* Istituto di Geoscienze e Georisorse, CNR, Pisa.
- Einarsson, Þorleifur (1994) *Geology of Iceland. Rocks and landscape. Translated by Georg Douglas*. 1st edition. Reykjavik, Mál og menning.
- Franzson, Hjalti et al. (2001) *Petrophysical Properties of Icelandic Rocks*. Proceedings of the 6th Nordic Symposium on Petrophysics, Trondheim, May 16-17.
- Gupta, Harsh and Roy, Sukanta (2007) *Geothermal energy: An Alternative Resource for the 21st century*. 1st edition. Amsterdam, Elsevier.
- Hall, Anthony (1996) *Igneous Petrology*. 2nd edition. Essex, Longman.
- Hamm, Karsten and Theusner, Markus (2010) *Lambda-Mess-Center LMCI*, Installation and Operation.
- Jakobsson, Svein P. and Gudmundsson, Mágnus T. (2008) Subglacial and intraglacial volcanic formation in Iceland, *Jökull*, 58, 179-196.
- Jakobsson, Svein P. et al. (2008) The Three Igneous Rock Series of Iceland, *Jökull*, 58, 117-138.
- Jóhannesson, Haukur et al. (2010) *Geological map of Southwest Iceland, 1:100 000*. Reykjavik, Iceland GeoSurvey.
- Lowrie, William (1997) *Fundamentals of Geophysics*, Cambridge University Press.
- Lund, John W. (2010) *Direct Utilization of Geothermal Energy 2010 Worldwide Review*. Proceedings World Geothermal Congress, Bali, 25-29 April.
- Plate, Erich J. (1993) *Statistik und angewandte Wahrscheinlichkeitslehre für Bauingenieure*. Berlin, Ernst.

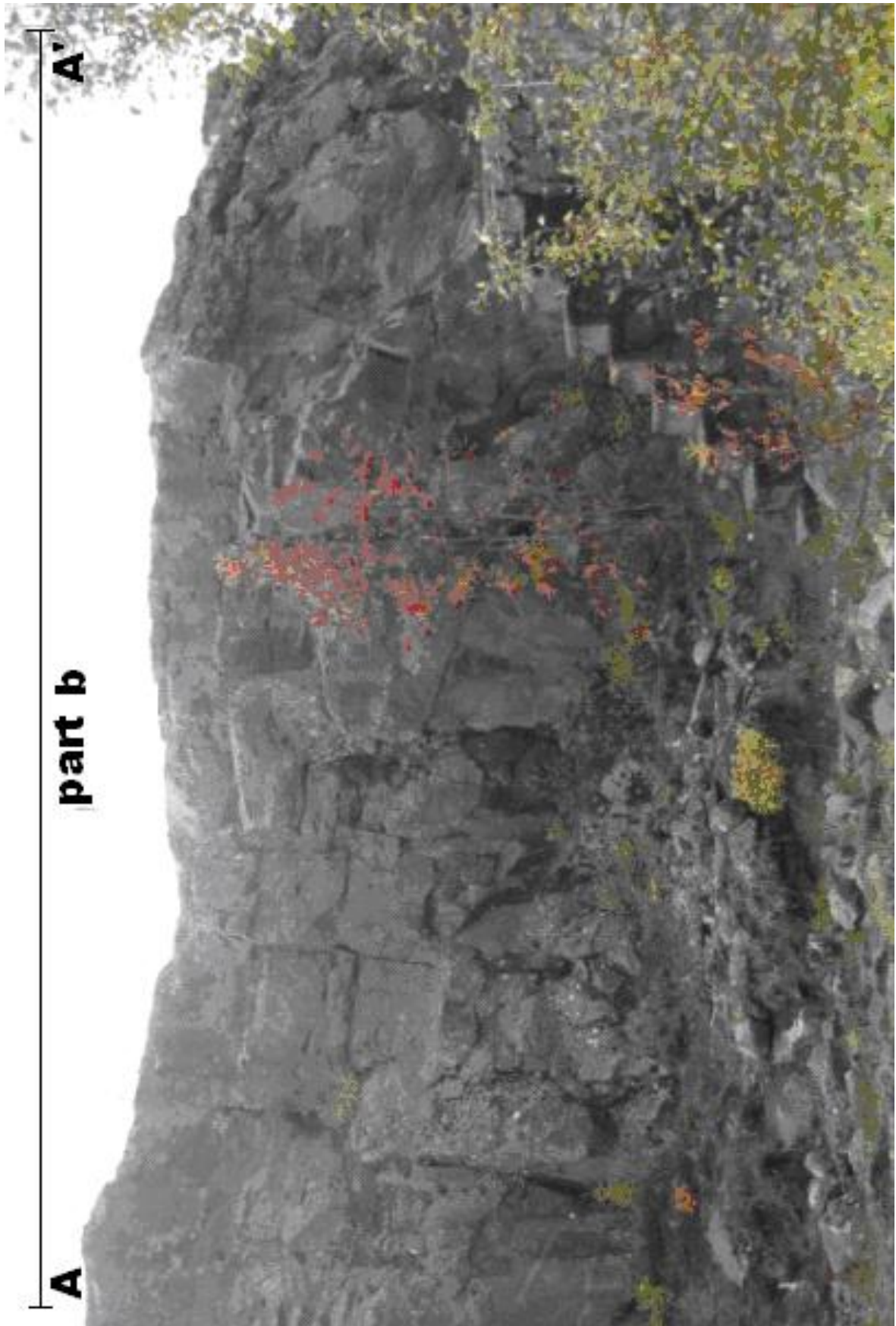
- Popov, Yuri A. et al (1983): Complex Detailed Investigations of the thermal properties of rocks on the basis of a Moving Point Source, *Physics of the solid earth*.21(1), 64-70.
- Popov, Yuri A. et al. (1985) Noncontact Evaluation of Thermal Conductivity of Rocks with the Aid of a Mobile Heat Source, *Physics of the solid earth*. 19(7), 563-567.
- Rykalin, N N. (1952) *Die Wärmegrundlagen des Schweißvorganges. Die Wärmeausbreitungsvorgänge bei der Lichtbogenschweißung*. Berlin, Technik.
- Sass, Ingo and Buß, Arne (2007) *Geothermische Kartierung – Korrelation von Wärmeleitfähigkeit und Permeabilität*. Proceedings of Der Geothermiekongress 2007, Bochum.
- Sass, Ingo (2010) *Introduction to Geothermal Energy, Part III*. Lecture Notes RES- The School for Renewable Energy Sciences. Geothermal Energy Specialization 2010. Geothermal Energy Sciences Course GEO-601: Geothermal Systems.
- Sædmundsson, Kristján (1979) Outline of Geology of Iceland, *Jökull*, 29, 7-28.
- Schmidt, Kai (2009) *Untersuchungen zum Einfluss der thermischen Umgebungsbedingungen bei berührungslosen Messverfahren zur Bestimmung der Wärmeleitfähigkeit von Gesteinen*. Diploma thesis. Institute of Applied Geosciences, Technical University of Darmstadt.
- Shelley, David (1993) *Igneous and metamorphic rocks under the microscope*. First edition. London, Chapman & Hall.
- Sigurðsson, Ómar et al. (2000) *Database on igneous rock properties in Icelandic geothermal Systems. Status and unexpected results*. Proceedings World Geothermal Congress 2000, World Geothermal Congress, Kyushu- Tohoku, May 28- June10.
- Stelzer, Friedrich (1971) *Wärmeübertragung und Strömung*. Berlin, Karl Thiemig.
- Trønnnes, Reidar G. (2002) *Geology and geodynamics of Iceland*. Nordic Volcanological Institute, University of Iceland, Reykjavik.
- Weinbruch, Stephan (2003) *Statistik für Geowissenschaftler. Vorlesungsskript*. 2nd edition. Lecture Notes Institute of Applied Geosciences, Technical University of Darmstadt.
- [www.fe-lexikon.info/images/Gauss\\_Kurve.jpg](http://www.fe-lexikon.info/images/Gauss_Kurve.jpg), Web-page
- [www.geo.tu-darmstadt.de/fg/angeotherm/geotherm\\_forschung/TCS.de.jsp](http://www.geo.tu-darmstadt.de/fg/angeotherm/geotherm_forschung/TCS.de.jsp), Web-page
- [www.knowledgerush.com/kr/encyclopedia/Normal\\_distribution](http://www.knowledgerush.com/kr/encyclopedia/Normal_distribution), Web-page



## **APPENDIX A**

### **Photos of the Öskjuhlíð outcrop**

























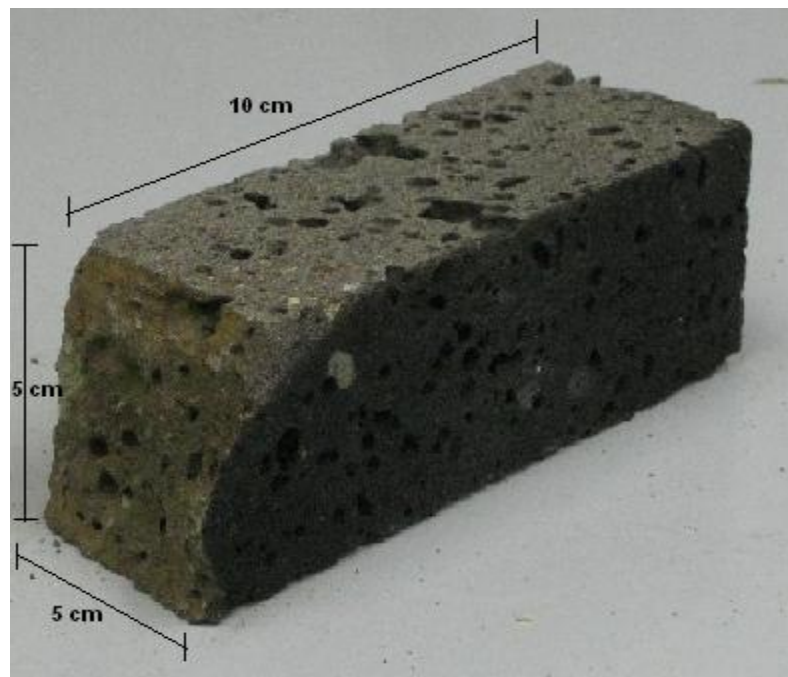
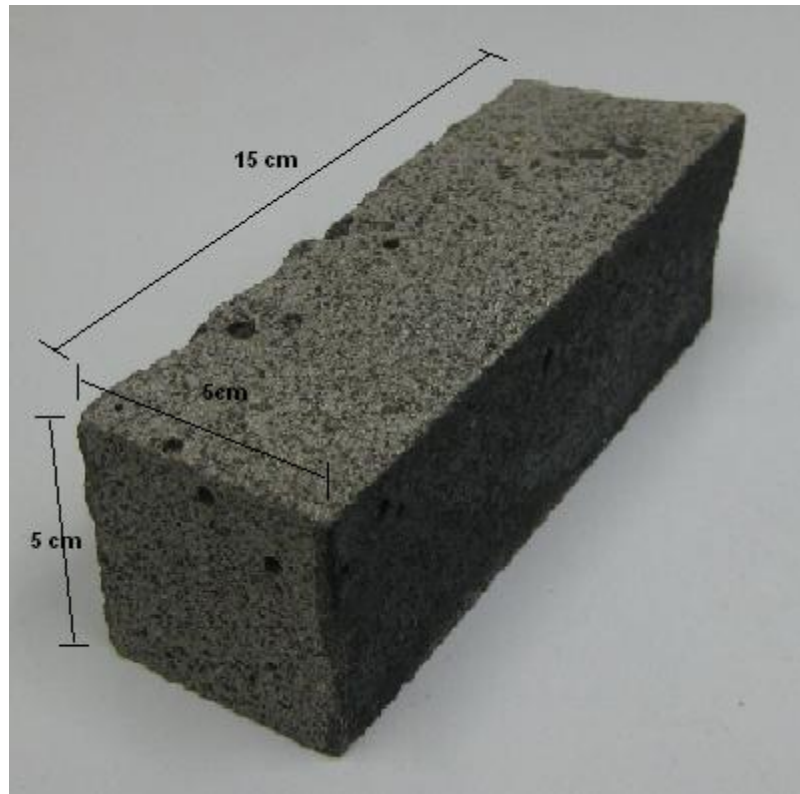






## APPENDIX B

### Photos of the cuboids





## Photos of cores

